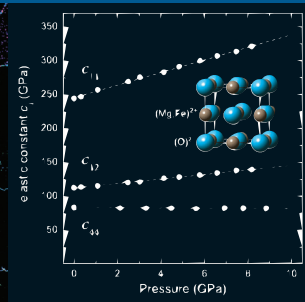
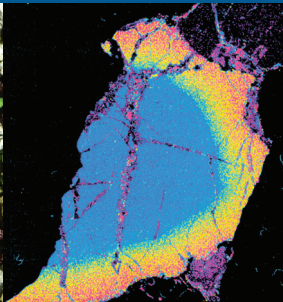
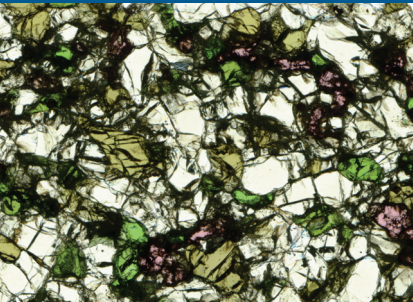


FROM CRUST TO CORE AND BACK

GEOMATERIALS RESEARCH AT BAYERISCHES GEOINSTITUT



Editor: Friedrich Seifert

Contributors: Tiziana Boffa Ballaran, Geoffrey Bromiley, Sylvie Demouchy, Natalia Dubrovinskaia, Leonid Dubrovinsky, Dan Frost, Florian Heidelbach, Steven Jacobsen, Stefan Keyssner, Kurt Klasinski, Falko Langenhorst, Christian Liebske, Fred Marton, Catherine McCammon, David Rubie, Friedrich Seifert, Gerd Steinle-Neumann, Hidenori Terasaki, Michael Terry

Layout by: Andreas Gaube, PR- & Werbeagentur A-G-SYSTEMS, Bayreuth,
Tel: 09 21 - 5 07 14 41, E-Mail: info@a-g-systems.de

Printed by: Druckerei Heinz Neubert GmbH, Bayreuth, Tel. 09 21 - 6 47 21

All rights reserved. No part of this book may be reproduced or transmitted in any form or by any means, electronic or mechanical, including photocopy, recording, or any information storage and retrieval system, without permission in writing from Bayerisches Geoinstitut.

FROM CRUST TO CORE AND BACK

GEOMATERIALS RESEARCH AT BAYERISCHES GEOINSTITUT



Universität Bayreuth
D-95440 Bayreuth
Germany

Tel. +49 (0) 9 21 - 55 37 00
Fax +49 (0) 9 21 - 55 37 69

e-mail bayerisches.geoinstitut@uni-bayreuth.de
Homepage: <http://www.bgi.uni-bayreuth.de>



In contrast to some of the other bodies in the Solar System, the Earth is a “living” and highly dynamic planet. This fact is appreciated especially by people who live in areas that are prone to

natural disasters such as those caused by earthquakes and volcanic eruptions. An additional aspect, also of great importance for mankind, is the exchange or cycling of chemical components (such as water and carbon dioxide) between the Earth’s atmosphere and the deep interior that can play an important role in determining the composition of the atmosphere and can thus greatly influence climate change. Such factors have motivated scientists for more than a hundred years to seek a detailed understanding of how the Earth functions as a chemical and physical system. Because “System Earth” is highly complex, a sustained multi-disciplinary approach is necessary to achieve this objective.

In the 1960’s a major scientific breakthrough occurred in the Earth Sciences with the formulation of the theory of Plate Tectonics. This theory, which explained many observations that previous appeared to be unconnected, still provides an integrated framework for understanding how the Earth works. In the last 40 years, our understanding of the structure and dynamics of the Earth’s interior and how these affect phenomena that occur at the surface has improved enormously. Such advances result from efforts in all branches of the Earth Sciences, including observational disciplines such as seismology, petrology and geochemistry, experimental studies, and theoretical approaches that often involve complex numerical

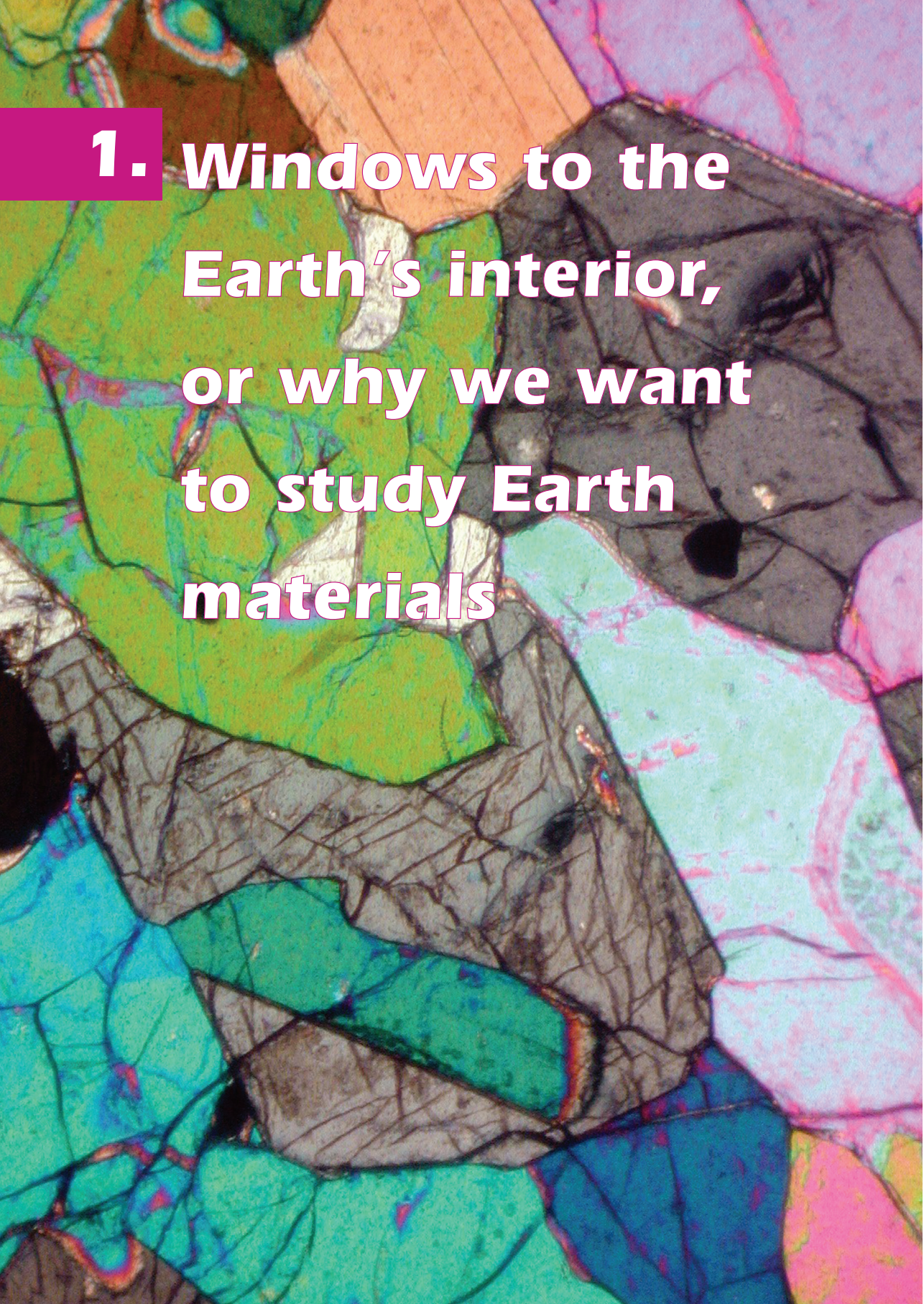
models of geological materials and processes. Experimental approaches are critical in the Earth Sciences for understanding the evolution of the Earth, its internal structure and composition, and the wide range of processes that occur within its interior. For example, seismology provides basic information about the density and elastic properties as a function of depth in the Earth. However, such data can only be used to understand the chemistry and mineralogy of the Earth in combination with information on how the density and elastic properties of Earth materials (i.e. minerals and rocks) vary with pressure and temperature - in other words, input from experimental geosciences is essential.

The Bayerisches Geoinstitut was founded by the Free State of Bavaria in 1986 with the aim of studying Earth materials experimentally at high pressures and temperatures, thus providing scientific data and ideas that are essential for developing a better understanding of how the Earth functions. In this brochure, we provide an overview of some of the main research areas that are pursued at the Geoinstitut. These research areas often overlap significantly with other fields, such as solid-state physics and chemistry and material science. Our intention is to convey to scientists from other disciplines and also to the general public the aims of experimental geosciences and how this research field contributes to the Earth Sciences as a whole. In this respect, I hope that you, the reader, will have much pleasure in browsing through this brochure.

A handwritten signature in black ink, appearing to read 'D. Rubie', with a long horizontal stroke underneath.

David Rubie

chapter	page
1. Windows to the Earth's interior, or why we want to study Earth materials	6
2. The tools	12
3. A look to outer space: Meteorite and impact research	16
4. Early differentiation of the Earth	20
5. Viscosity of melts under high pressure	24
6. Fluid transport and release during subduction: Water recycling into the Earth's deep interior	28
7. Structure and elasticity of minerals	34
8. Mineral phase transformations in the mantle and seismic discontinuities	40
9. The oxygen content of the Earth	44
10. The most common but unseen terrestrial mineral	48
11. Rheology of the deep Earth	52
12. The core-mantle boundary - Earth's major interface	56
13. The Earth's core	60
14. A view to technical applications: Synthesis of new superhard materials at extreme conditions	64
About Geoinstitut	68
Source of Figures	72



**1. Windows to the
Earth's interior,
or why we want
to study Earth
materials**

The surface of the Earth on which we live is an interface, with interactions of endogenous (inner) and exogenous (outer) forces. For example, heat is supplied to us both by radiation from the sun, and by heat flux from the Earth's interior. Volcanic exhalations contribute to greenhouse gases, and aerosols generated by volcanoes can change the albedo of the Earth, which may lead to variations in surface temperature. Earthquakes originate from stress release in the Earth's brittle crust. Geochemical cycles may reach from the stratosphere down to the depths of the Earth's mantle, and auroras in the ionosphere are closely connected to the magnetic field originating from convection of liquid metal in the Earth's

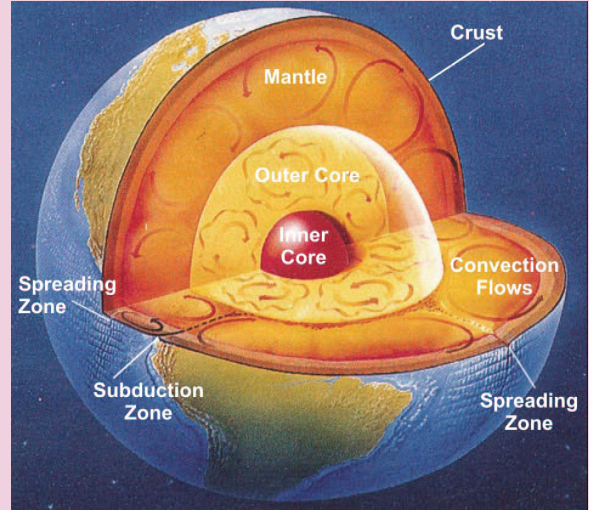
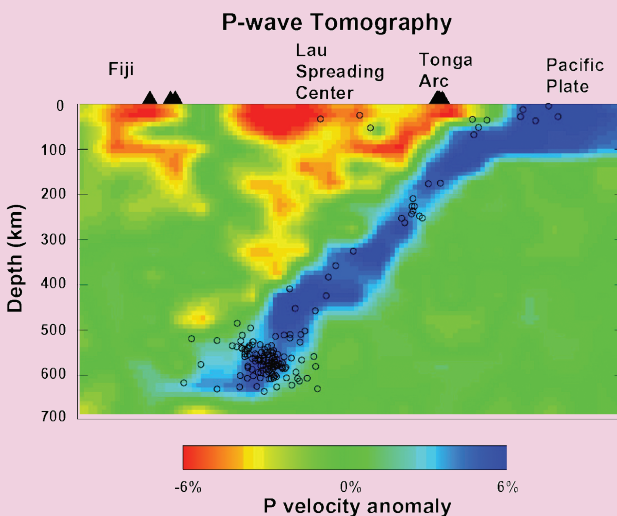


Fig. 1.1: Schematic cross section through the Earth, showing the major units and several convection processes. Modified from GEO

Fig. 1.2: East-west vertical cross section of P wave velocity from 0 to 700 km across the Tonga subduction zone and Lau ridge. Red and blue colours denote slow and fast velocities, respectively (see velocity perturbation scale). Solid triangles indicate active volcanoes, while earthquakes within a 40 km width from the cross section are marked by circles. Taken from Zhao et al., *Science* 278, 254 (1997).



outer core. To understand the origin of all these phenomena, we have to investigate the processes – both present and past – that occur in the Earth.

Fig. 1.1 shows our present understanding of the nature of the Earth's interior. The Earth may be described in an oversimplified "onion-shell" model (assuming only radial variations in physical and chemical properties) as consisting of a thin crust (close to an average composition of granite on the continents and basalt under the oceans) with an ultrabasic mantle (rock name peri-

dotite) reaching down to about 2900 km depth. The mantle can be further subdivided on the basis of distinct mineral species into an upper mantle, a transition zone, and a lower mantle. The crust and the upper part of the upper mantle (to about 100 km depth) form the brittle “skin” of the Earth, called the lithosphere, which constitutes the rigid plates. These plates “swim” on the much more ductile (but still solid) rest of the mantle. Further down, the core extends from 2900 km to the Earth's centre at 6371 km depth. It consists mostly of iron, and is subdivided into a molten outer core and a solid inner core.

The Earth is a lively planet, and it is the dynamic nature of the processes that we feel as endogenous benefits or threats at the surface. Essentially, these dynamic processes are driven by a two-stage heat engine which derives its energy from the temperature gradient between the centre of the Earth and its surface. In the outer core, rapid convection in the liquid metal creates the dynamo which produces the Earth's magnetic field. In the mantle, the solid materials are at such high temperatures that



they flow plastically like toothpaste, where hotter and less dense materials rise slowly as diapirs, while colder and denser materials descend in the slabs at subduction zones. How has the picture of the Earth presented in Fig. 1.1 been derived? Despite a recent bold proposal to probe the interior of the Earth directly, we have to rely on a combination of more or less indirect but interlinked approaches:

Observational astronomy, geophysics and geodesy: A number of properties of the Earth can be measured directly, such as the shape of the Earth (the geoid), the mass and moment of inertia, the magnetic field and its variation, post-glacial rebound, the

Fig. 1.4: Sample from the Earth's mantle enclosed within basalt. This greenish peridotite nodule, which consists of olivine, pyroxenes and spinel, was transported by the basaltic melt and then ejected. From Dreiser Weiher, Eifel Mountains, Germany. Collection GeoMuseum Universität Köln. The length of nodule is ca. 12 cm.



velocities of seismic waves and their depth dependence, the electrical conductivity and so on. In recent years, dramatic progress has been achieved through seismic tomography, where wave velocities are mapped in three dimensions with a spatial resolution on the order of less than 100 km, clearly showing evidence for rising hot plumes or subducting cold slabs (Fig. 1.2). However, the chemical and mineralogical nature of these features is not always clear.

Cosmochemistry: According to theories for the origin of the solar system, the proto-Earth had a so-called chondritic composition which we still encounter today in the form of undifferentiated meteorites, the carbonaceous chondrites (Fig. 1.3). Assuming a metallic core and knowing the chemical composition of the crust, we may then calculate the chemical composition of the mantle.

For more direct estimates, there are geological processes that bring to the surface materials from great depth: for example, metamorphic rocks in mountain ranges may have formed at depths up to 100 km or

Fig. 1.3: Optical photomicrograph (crossed polarisers) of a carbonaceous chondrite with numerous chondrules (spheres) embedded in a dark, fine-grained matrix that contains organic matter. The chondrules display various textures and are composed of olivine, pyroxene and glass.

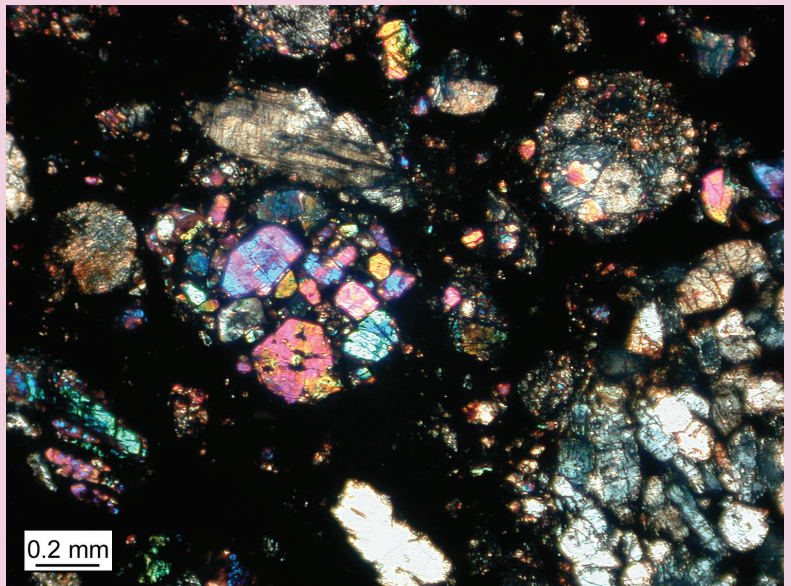




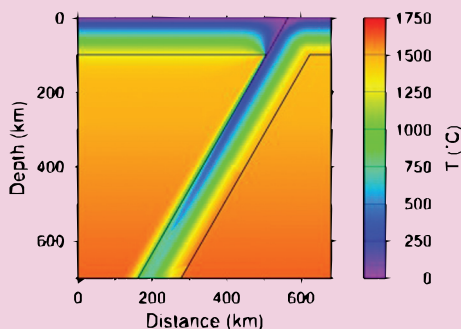
Fig. 1.5: Bright red garnet inclusion in a round brilliant diamond.

more and then be uplifted again, or magmas may carry along samples from the mantle. Basalt melts are generated in the upper parts of the Earth's mantle and, during their ascent, sample wall rocks such as the peridotite nodule shown in Fig. 1.4 which "swims" in vesicular basalt. This particular nodule consists of abundant olivine, two pyroxenes and a small amount of spinel.

Such rocks therefore provide information on the chemical and mineralogical constitution of the Earth down to the source region of basalts, which come from depths of a few tens up to ca. 100 km below the surface.

Samples from even greater depths can be preserved as inclusions in diamonds (Fig. 1.5). While most diamonds originate within the upper approximately 200 km of the mantle, a select few appear to originate from greater depths, including some from below 670 km which therefore represent samples of the Earth's lower mantle. The hard and resistant diamonds encapsulate mineral inclusions like a safe and protect them from chemical alteration during ascent. Shown here is a red garnet inclusion in a diamond (already cleaved and polished into the shape of a round brilliant) – the shock or dismay of the jeweller may turn into the joy of the mineralogist.

Fig. 1.6: Calculated temperature distribution within a subducting slab. The cold subducting crust forms a wedge within hotter mantle material.



Modelling: Large scale geological processes such as subduction of oceanic crust or rising of mantle plumes may be successfully modelled in two or even three dimensions using tools such as finite element methods. In this way the distribution of physical parameters such as temperature, stress and buoyancy as well as the shape of chemical heterogeneities or the regions of stability or metastability of individual mineral structures can be predicted. Fig. 1.6 shows the calculated temperature distribution in and around a cold subducted slab. Such models require a detailed knowledge of material properties such as thermal conductivity for this specific example.

Finally, there is experimental geochemistry and geophysics. This involves the laboratory determination of the properties of Earth materials under well-defined conditions of pressure, temperature and chemical composition, which is what most of this pamphlet is actually about. This approach can be considered a particular type of material science – the physics and chemistry and physical chemistry of matter, mostly specialised to extreme temperatures and pressures, and more or less confined to the chemical compositions that we expect in the Earth. Such laboratory data then provide constraints for the interpretation of observational data, for example the elastic properties derived from seismic wave velocities must conform to those of materials that are stable at the corresponding depths and chemical compositions. Laboratory data are also the basis for most modelling approaches, as exemplified by Fig. 1.6. On the other hand, the output of the experimental ap-

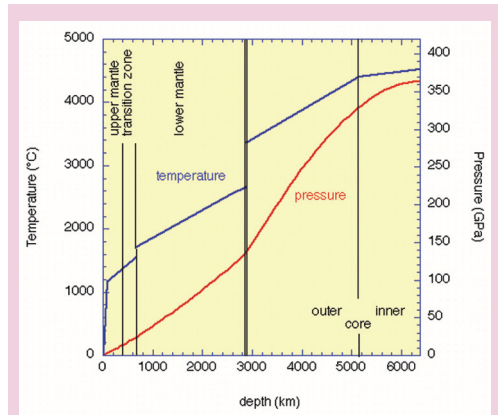
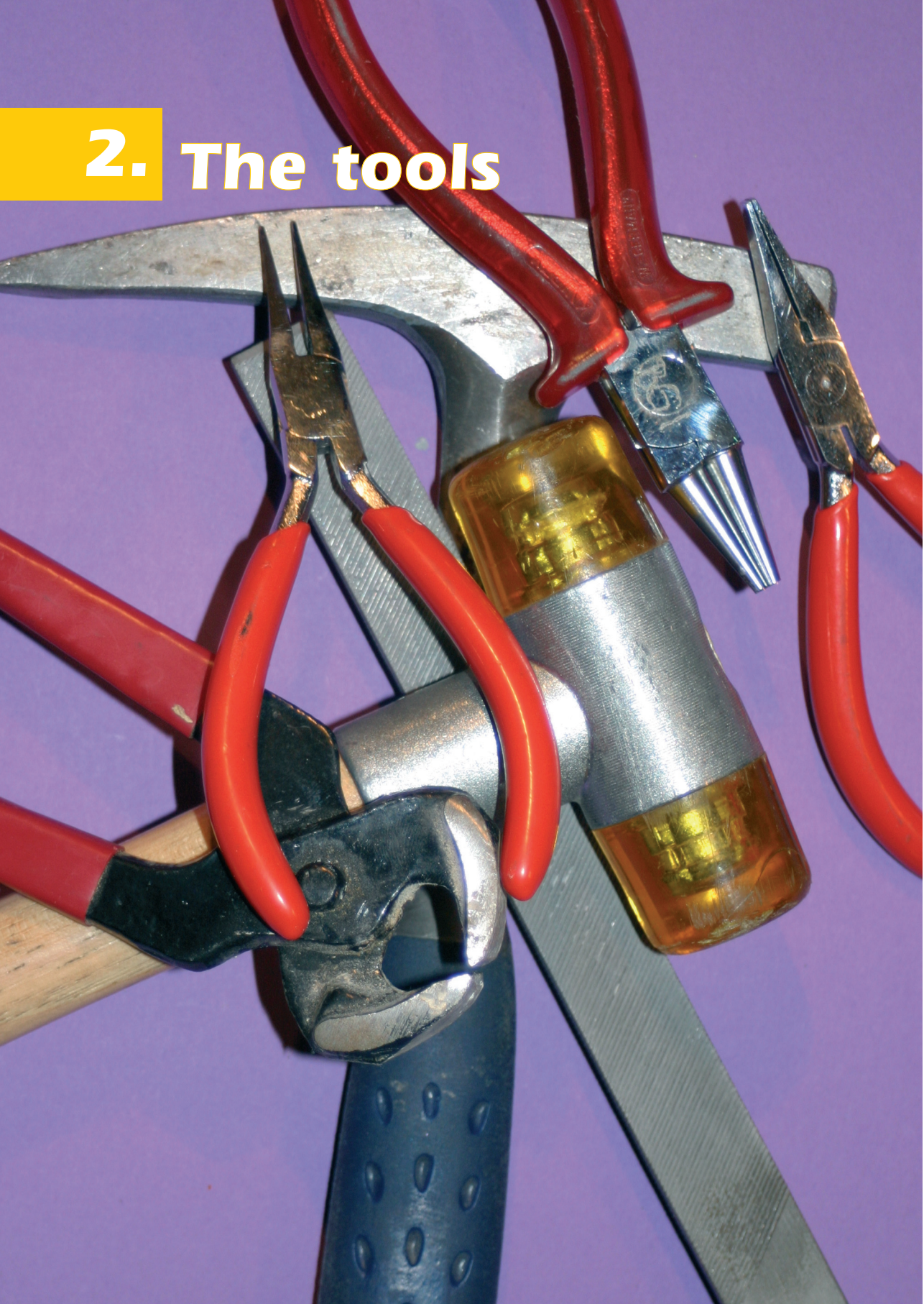


Fig. 1.7: Pressure distribution in the Earth according to the Preliminary Reference Earth Model. The temperature estimate is uncertain, and at large depths is on the order of at least 1000°C.

proach depends on the input (the chemical composition, for example), so ground truthing of experimental data by observations is therefore necessary.

In summary, we have to explore all relevant physical and chemical properties of Earth materials at the relevant conditions of pressure and temperature, as well as possibly others such as the fugacity of volatile species (water, for example). Pressure and temperature alone are a challenge: as shown in Fig. 1.7 we have to cover a pressure range from *ca.* 0 to 365 GPa (1 Giga-pascal = 10 kilobars \approx 10 000 atmospheres) and a temperature range from *ca.* 0° to 5000°C in order to straddle the conditions from the Earth's surface down to its centre. In the next section, we will therefore look at the available methodology. ■

2. The tools



To simulate the state of matter in the Earth's interior we may use a laboratory (or experimental *sensu stricto*) approach or computer modelling or – better still – a combination of both. The task is not trivial: as indicated in Fig. 1.7 pressures cover the range from 0 at the Earth's surface to 365 GPa in the centre of the core, temperatures vary from *ca.* 0° to *ca.* 5000°C, materials include metals, oxides, sulphides, *etc.*, aggregate states range from solid to molten to fluid, crystal structures include both simple and complex, bonding varies from metallic to covalent to ionic, and so on. However, methodological development at Bayerisches Geoinstitut (and elsewhere in the world) has made it possible to tackle these tasks.

Pressure P is defined as

$$P = \frac{F}{A}$$

with F = force and A = area, and high pressures can be therefore generated in basically two ways: increasing the force or decreasing

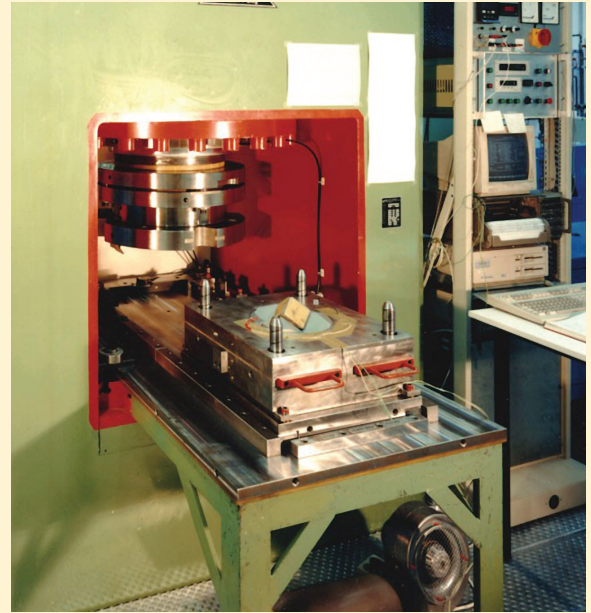


Fig. 2.2: The 1000 ton multi-anvil press, opened for loading a sample assembly. The lower guide block (centre) contains the set of three outer anvils and the cubic arrangement of eight inner anvils (*cf.* Fig. 2.3), electrically insulated by green epoxy sheets

Fig. 2.1: The multi-anvil laboratory at Bayerisches Geoinstitut showing (from right to left) the 1200, 1000 and 5000 ton presses.



ing the area. The approaches are complementary, and both are used in Bayreuth.

Maximising force: Bayerisches Geoinstitut operates three big presses (with nominal capacities of 1000, 1200, and 5000 tons – Fig. 2.1) using multi-anvil technology, which achieve pressures up to 26 GPa (corresponding to some 700 km depth), temperatures up to 2500°C, and “large” (several mm³ to cm³) volumes. They operate by application of a large force (Fig. 2.2) to a sample assembly

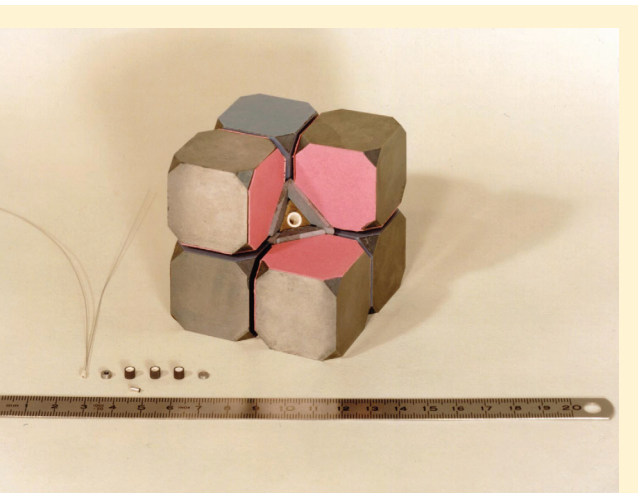


Fig. 2.3: The set of eight inner tungsten carbide anvils, with one cube removed to show the ceramic octahedron serving as a pressure-transmitting medium. The thermocouple and the ceramic parts forming the furnace are shown on the lower left of the cube assembly.

which incorporates a heater and a thermocouple (Fig. 2.3). The 5000 ton press is the biggest operational multi-anvil press in the world. Its large sample chamber makes it particularly useful for synthesising large quantities of high-pressure materials, growing large crystals, and for *in situ* measurements such as thermal or electrical conductivity.

Minimising area: In diamond anvil cells (DACs) two anvils made from superhard materials squeeze a tiny (10-500 μm) sample; hence the required forces are relatively moderate. In this way pressures up to several hundred GPa may be attained. Heating may be external (up to about 1200°C) or internal using a laser. DACs have the great advantage that the anvils are transparent to a wide range of electromagnetic radiation (X-rays, visible and infrared ra-

diation *etc.*) and samples can therefore be monitored during the experiments (Fig. 2.4).

Some high-pressure materials may be brought back to room pressure without loss of structure or change in chemistry, and can be studied at ambient conditions using a wide spectrum of methods such as electron microscopy, diffraction of X-rays or neutrons or electrons, and various types of spectroscopy (see equipment list in the Appendix). In contrast, however, other materials decompose during decompression or change to a different structural state, and therefore require characterisation at high pressure and/or temperature by so-called *in situ* measurements (Fig. 2.5). Also, some critical properties of materials such as compressibility or thermal conductivity can only be studied at elevated pressures and temperatures. Work at Bayerisches Geoinstitut has solved some of these methodological chal-

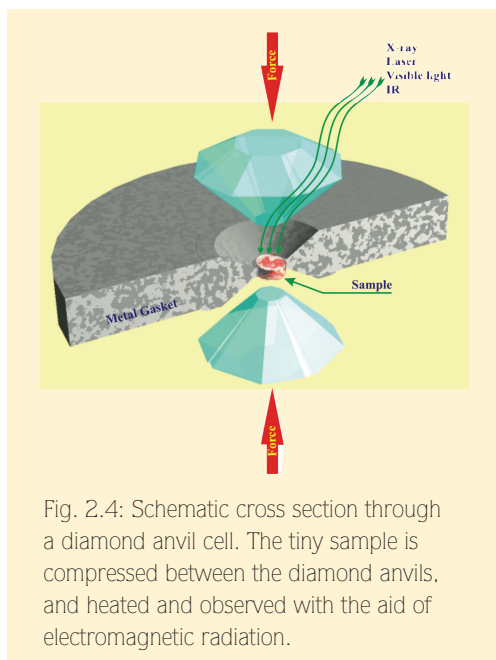


Fig. 2.4: Schematic cross section through a diamond anvil cell. The tiny sample is compressed between the diamond anvils, and heated and observed with the aid of electromagnetic radiation.

lenges, and specific examples are given in the following sections.

Computational methods increasingly supplement the experimental efforts in mineral physics (Fig. 2.6). Progress in the methodology of computational solid state physics, primarily density functional theory, and advances in computer technology make it now possible to reliably predict material properties. Such computations do not use information from experiments and are based on our quantum-mechanical understanding of the structure of matter (first principles calculations). They rely exclusively on the chemical composition of the material to be studied and an educated estimation of its crystal structure and unit cell volume. Of central importance in this context are the electrons that are responsible for bonding in the solid. In density functional theory their energies (band structure) are calculated, and depend on the other electrons and atomic nuclei through electrostatic interactions, and vary as a function of structure and unit cell volume. Through variation of the volume, compression (and therefore high pressure) can be accessed relatively easily. High temperatures (obviously relevant for the Earth's interior) are achieved through molecular or lattice dynamics, and all thermodynamic equilibrium properties (including pressure, elasticity, specific heat and thermal expansivity) can be obtained from such simulations which are of central importance in the solid Earth sciences. ■

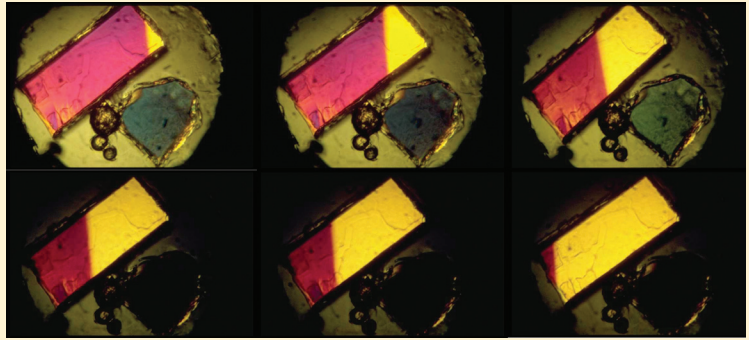


Fig. 2.5: *In situ* observation of a phase transition in the diamond anvil cell as seen in polarised light. The spodumene crystal (a pyroxene of composition $\text{LiAlSi}_2\text{O}_6$) transforms from a low-pressure (yellow) to a high-pressure (violet) form. A slight volume decrease at 3.2 GPa sweeps the interface (corresponding to the locus of the phase transition) between the two structures through the crystal. The high-pressure structure cannot be quenched, so measurements such as X-ray structure determination can only be made *in situ* at high pressure.

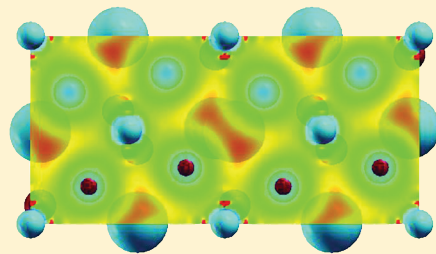


Fig. 2.6: Calculated charge density of MgSiO_3 perovskite shown for the a - c plane. The structure is depicted as follows: Mg atoms (large blue spheres), Si atoms (small blue spheres) and O atoms (red spheres). The octahedral tilt of SiO_6 octahedra in the orthorhombic $Pbnm$ structure is apparent by two O atoms above the a - c plane, and two O atoms below the plane. The charge density in the plane is displayed on a logarithmic scale: high charge density is dark brown and low charge density is red.



**3. A look to
outer space:
Meteorite and
impact research**

Meteorites are the oldest rocks in the solar system and mostly represent fragments of asteroids. They provide witness of early solar processes that are not preserved on the Earth due to its high geological activity. The information contained in these early messengers ranges from the condensation of the first solid phases in the solar nebula to the accretion of planets by collisions of smaller bodies (planetesimals). The study of meteorites provides important constraints on the composition of the proto-Earth and helps to decipher the role of impact processes in the formation and early evolution of the Earth.

The cratered surfaces of the terrestrial planets and their satellites provide evidence for an early heavy bombardment. As established on the Moon, the early high cratering rate declined significantly within the first 1.5 billion years and then reached a steady level (Fig. 3.1). Due

to erosion and plate tectonics, the traces of such impact events (i.e. impact craters) are difficult to detect on Earth, where so far, about 150 craters have been recognised (Fig. 3.2). Some impacts were large enough to cause global effects, where the best example is the 180 km diameter Chicxulub impact crater at Yucatan peninsula, Mexico. The current consensus is that this impact event caused the mass extinction at the Cretaceous-Tertiary (K/T) boundary.

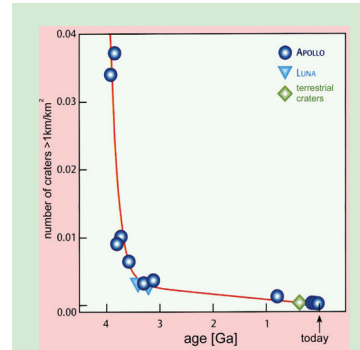
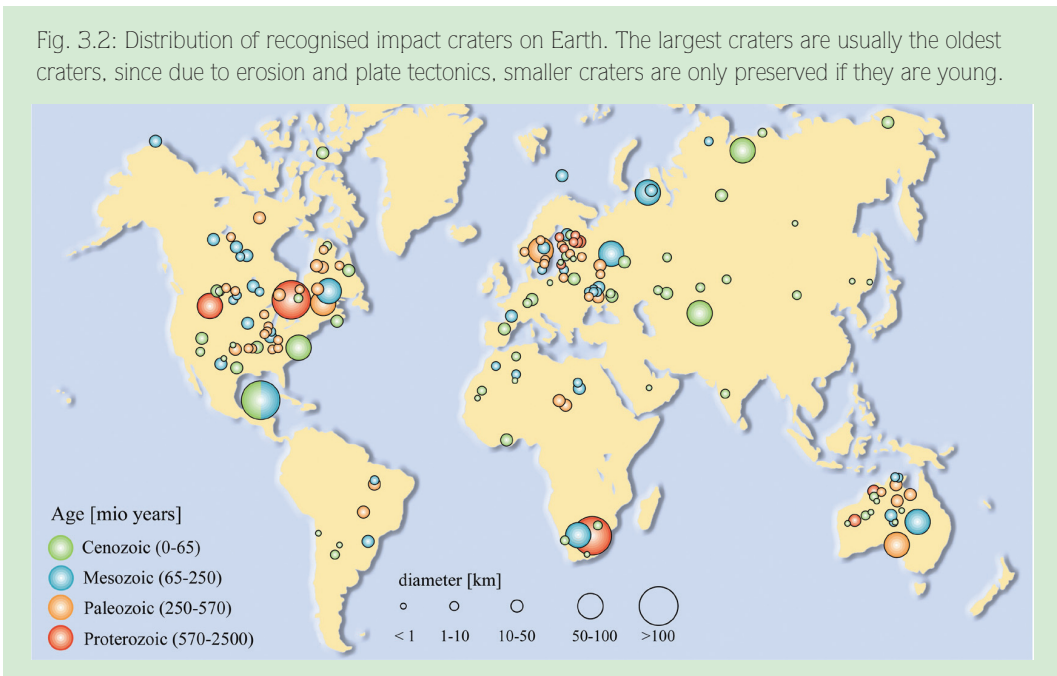


Fig. 3.1: The cratering record of the Moon. The curve shows the number of craters per area as a function of time. The young terrestrial value fits well on the lunar curve and illustrates that the flux of projectiles was the same for Earth and Moon.

Fig. 3.2: Distribution of recognised impact craters on Earth. The largest craters are usually the oldest craters, since due to erosion and plate tectonics, smaller craters are only preserved if they are young.



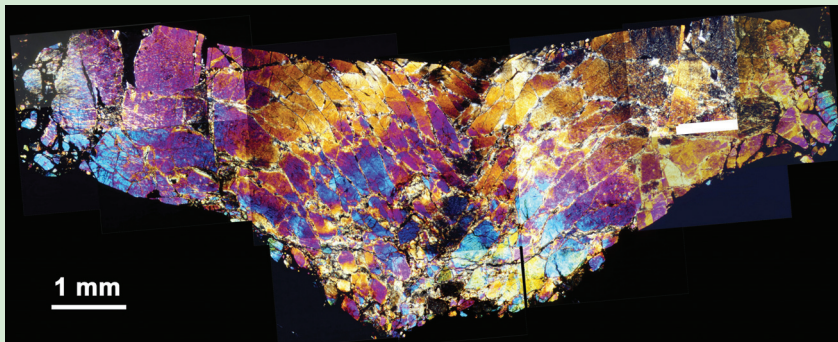
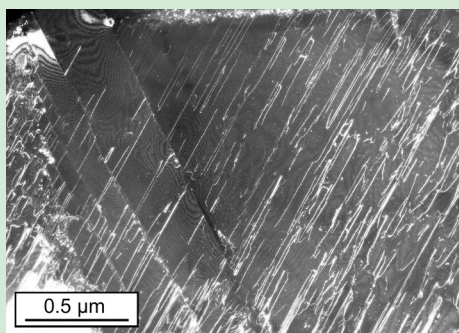


Fig. 3.3: Photomicrograph (crossed polarisers) of a cross section through an experimentally shocked olivine crystal that was strongly sheared in a shock experiment. As a consequence, numerous melt veins have formed in the central part of the sample.

Our current research in this field focuses on high-pressure phase transformations in meteorites and terrestrial impact rocks, and impact-induced gas release from carbonates and sulfates with potential consequences for the climate. Questions regarding these subjects are addressed by combining natural observations with experimental simulations and modelling. Shock experiments are performed in collabo-

Fig. 3.4: Dark-field transmission-electron microscope (TEM) image of an experimentally shock-deformed olivine crystal adjacent to the shock veins shown in Fig. 3.3. The numerous straight dislocations originate at planar fractures.



ration with other institutes (ENSMA, Poitiers; EMI, Freiburg; Institute of Planetology, Münster), using various experimental designs such as high-explosive setups, laser and electric discharge guns.

High-pressure minerals are perhaps the most spectacular manifestations in impact rocks. The study of high-pres-

sure minerals in meteorites provides crucial information on the collision history of their parent bodies. Certain groups of meteorites such as L6 ordinary chondrites and the Martian (SNC) achondrites have recorded very high shock pressures and temperatures. These meteorites represent our only access to natural samples of high-pressure silicates (*e.g.* ringwoodite, majorite) that are otherwise believed to exist in the Earth's deep mantle but decompose before they can reach the surface. The high-pressure minerals occur in thin melt veins (so-called shock veins), which have been formed due to friction along shear faults. High-pressure phases crystallise from these melt veins upon decompression, *i.e.* at still enhanced pressures. To reproduce shock veins and deformation effects in adjacent minerals experimentally, we have successfully developed a new setup designed to produce large shear (Figs. 3.3 and 3.4).

Another spectacular example of a shock-induced phase transformation is the formation of diamond in terrestrial impact craters such as Popi-

gai, Lappajärvi and the Nördlinger Ries (Fig. 3.5). These diamonds have a tabular shape and contain numerous planar lattice defects. Our observations show that impact diamonds form directly from graphite by a solid-state mechanism. As a result of the internal disorder, they display unusual physical properties such as great hardness and high birefringence, which may have applications in material sciences.

The study of shocked carbonates and sulfates addresses the question of how impact events affect the climate. The perturbation of the atmosphere by carbon dioxide and sulphur oxides released from carbonates and sulfates and the resultant climatic changes seem to have played an important role in the deadly scenario at the K/T boundary. Carbon dioxide is believed to have produced a greenhouse effect, whereas sulphur oxides probably caused a prolonged "impact winter". To gain insights into this problem, we are studying the recently recovered drill cores from the Chicxulub crater and conducting shock experiments on calcite and anhydrite. The results show that the main response of carbonates and sulfates to strong shock compression is melting (Fig. 3.6). Decomposition occurs after decompression if post-shock temperatures are sufficiently high and the effective back reactions can be avoided by separation of dissociated species. Altogether, the Chicxulub event demonstrates that impacts exert an important control on global transport cycles in the Earth such as the carbon cycle. To understand these

effects, a multi-disciplinary approach is needed, combining natural observations, experiments and modelling. ■

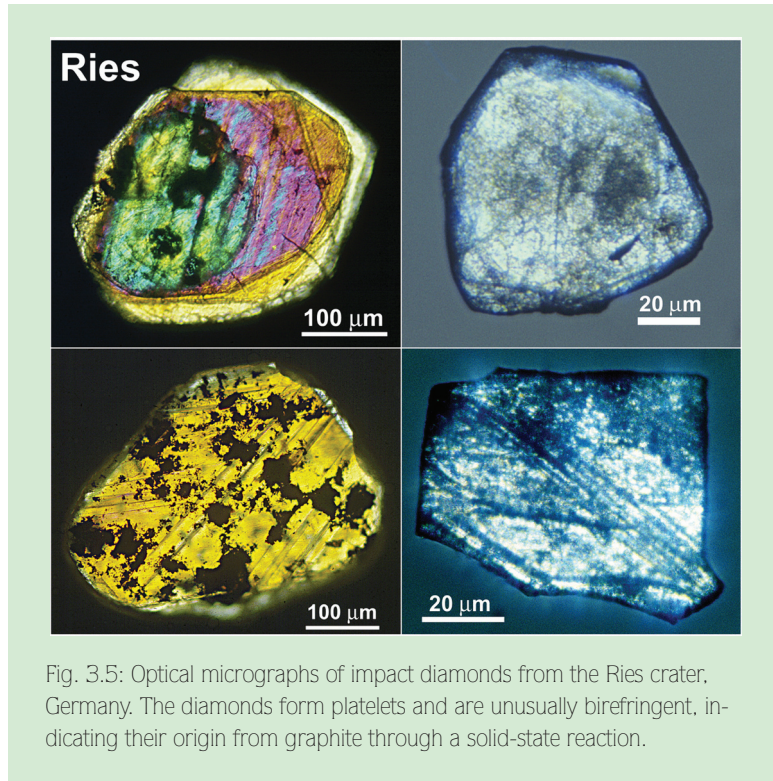
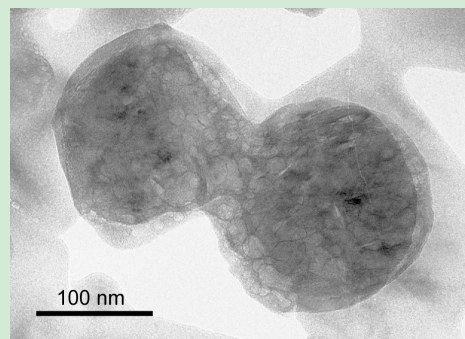


Fig. 3.5: Optical micrographs of impact diamonds from the Ries crater, Germany. The diamonds form platelets and are unusually birefringent, indicating their origin from graphite through a solid-state reaction.

Fig. 3.6: Bright-field TEM image of experimentally shocked calcite. The sample was melted and started to degas, as indicated by the foamy surface structure of the droplets.



4. Early differentiation of the Earth

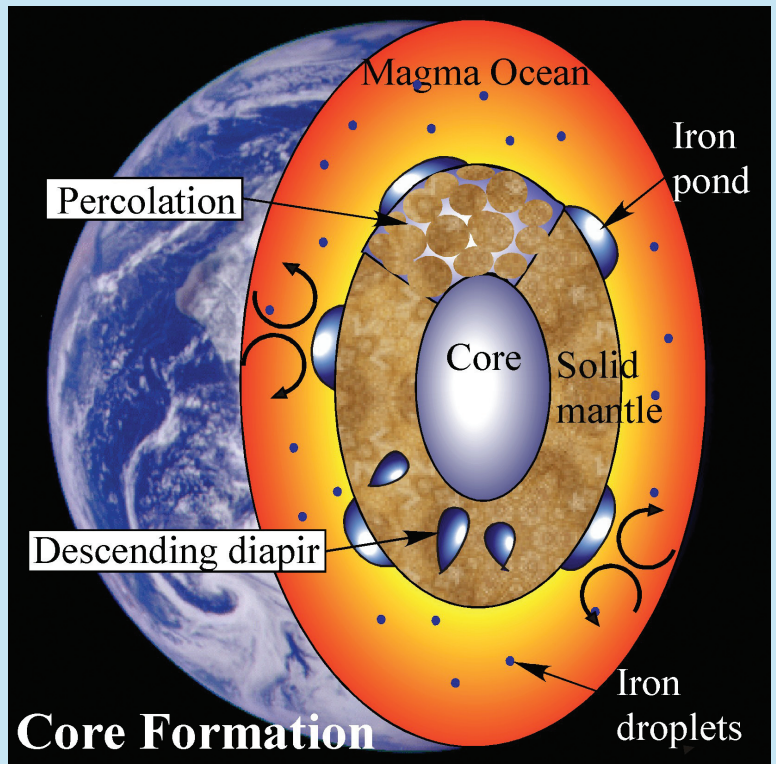


The Earth formed about 4.6 billion years ago largely by the accretion of small “planetesimals” or proto-planets. These consisted of material that is currently represented by the chondritic meteorites – the oldest known bodies in the solar system. Such meteorites thus provide crucial information concerning the bulk chemical composition of the Earth. The fact that the Earth’s interior consists now of chemically distinct regions – the metallic iron-rich core and silicate mantle – indicates that a major differentiation event occurred during the early history of the Earth that caused metal to segregate from silicate and to migrate to the Earth’s central region to form the core. (Fig. 4.1) For this process to be physically possible, the metal, and possibly also the silicate, must have been in a molten state. Thus the mechanisms of metal-silicate separation during core formation are of major interest for understanding the early thermal history of the Earth. In particular, the giant impact theory can be tested, according to which the Earth is postulated to have collided with one or more Mars-sized bodies during the late stages of accretion (Fig. 4.2). The enormous energy involved in such collisions would have partly or wholly melted the

Earth, leading to the formation of a deep magma ocean (Fig. 4.1).

A record of the process of core formation is preserved in the geochemistry of the Earth’s mantle. It is well known that siderophile (or “metal-loving”) elements, such as Ni, Co, Mo, W, Re and Pt, partition strongly into metal, so that the concentrations of these elements in coexisting silicates is very low. Indeed, the

Fig. 4.1: Schematic view of the Earth’s interior during core formation. A deep convecting magma ocean enables droplets of liquid iron-rich metal to separate efficiently from liquid silicate and to accumulate as “ponds” above crystalline lower mantle. The ponded metal may descend further towards the proto-core either as large diapirs (with little chemical interaction) or by grain-scale percolation through the polycrystalline silicates.



Earth's mantle is depleted in such elements as a consequence of metal separation during core formation. However, based on experimental studies of element partitioning at low pressure (1 bar) and moderate temperatures, the depletion is much less than expected and the concentrations of siderophile elements in the mantle appear to be too high, often by orders of magnitude. One possible explanation for this apparent anomaly is that pressure and/or temperature have a significant effect on the partitioning behaviour of the siderophile elements. Thus, over the last few years, numerous experimental studies have been performed to study the effects of pressure, temperature and oxygen fugacity on the

partitioning of siderophile elements between metal, silicates and oxides up to 25 GPa and 2800 K using multianvil apparatus. Results show that the high concentrations of at least some siderophile elements in the mantle can be explained by equilibration between metal and silicate at pressures and temperatures of at least 25 GPa and 2400 K and possibly as high as 35 GPa and 3600 K. At such high temperatures, both silicate and metal would be in the molten state. These results are therefore consistent with metal-silicate separation occurring in a deep magma ocean and thus support the giant impact theory. With the acquisition of more experimental data for all the siderophile elements, it will eventually be possible to constrain the depth of the magma ocean and the details of the early thermal history of the Earth.

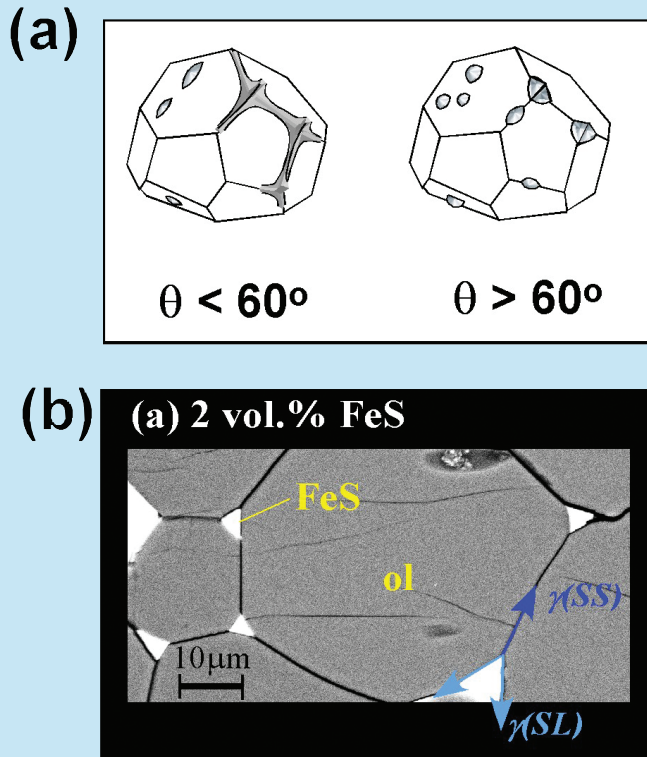
strain the depth of the magma ocean and the details of the early thermal history of the Earth.

An additional question concerns whether or not the Earth had to be completely molten for core formation to occur. This can be answered by experimentally investigating if liquid metal can percolate through a matrix of crystalline silicates by forming an interconnected network, or if the metal remains trapped in the silicate as isolated blebs. Interconnectivity depends on the magnitude of the angle between metal-



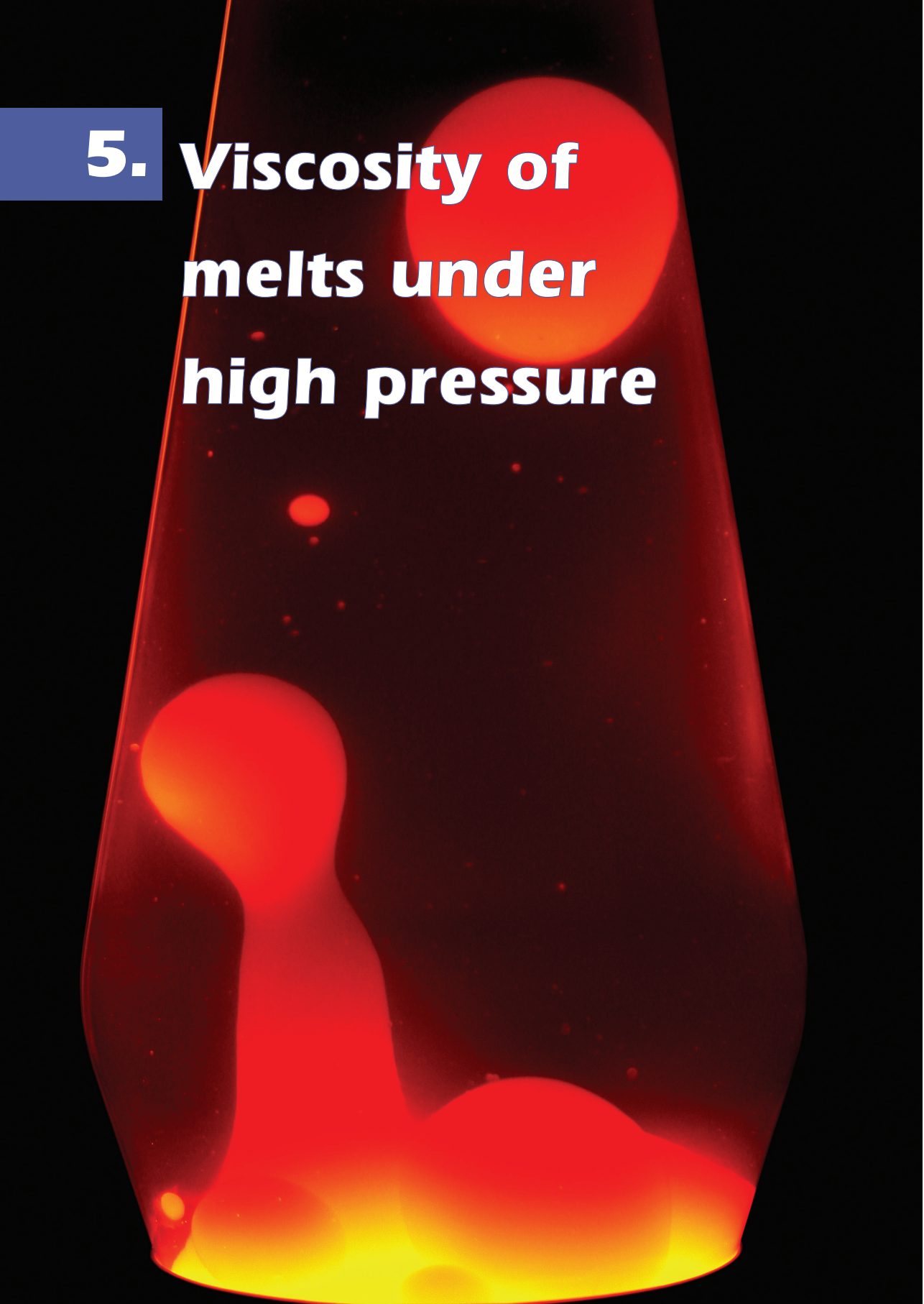
Fig. 4.2: Artist's view of the giant impact – a collision between the Earth and a Mars-sized planet – that led to large-scale melting and the formation of a magma ocean.

Fig. 4.3: (a) Schematic diagram showing the θ effect of the dihedral angle on the morphology and interconnectivity of liquid metal in a matrix of crystalline silicates. (b) Experimental sample consisting of olivine and liquid FeS showing the concentration of the liquid along the edges of olivine grains. This sample was annealed in a multianvil apparatus at 5 GPa and 1830 K. The measured dihedral angle in this sample is 72° , which indicates no interconnectivity when small fractions of liquid are present. Also shown is the equilibrium between solid-solid (SS) and solid-liquid (SL) interfacial energies (γ).



silicate interfaces – the so-called dihedral angle (Fig. 4.3). If the dihedral angle is less than 60° , metal is interconnected and can move by percolation; whereas if it is greater than 60° there is no interconnectivity and percolation is not possible (Fig. 4.3a). The dihedral angle depends on the energy of the metal-silicate interface, and is likely to depend on variables such as pressure, temperature, metal composition and silicate crystal structure. These effects can be investigated through high-pressure experiments (Fig. 4.3b).

In addition to the siderophile elements, experimental studies of the partitioning of elements such as oxygen, silicon and sulphur between metal and silicate at the conditions of core formation are necessary for understanding the geochemical evolution of the Earth and the nature of the light elements that are currently present in the Earth's core. ■

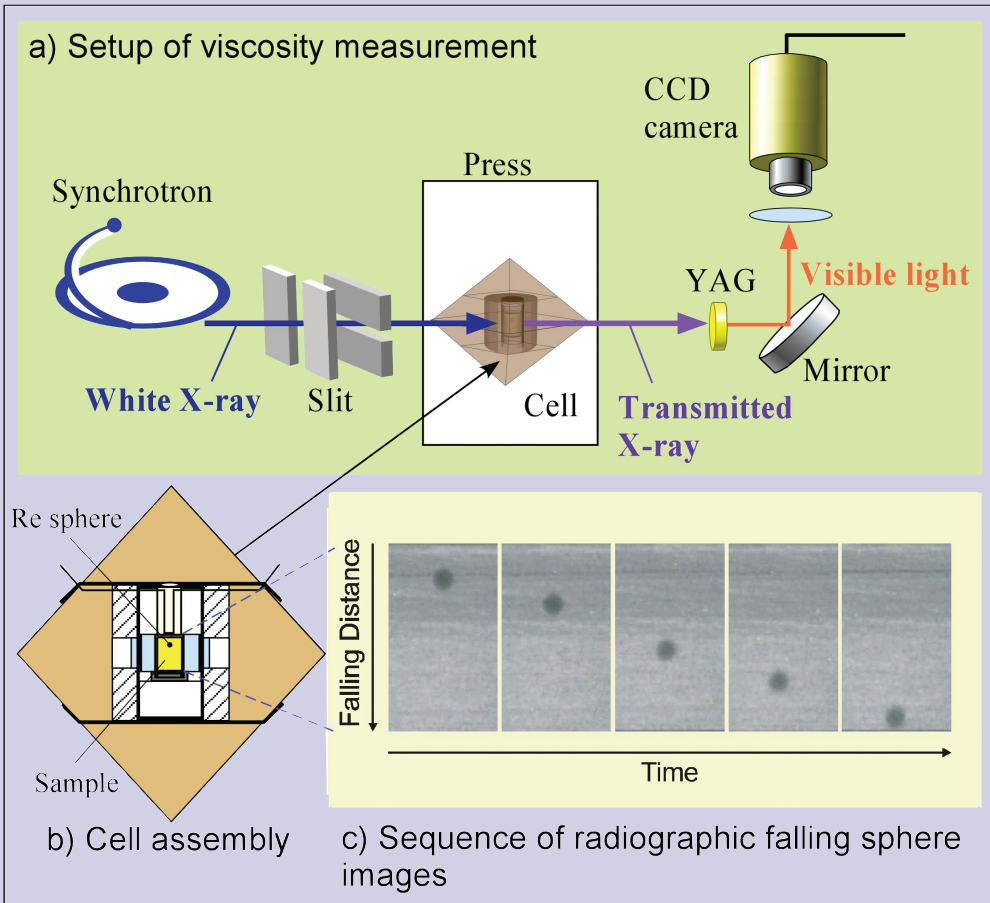


**5. Viscosity of
melts under
high pressure**

Melting is certainly one of the most effective mechanisms causing chemical differentiation throughout the entire history of the Earth. To understand the kinetic aspects of processes such as present day volcanism or the separation of liquid metal through a magma ocean to form the Earth's core, the viscosities of the liquids have to be known as a func-

tion of several parameters, for example temperature or chemical composition. However, many differentiation mechanisms occur tens or hundreds of kilometres beneath the Earth's surface; hence detailed knowledge about the influence of pressure on the viscous flow behaviour of melts is required.

Fig. 5.1: (a) Experimental set-up of viscosity measurement. Radiography images were observed by the CCD camera coupled with the YAG fluorescence screen with a resolution of about $5\ \mu\text{m}$. (b) Schematic cross section of the high pressure cell assembly used for viscometry. (c) Continuous radiographic images of a falling sphere. The Re sphere can be observed as a black shadow in the sample due to its high density.



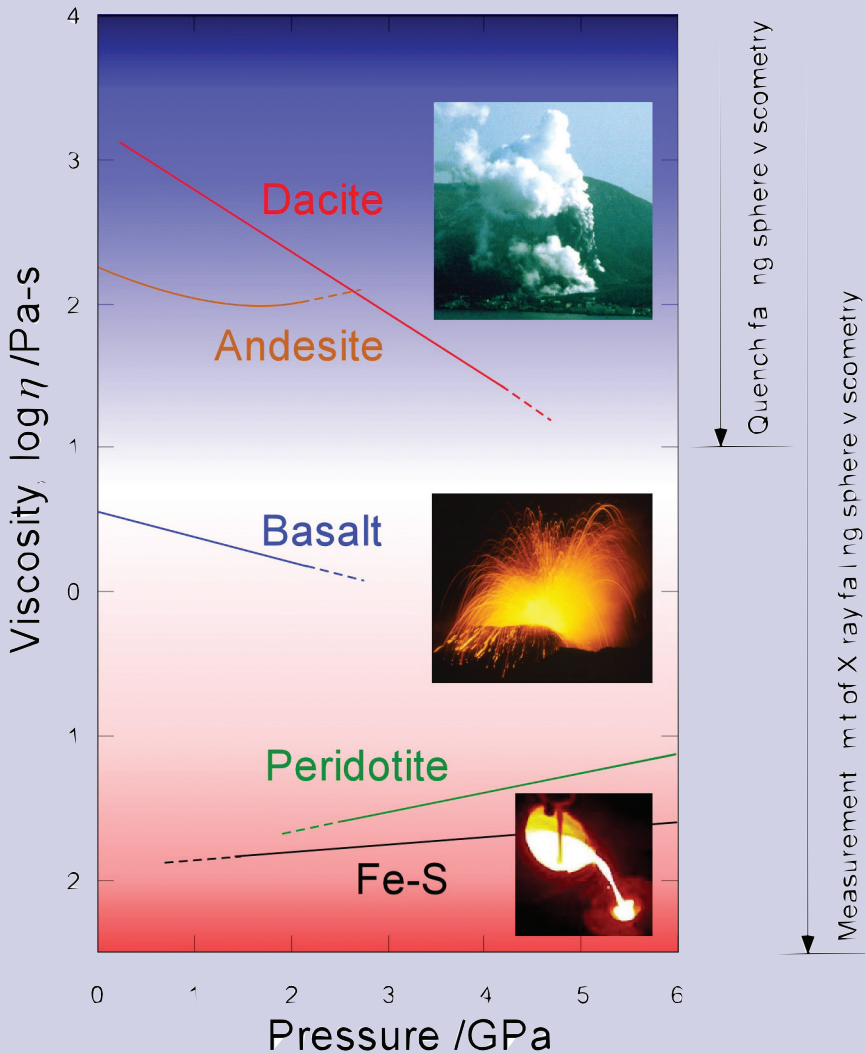


Fig. 5.2: Pressure effect on viscosity of magmatic liquids. Viscosity of dacitic melt was calculated from diffusivity data at 1460°C. Andesitic and basaltic melt viscosities were measured using quench falling sphere viscometry at 1350° and 1400°C, respectively. Peridotitic and Fe-S eutectic melt viscosities were measured using X-ray radiographic falling sphere viscometry at 1900° and 1040°C, respectively.

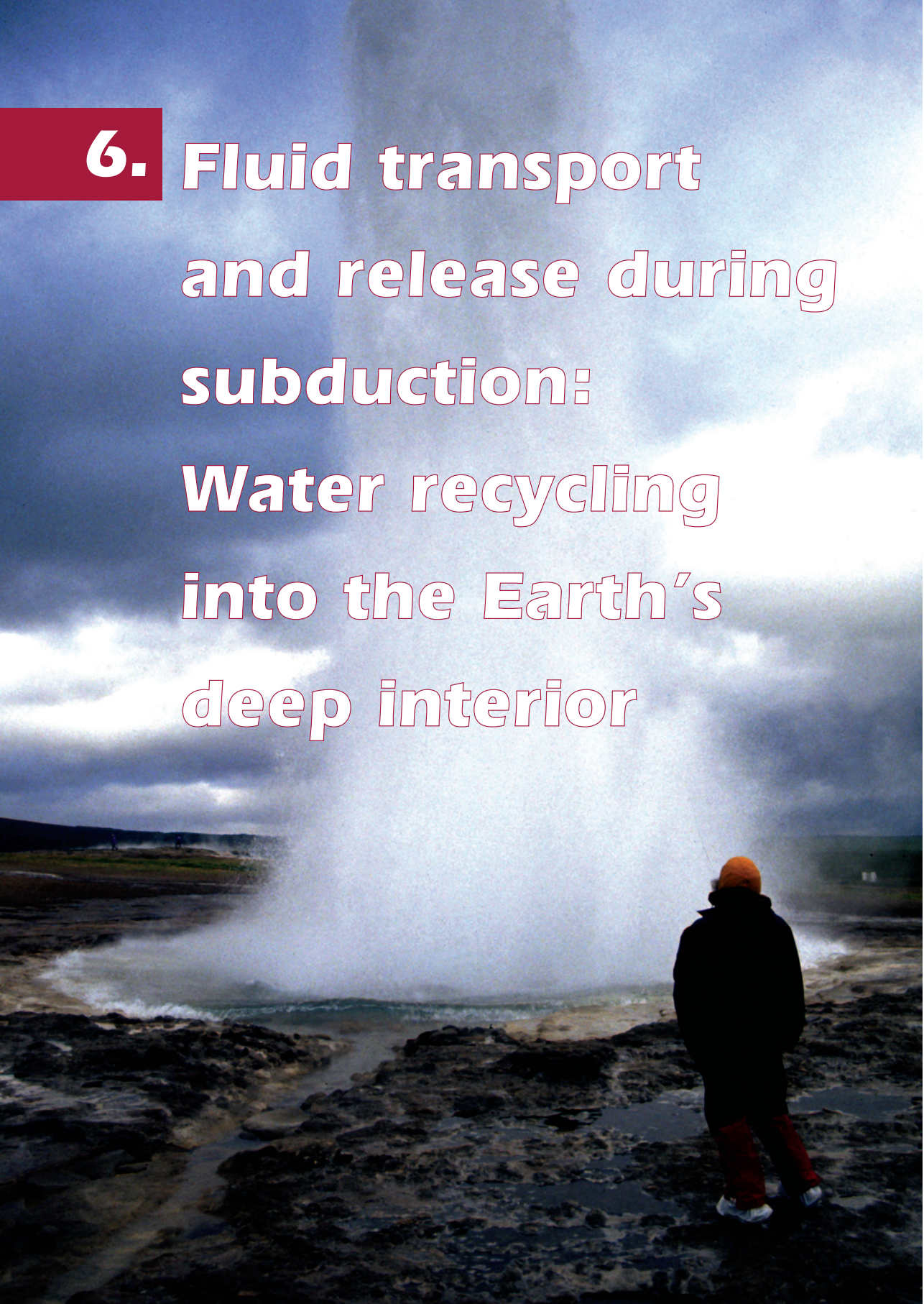
Over the past decades the falling sphere method has been successfully applied to investigate the viscosity of magmatic liquids

under elevated pressures. A sample containing a sphere that is denser than the surrounding material is pressurised, heated rapidly

to a temperature above its liquidus, and then quenched (brought back to room temperature and thus frozen) after a distinct time period. The velocity of the falling sphere can then be determined from the final position of the sphere in the recovered sample (assuming the initial position is known), and the viscosity of the liquid is calculated using Stokes' law. However, the determination of viscosities with a reasonable accuracy using quench techniques is limited to liquids with high viscosities such as basalts or andesites. More fluid silicate melt compositions such as peridotite or metallic liquids require measurements using an *in situ* technique that involves intense synchrotron radiation. Using a radiographic method the falling of the "marker" sphere can be monitored in real time as an X-ray shadowgraph (Fig. 5.1) while the sample is kept under high pressure and temperature conditions. From the illustrated shadowgraphs the velocity of the falling sphere can be precisely determined, which is essential to obtain high quality viscosity data.

Silicate melts are generally described as a disordered arrangement of more or less ordered building units, the coordination polyhedra of the cations. So-called network formers (mostly Si, but a portion of Al) are tetrahedrally coordinated to oxygen, and such tetrahedra are interlinked ("polymerised") via joint corners. Increasing concentrations of silicon and tetrahedrally coordinated aluminium therefore lead to an increasing degree of polymerisation. The role of the other cations (*e.g.* alkalis and alkaline earths) is that of so-called network modifiers – they have larger oxygen coordination numbers, and an increase in

their concentration leads to a depolymerisation of the network. The viscosity of general molecular or metallic liquids increases with pressure. This behaviour is simply the result of the decreasing interatomic spacings in the liquid due to pressure-induced compaction. Relatively polymerised silicate melts, such as dacite and andesite, show a peculiar, opposite behaviour with pressure: their viscosities decrease with increasing pressure as shown in Fig 5.2. This behaviour can be interpreted as due mostly to changes of the coordination number of network-forming cations and an increasing depolymerisation of the melt with pressure: both aluminium (at low pressures) and silicon (at higher pressures) change their coordination number from 4 to 5 or 6, thus transforming from network formers to network modifiers and breaking up the network. Once this transformation is complete, viscosity should increase again simply due to further compaction, and this effect might be visible in the andesite data shown in Fig. 5.2. The present results for basalt, as an example, suggest that kinetic processes such as crystal fractionation may change with depth of the magma chamber. Because temperature increases along a geotherm with increasing pressure and depth, and because viscosities in polymerised melts decrease with both increasing pressure and temperature, a "run-away" situation is encountered, and thus liquidus crystals may separate more effectively from the liquid at higher pressures or greater depth. Investigation of the negative pressure effect on viscosity is therefore of interest not only for the general chemical or physical properties of melts, but also for the important constraints it provides for differentiation processes within the Earth. ■

A person wearing a dark jacket and an orange hat stands on a rocky shore, looking out at a large splash of water in the ocean. The sky is overcast and grey. The text is overlaid on the image in a white, outlined font.

**6. Fluid transport
and release during
subduction:
Water recycling
into the Earth's
deep interior**

In addition to being a prerequisite for life on Earth, water plays a pivotal role in the dynamic processes of plate tectonics. Fig. 6.1 shows a schematic cartoon cross-section of the Earth, illustrating some of these processes. At mid-oceanic ridges (A), new oceanic crust is created by partial melting of the underlying upper mantle. Circulation of sea-water through hot, newly created crust leads to partial hydration, and the crystallisation of hydrous minerals such as serpentine and talc in the crust and possibly also deeper into the lithosphere. The famous “black smokers” (Fig. 6.2) on the sea floor near mid-oceanic ridges are perhaps the most spectacular manifestations of this water circulation and rock-water interactions. Conversely, at subduction zones (B), oceanic lithosphere is recycled back into the deep Earth interior. During subduction, oceanic lithosphere is dragged downward and subjected to increasing pressures and temperatures, resulting in reactions of minerals. Breakdown of hydrous minerals stable at lower pressures releases water from the lithosphere during subduction. Most of the released water is expected to rise upward into the overlying mantle wedge (C), leading to partial melting of the mantle. Such magmas rise up through the mantle and crust and eventually produce the extensive and explosive volcanism which is characteristic of subduction zones. Subduction of cold, oceanic lithosphere therefore results in extensive melting of the mantle and concurrent volcanism.

A question which remains largely unanswered, however, is whether subduction can provide a mechanism for transporting water beyond the depths of sub-arc magmatism and

deeper into the mantle. Extensive work has been conducted to determine the stability of hydrous minerals in the various bulk compositions present in subducting material. Known pressure-temperature paths for most subduction zones indicate that complete dehydration of the subducting slab is expected to occur at depths of over 100 km. However, over recent years considerable focus has been placed on the capacity of nominally an-

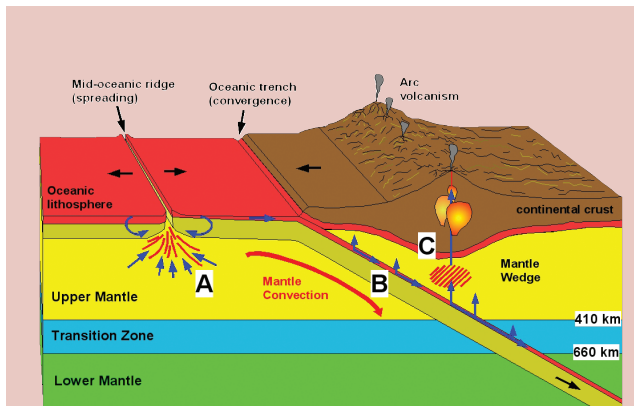


Fig. 6.1: Schematic cross-section (not to scale) showing some of the features of plate tectonics. Blue arrows represent movement of water-rich fluids, and black arrows represent movement of tectonic plates. Letters are processes mentioned in the text: (A) Partial melting of the upper-mantle at mid-oceanic spreading sites. Water partitions more readily into the melt. Melt rises upwards and forms new oceanic crust. Sea-water circulation through hot, fractured oceanic lithosphere leads to partial hydration. (B) Subduction of partially hydrated oceanic lithosphere. Fracturing of lithosphere during bending of the subducting slab may provide an additional mechanism for hydration. (C) Breakdown of hydrous phases with increasing P - T results in fluid release from the subducting slab. Water-rich fluids rise up into the overlying mantle wedge resulting in partial melting. Resulting magma rises up into overlying continental (or oceanic) crust, producing extensive volcanism.

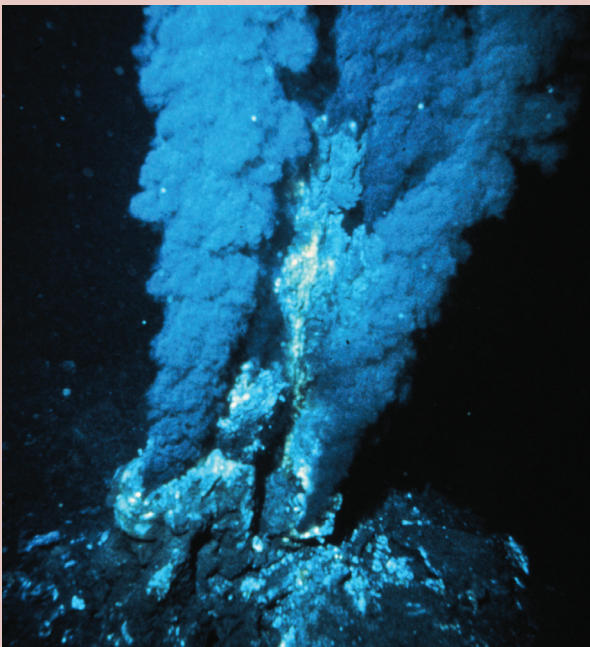
hydrous minerals (NAMs) to incorporate small amounts of water. Investigations of ultramafic xenoliths (i.e. parts of the upper mantle carried up into the crust by magmas, *cf.* Fig. 1.4) have shown that minerals such as olivine, pyroxene and garnet can contain trace amounts of water (on the order of 100s to 1000s ppm H₂O, where 1000 ppm = 0.1 wt. %), in the form of hydrogen associated with point defects in the mineral structures. Even though the amounts of water contained in such minerals is small, incorporation of water by NAMs could provide an efficient mechanism for transporting large quantities of water back into the deep Earth interior. Un-

derstanding the role of NAMs as repositories for water in subducting lithosphere is therefore crucial for elucidating the internal water cycle of the Earth.

Exposure of high- and ultra-high-pressure (UHP) eclogitic rocks in ancient and modern orogenic belts provides us with information on stable minerals and their relations in subducting oceanic crust at depths of up to some 200 km. Stable mineral assemblages for rocks that had a basaltic composition are dominated by the pyroxene omphacite, garnet and quartz/coesite. Direct evidence of high water contents in omphacite under UHP conditions has recently been demonstrated via exsolution textures in natural UHP omphacites (Fig. 6.3). The omphacite contains exsolution lamellae of silica and hornblende (a hydrous mineral). Exsolution of silica from UHP omphacites demonstrates that the composition of omphacite varies considerably as a function of pressure, while exsolution of hornblende implies that the precursor pyroxene was relatively water-rich. It is possible to determine the proportions of exsolved minerals, and therefore recalculate the composition and water content of the precursor. Exsolution from the precursor mineral provided a mechanism for trapping at least some of the water present at UHP conditions, and the calculated original water content, 2400 ppm H₂O, therefore provides a lower limit of water solubility.

The rate of hydrogen diffusion and diffusion of hydrogen related to vacancy mobility has been experimentally determined for a number of mantle minerals. Measured values suggest that during exhumation, significant

Fig. 6.2: Picture of a "black smoker", a type of hydrothermal vent on the sea floor where super-heated, mineral-rich water is released that has circulated through the oceanic crust. The black colour is due to precipitated sulfides.



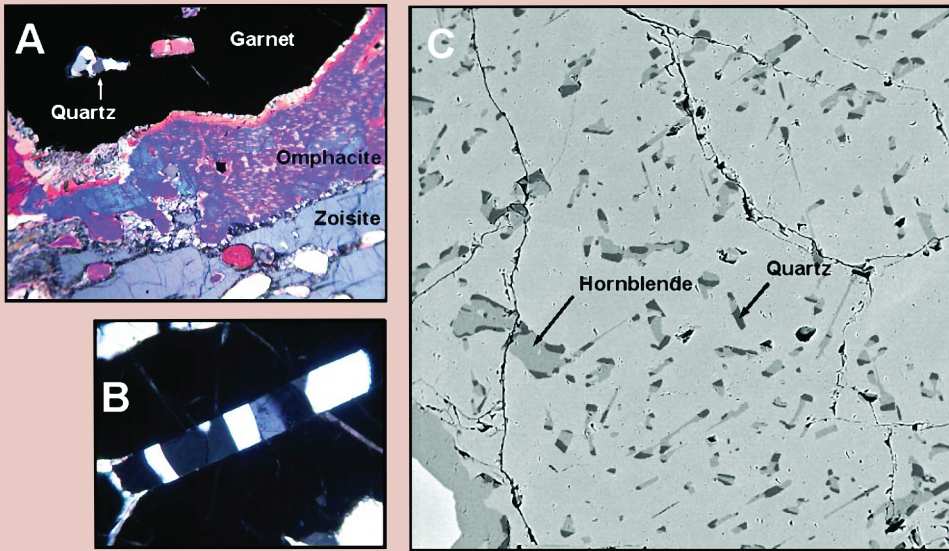


Fig. 6.3: Exsolution texture in omphacite from an UHP kyanite-eclogite, Western Norway. (A) Photomicrograph showing principle minerals and exsolution lamellae in omphacite. (B) Photomicrograph of individual lamella shows the presence of at least two minerals. (C) Back-scattered electron image of exsolution texture. Chemical analysis shows that lamellae are an intergrowth of hornblende and quartz, implying that the precursor pyroxene contained many vacancies and was relatively water-rich.

water loss from minerals should take place. Our recent work has, for the first time, demonstrated diffusion profiles in olivine from a mantle xenolith (Fig. 6.4). Analyses by infrared (IR) spectroscopy of large olivine crystals in the sample reveal rims depleted in water, indicating that water was more readily partitioned into the surrounding melt (basaltic magma) during transport. Using data on hydrogen diffusion in natural olivine, the ascent rate of the entrapped xenolith can be estimated. The calculated ascent rate of 14 km/h demonstrates that even with rapid exhumation, measured water contents in mantle samples are unlikely to represent equilibrium values, especially for eclogites where

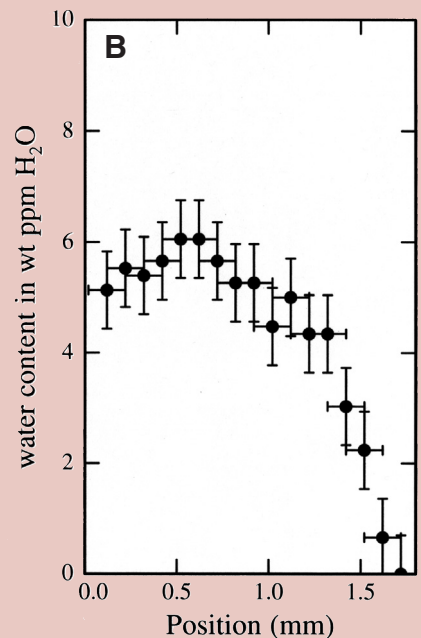
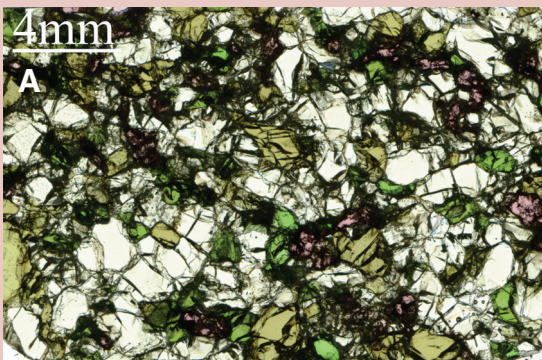
exhumation is several orders of magnitude slower. In order to determine the capacity of subducted material to act as a repository for water, we therefore need to conduct high-pressure experiments to determine the maximum solubility of water in NAMs.

Large (several hundred microns in diameter) crystals of pyroxene can be synthesised over a large range of P - T conditions using high-pressure equipment, and water incorporation studied using Fourier-Transform Infrared (FTIR) spectroscopy. FTIR spectroscopy is the most powerful technique for analysing structurally-incorporated hydrogen, and provides information on absolute water solubility, as

well as mechanisms for hydrogen incorporation. Natural omphacite can be considered largely a solid solution between the pyroxene end members jadeite ($\text{NaAlSi}_2\text{O}_6$) and diopside ($\text{CaMgSi}_2\text{O}_6$), with small amounts of additional components. Experimental work has been conducted to determine water incorporation in both end-member systems, and jadeite has been shown to provide a good model for understanding water incorporation mechanisms in more complex omphacitic compositions. Fig. 6.5 shows an IR spectrum from synthetic jadeite and a crystal model constructed based on IR data to show possible H incorporation mechanisms. H incorporation is related to a local charge deficit produced by cation vacancies (*i.e.* unoccupied structural positions) or by incorporation of

low-valence atoms (such as Na^+) instead of high-valence atoms (such as Ca^{2+} , Mg^{2+} , Fe^{2+}) on the *M2* and *M1* sites in the pyroxene structure. Hydrogen is strongly bonded to oxygen in the structure, and provides local charge balance for nearby cation sites. Evidence from experimental investigations and from exsolution textures in natural UHP pyroxenes suggest that the vacancy content in omphacite (especially the number of *M2* vacancies) increases with increasing pressure. Therefore, it seems likely that the capacity of omphacite to store water increases during subduction, and omphacites in subducting oceanic crust may incorporate some of the water released following the breakdown of hydrous minerals. ■

Fig. 6.4: (A) Photomicrograph of a garnet-bearing lherzolite xenolith from the Pali-aike volcanic field (Chilean Patagonia). FTIR spectra obtained from large olivine crystals (colourless) reveal hydrogen depletion towards olivine rims and the development of hydrogen diffusion profiles (B). These diffusion profiles provide direct evidence of dehydration of mantle samples via hydrogen diffusion during transport into the crust.



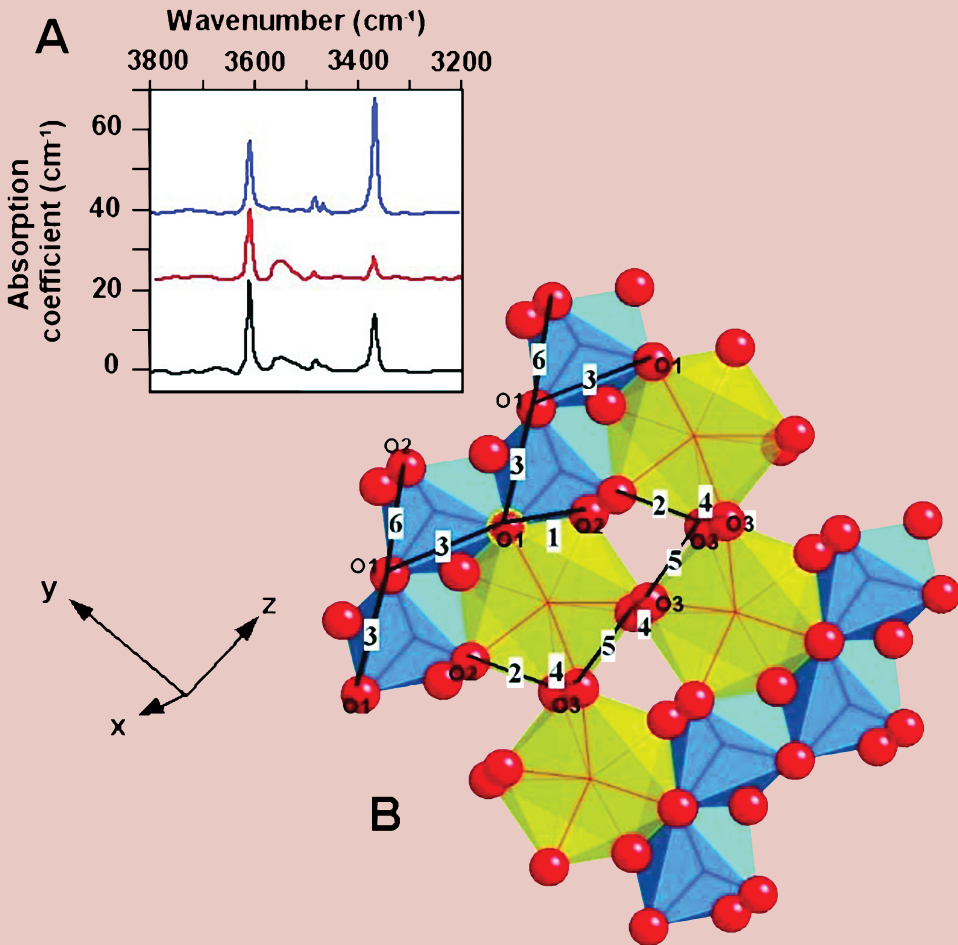
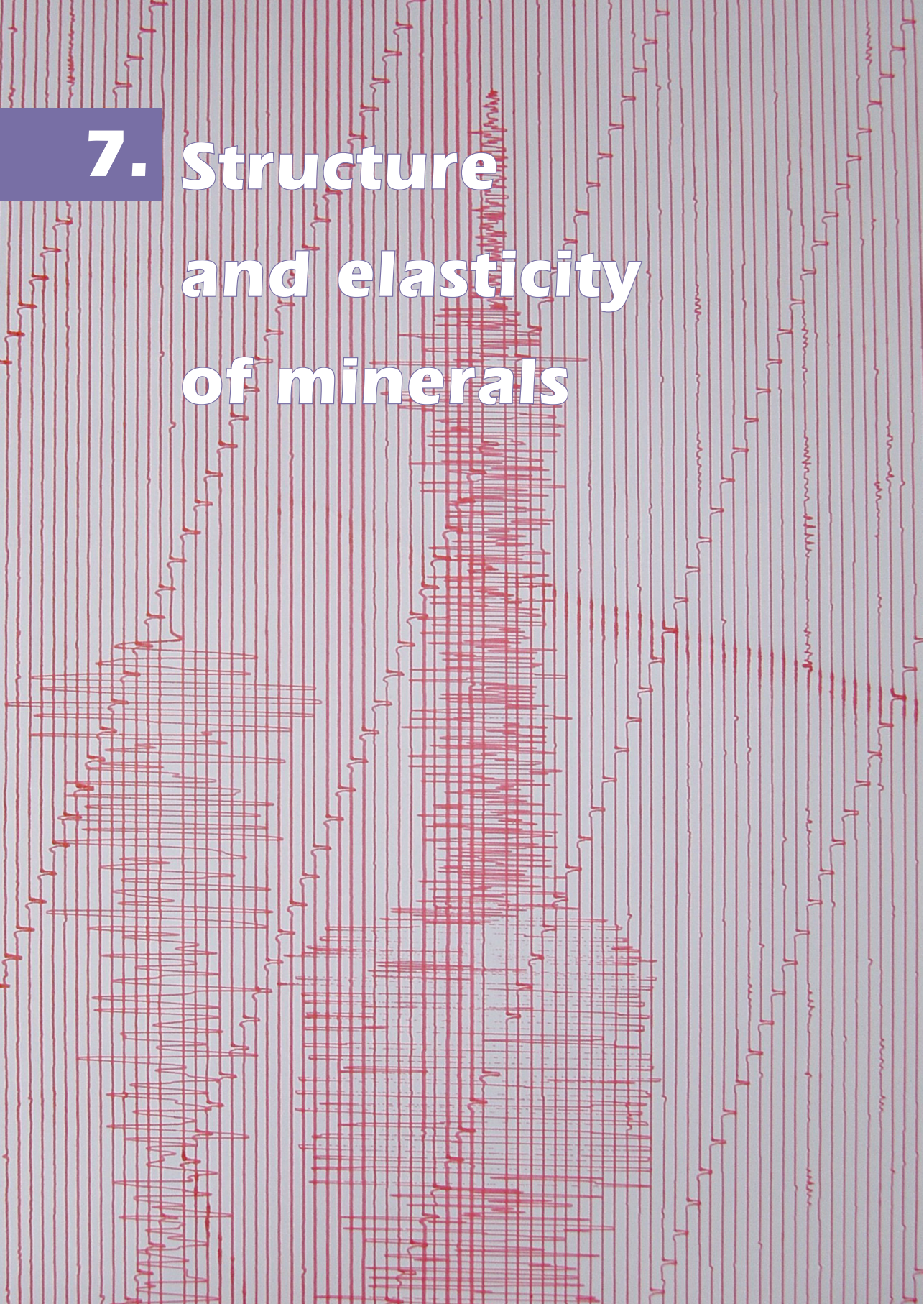


Fig. 6.5: Results from investigation of H incorporation and water solubility in synthetic jadeite. (A) FTIR spectra for water-saturated jadeite synthesised at 3.0 GPa, 600°C (black = unpolarised, red = radiation polarised perpendicular to c axis, blue = radiation polarised parallel to c axis). Peaks in the spectra imply absorption of radiation due to vibration of OH dipoles, indicating that H is present in the structure, associated with specific oxygen sites. (B) Representation of part of the jadeite structure showing mechanisms for H incorporation consistent with data from FTIR spectra. Model shows octahedral sheet (yellow = $M2$ sites, blue = $M1$ sites, red spheres = oxygen sites). Numbers refer to possible H incorporation mechanisms.



7. Structure and elasticity of minerals

Much of what we know for certain about the structure of Earth's deep interior is derived from global seismology. Compressional (P) and shear (S) elastic body waves from large earthquakes directly sample the mantle and core, revealing several major density discontinuities and the massive liquid outer core. P and S-wave travel times and the frequency of Earth's resonant vibrations or normal modes are used to construct globally averaged seismic Earth models, upon which the layered picture of our differentiated planet is based (Fig. 7.1). Interpretation of seismic structure in terms of mutually dependent variables such as composition, mineralogy or temperature variations require information on

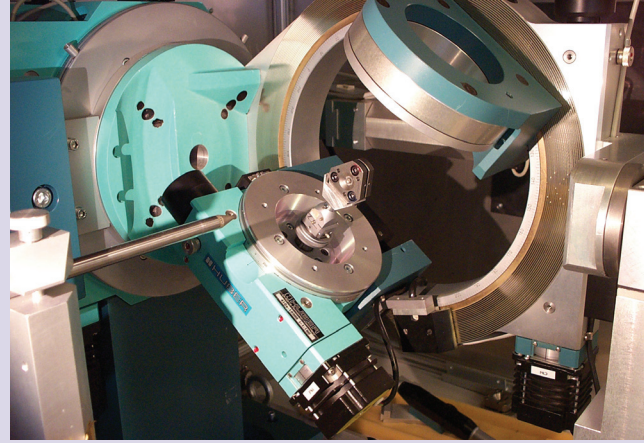
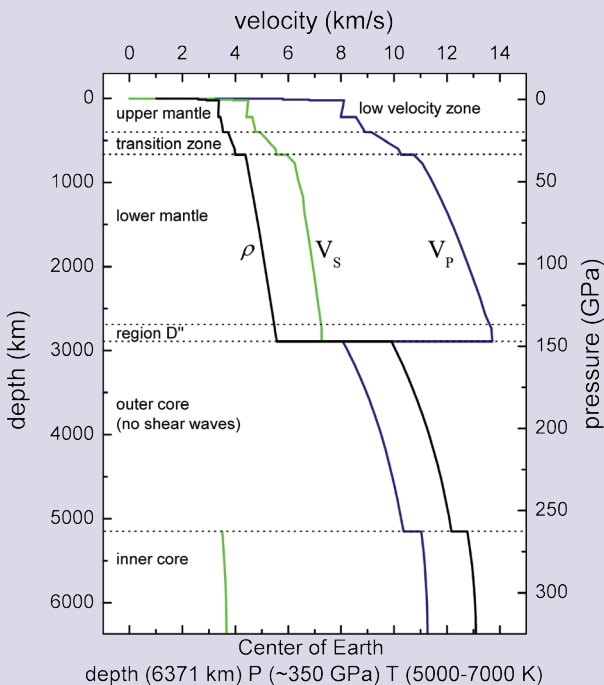


Fig. 7.2: Diamond anvil cell (centre) mounted on the four-circle X-ray diffractometer for structure and compressibility studies.

Fig. 7.1: The Preliminary Reference Earth Model (PREM), a seismic model defining the layered structure of the Earth.



the structure and elasticity of the Earth-forming minerals. It is thus a major goal of mineral physics and geophysics to measure or calculate the effects of pressure (P), temperature (T) and composition on the physical properties of minerals. In the following section we outline elasticity studies at Bayerisches Geoinstitut involving (1) static (isothermal) or dynamic (adiabatic) experiments, performed *in situ* in the diamond anvil cell at high pressure, and (2) computer simulations. X-ray diffraction experiments give the variation of mineral structures and volume (V) or density (ρ) with pressure, resulting in finite strain P - V Equations of State (EoS). In the ultrasonic laboratory, acoustic experiments inside

the diamond cell are used to measure P-wave and S-wave velocities (V_P and V_S) in single crystals at high pressures, resulting in the anisotropic elastic constants (c_{ij}) relating stress to strain in the elastic regime.

Compressibility studies by high-pressure X-ray diffraction experiments focus on the variation of mineral structures and density with pressure. Hydrostatic pressures up to around 10 GPa (or the pressure at approximately 300 km depth) are created inside a diamond anvil cell (DAC), where single-crystal samples can be studied optically or with X-rays directly through the anvils. The DAC is a small, light and versatile pressure chamber that can be mounted directly on a four-circle X-ray diffractometer, shown in Fig. 7.2. X-ray diffraction is an interference effect based on the fact that the wavelength of X-rays are on the order of the size and spacing between atoms, about several angstroms (where $1 \text{ \AA} = 10^{-10} \text{ m}$). The geometry and intensity of the recorded diffraction patterns provide information not just on lattice periodicity (cell parameters) but also on the total charge density from which actual crystal structures are modelled. Additional information can be obtained from molecular modelling of the compression behaviour of minerals; this is particularly useful for stud-

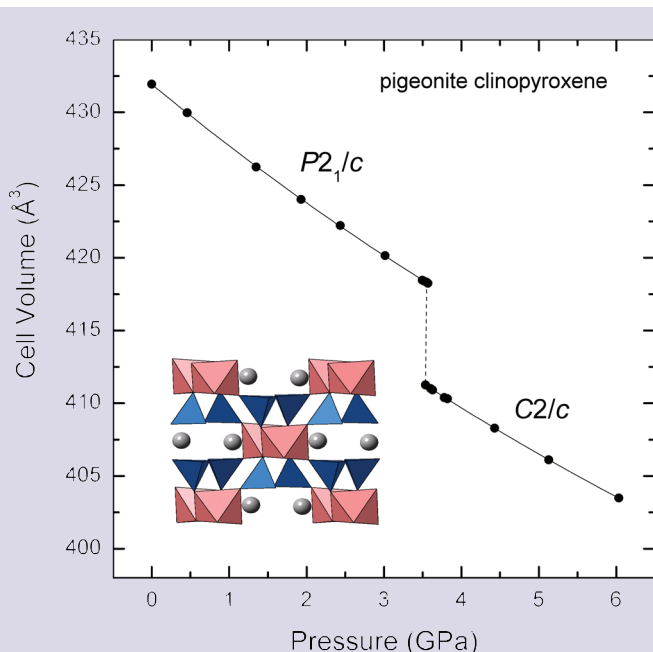


Fig. 7.3: Volume compression of a clinopyroxene crystal, pigeonite (Mg,Fe,Ca) $_2\text{Si}_2\text{O}_6$, illustrating a large volume change (density jump) related to a first-order phase transition around 3.5 GPa.

ies in which X-ray diffraction does not yield high quality data, for example due to extreme P or T conditions, or for cases where poor X-ray scattering atoms such as hydrogen are involved.

The variation of cell parameters with pressure provides information on the change in volume (or density) of minerals with depth, and is also a key indicator of lattice strain and phase transitions. The isothermal change in volume with pressure for a solid is given by the bulk modulus K_T , and its pressure derivative K_T' ,

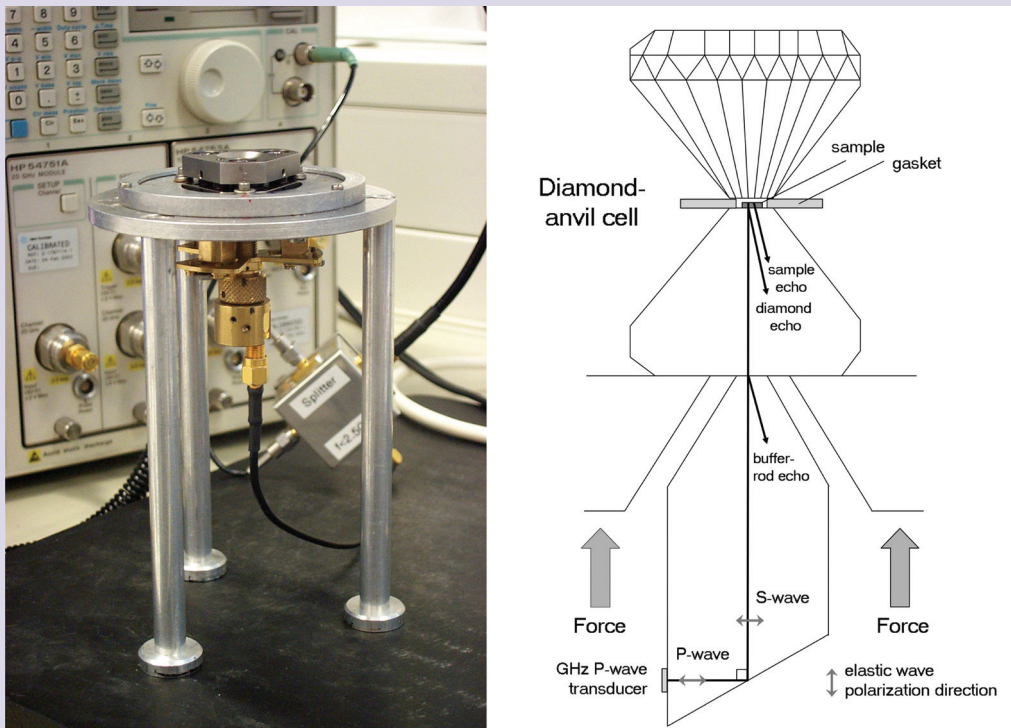
$$K_T = -V(dP/dV)$$

$$K_T' = \partial K_T / \partial P$$

As an example, the volume compression of a clinopyroxene crystal is shown in Fig. 7.3. At each pressure, the volume of the sample is determined from the position or angles (2θ) of various diffracted X-rays passing through the diamond anvils. In DAC experiments, the pressure is determined using an internal standard, for example by measuring the cell volume of a quartz crystal next to the sample (with known EoS) or by using the calibrated pressure shift of ruby light fluorescence. The set of pressure-volume data can be evaluated for EoS parameters (K_T and K_T') using equations such as the Birch-Murnaghan (BM) EoS.

In Fig. 7.3, the initial volume compression of the sample is shown by filled circles, and the solid curve is the fitted BM-EoS. The abrupt change in volume (density) at ca. 3.5 GPa is the result of a phase transition, accompanied by a change in space group symmetry. In addition to the cell parameters, the atomic structure of the high-pressure clinopyroxene phase was determined *in situ* using single-crystal X-ray diffraction, also shown in Fig. 7.3. Structural phase transitions in minerals at high pressures are important to understanding the seismic model (shown in Fig. 7.1) because many of the seismic reflectors or discontinuities appear to result from abrupt changes in density caused by phase transitions.

Fig. 7.4: Ultrasonic diamond anvil cell (left) with schematic detail (right). Acoustic interferometry is used to determine P- and S-wave travel times for mineral elasticity studies.



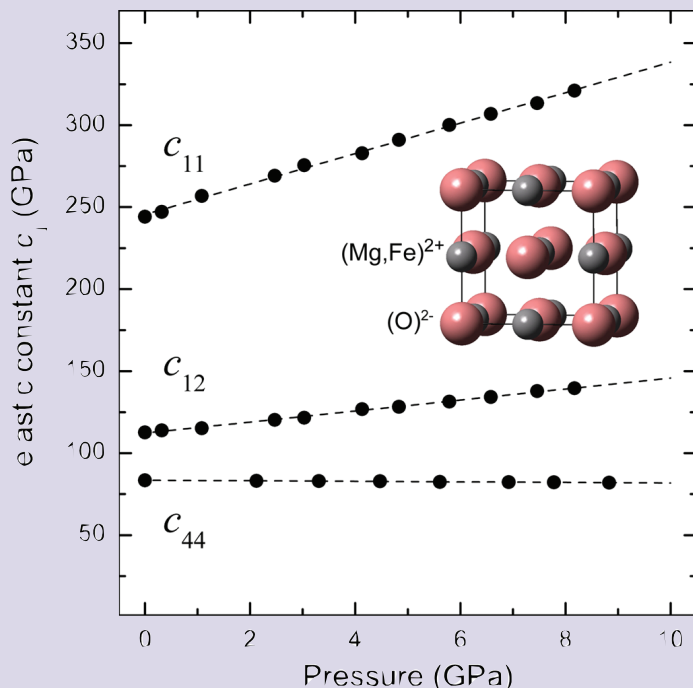


Fig. 7.5: The complete elastic tensor of ferropericlase (Mg,Fe)O to ca. 10 GPa, determined by GHz-ultrasonic interferometry. This phase is likely the most abundant non-silicate mineral in the planet. The elasticity of this cubic structure, shown in the inset, is completely defined by the three elastic constants c_{11} , c_{12} and c_{44} .

Elasticity: Elastic wave propagation in solids at the limit of infinitesimal strain is governed by a linear relationship between the stress tensor (σ_{ij}) and strain (ϵ_{kl}), given by the elastic constants (c_{ijkl}) in Hooke's law of elasticity. Compressional (V_p) and shear (V_s) elastic wave velocities can be measured ultrasonically in the laboratory, or the full elastic constant tensor can be computed by a variety of approaches in molecular modelling that will be discussed below. For comparison to Earth (PREM, Fig. 7.1), the bulk sound velocities and density from static compress-

ion (see above) determine the adiabatic bulk (K_s) and shear (G) elastic moduli at pressure,

$$K_s = \rho(V_p^2 - 4/3V_s^2)$$

$$G = \rho V_s^2$$

Laboratory ultrasonic measurements are traditionally carried out at MHz frequencies on polycrystalline samples of several millimetres in size. However, the high-pressure mantle phases that can now be synthesised in the large-volume multianvil press are still usually sub-millimetre in size. Furthermore, *in situ* ultrasonic experiments at high pressures in the diamond anvil cell require samples less than 0.1 mm in thickness. To meet these demands, a new high-frequency (gigahertz, GHz) ultrasonic interferometer has been developed featuring pure elastic strain waves with wavelengths on the order of 0.01 mm. The aim is to

measure the elastic constants c_{ij} of single-crystal minerals at high pressure in the diamond anvil cell.

Ultrasonic P waves are generated at a piezoelectric thin-film transducer, bonded to an acoustic buffer rod that delivers the strain wave either directly to a sample, or through an anvil of the diamond cell. To produce high-frequency S waves, a compression wave is converted to shear on the facet of a gem acoustic buffer rod, shown attached to the anvil in Fig. 7.4. In separate P-wave and S-

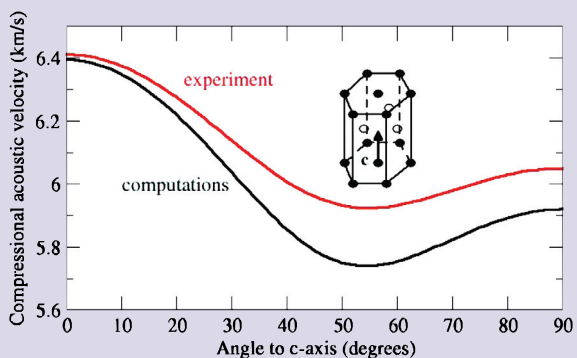
wave experiments, echoes are produced at each impedance contrast (between the buffer rod and diamond, and at the diamond-sample interface). Using time-delayed phase coherent pulses, the returning echoes can be overlapped so as to produce an interference pattern from which the travel time is determined. The travel times are converted to velocities using the sample length, measured mechanically in air, or at high pressures it is calculated from the isothermal equation of state (see above). Combining information on the density and velocities at room pressure gives the adiabatic elastic moduli, and data at high pressure give their derivatives for extrapolation to deep-Earth pressures.

Fig. 7.5 shows the complete elastic tensor of ferropericlase (Mg,Fe)O containing about 50% iron. This dense oxide has the rocksalt structure over this pressure range (shown inset) and is likely the most abundant non-silicate mineral in the Earth, coexisting with silicate perovskite (Mg,Fe)SiO₃ in Earth's lower mantle. The c_{ij} in Fig. 7.5 define completely the anisotropic elastic behaviour of this mineral at high pressures.

Elastic properties of minerals are readily accessible in computational material physics at simultaneous high pressures and temperatures. In molecular dynamics simulations a supercell of the mineral structure is equilibrated at a particular pressure and temperature, and the strain fluctuations on this simulation cell are

evaluated in terms of the full elastic constant tensor of the system. The dependence of the phonon frequencies on the lattice direction (dispersion) carries the same information, and the dispersion of the three acoustic phonon branches can be inverted for the full elastic constant tensor, similar to the ultrasonic studies discussed above. One may also define elastic constants thermodynamically and calculate them as the second derivative of the free energy with respect to strain. This can be done at high temperature and static conditions (0 K), and is illustrated in an example in Fig. 7.6. ■

Fig. 7.6: Angular dependence of acoustic compressional wave velocity in hexagonal cobalt at ambient pressure from ultrasonic measurements (red line) and as determined from first principles calculations (black line). The angular dependence is defined with respect to the hexagonal c axis (see inset).



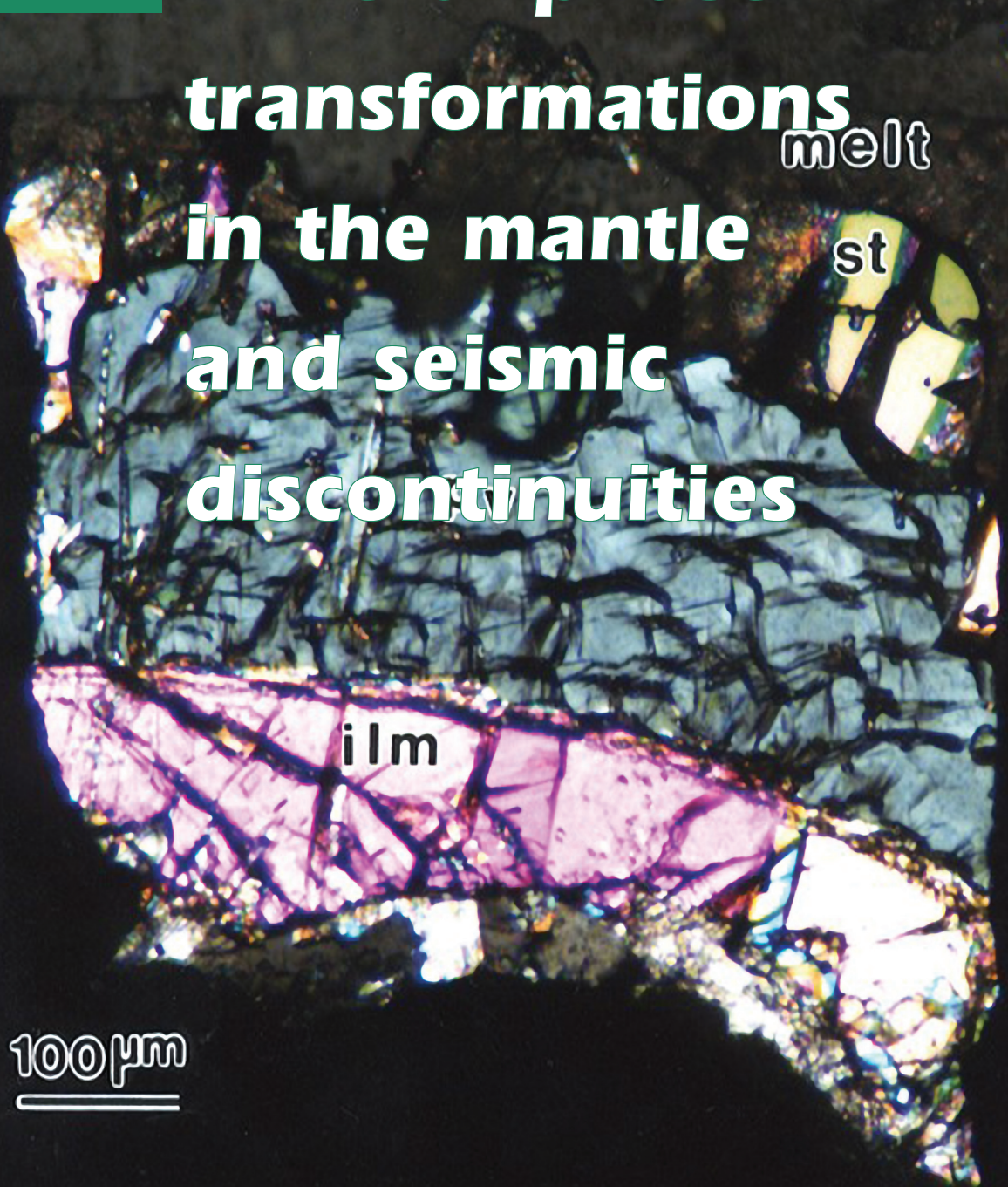
**8. Mineral phase transformations
in the mantle
and seismic discontinuities**

melt

st

ilm

100 μm

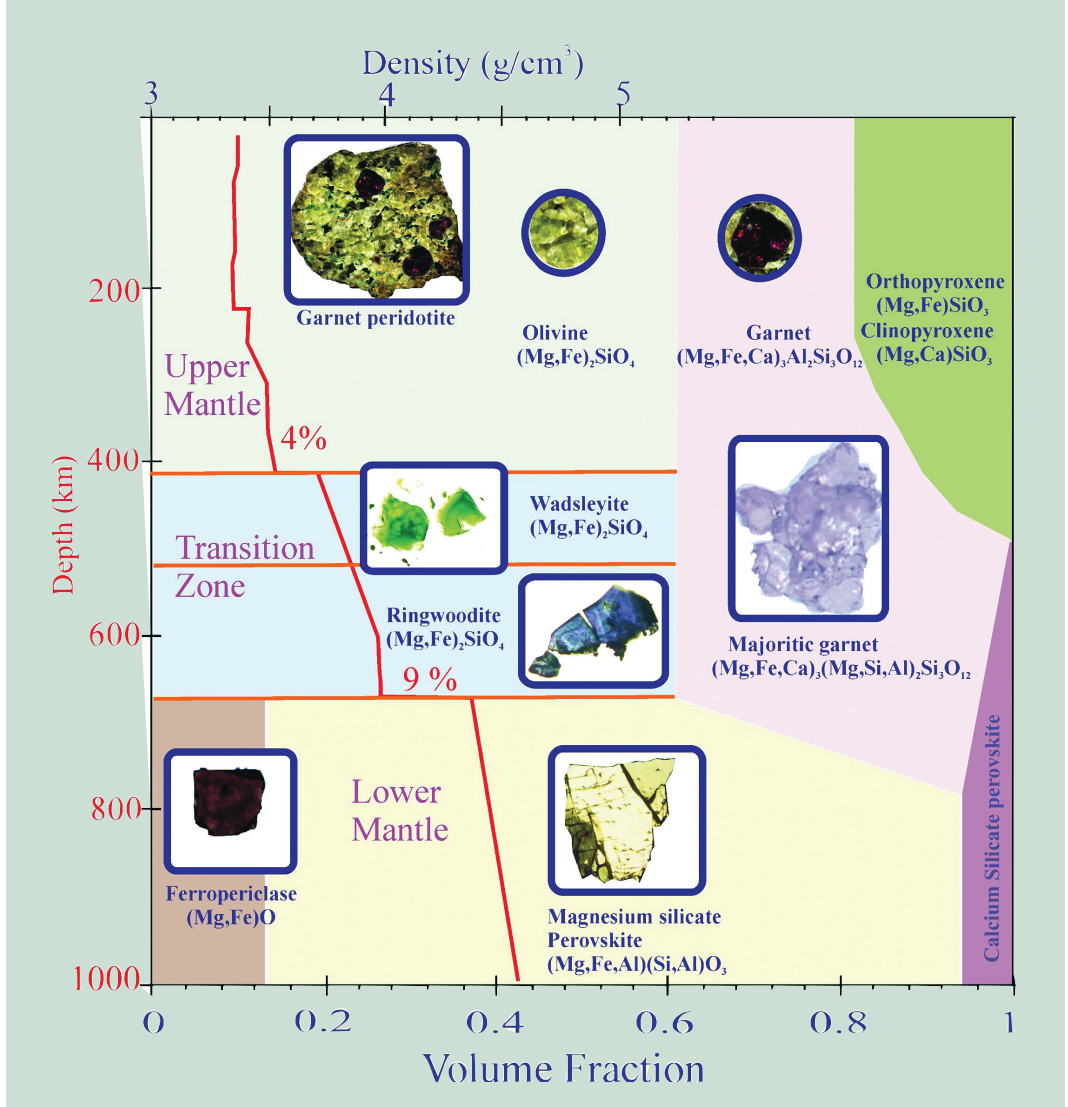


Rock samples from the mantle, brought to the surface in volcanic eruptions, mainly originate from depths of less than 200 km. What the remaining 2700 km of unsampled mantle is made from is, therefore, a very important question. The best evidence for the nature of the deeper mantle comes from seismology. Models developed from seismic wave travel times through the Earth indicate that the density of the mantle increases with depth both smoothly and discontinuously as shown in Fig. 8.1. There are two major discontinuities at approximately 410 and 660 km depth that are caused by jumps in mantle density of around 4% and 9%, respectively. It is believed that they result from phase transformations in silicate minerals of the mantle. Using seismic waves that are reflected off the discontinuities, seismologists can also provide regional details on the variations in depth and sharpness of the discontinuities. These observations can provide a wealth of information on the physical and chemical state of the mantle on a relatively local scale. Interpreting these findings, however, requires information on the mineral reactions that cause these discontinuities, which can only be obtained from laboratory experiments.

The 410 km discontinuity, for example, is caused by the transformation of $(\text{Mg,Fe})_2\text{SiO}_4$ from the olivine to the wadsleyite structure and seems to vary in depth in the bulk of the mantle by approximately 40 km. Using experimental determinations of the pressure-temperature slope for the olivine to wadsleyite transformation, this equates to regional temperature variations in the mantle of approximately 100°C. The sharpness or width of a discontinuity such as the “410”, *i.e.* the depth

interval in the Earth over which it takes place, can provide important evidence for the composition of the mantle in that region. As mantle olivine is a solid solution involving two components, Mg_2SiO_4 and Fe_2SiO_4 , it is not expected to transform sharply to wadsleyite at a specific depth, but rather the transformation will be smeared out over a broader depth interval. This can be seen in the phase diagram shown in Fig. 8.2, which has been calculated using the results of high pressure and temperature multianvil experiments. Because both olivine and wadsleyite contain iron, a two-phase transformation interval is entered where both minerals coexist. For a viable mantle olivine with a Fe_2SiO_4 content of 10 % (shown as the dotted yellow line), the transformation will take place over an 8 km wide depth interval. Seismic observations, however, show that in some regions of the Earth the 410 km discontinuity can occur over a 4 km interval while in other regions it appears broader than 20 km. At Bayerisches Geoinstitut we are particularly interested in understanding the factors that may cause this type of variation. By performing high pressure and temperature multianvil experiments we can examine the effects of various components and assemblages on the mineral transformations that cause seismic discontinuities. The pressure intervals of many mantle transformations are relatively narrow and challenge the precision in pressure determination of the multianvil apparatus. These transformations can, however, be accurately calculated using thermodynamic models. The width of the interval calculated in Fig. 8.2, for example, is strongly dependent on the thermodynamics of Fe-Mg mixing in both olivine and wadsleyite. Such thermodynamic quantities are rel-

Fig. 8.1: The mineralogy of the Earth's mantle. The coloured fields show the volume fractions of the various minerals of the mantle. In the upper mantle a garnet peridotite xenolith hand specimen is shown in the inset, which contains olivine, garnet, orthopyroxene and clinopyroxene. The inset diagrams at depths below 400 km show high-pressure minerals recovered from multianvil experiments, with the field of view in each diagram being approximately 0.2 mm across. The red curve indicates the PREM model for the density of the mantle as a function of depth. The 410 km and 660 km discontinuities can be seen with their respective density jumps indicated. No strong global discontinuities have been observed at depths greater than 660 km, which infers agreement with laboratory experiments that show magnesium silicate perovskite and ferropericlase to be stable throughout the lower mantle.



atively insensitive to pressure and can therefore be accurately determined using results from element partitioning experiments performed in the multianvil press.

There are many factors that may influence the width of mantle discontinuities such as the presence of H₂O, the redox state in the mantle, the rate of mantle upwelling, and the existence of non-transforming minerals such as garnet. All these factors must be carefully characterised if we are to extract meaningful information from seismic observations. Some very basic observations of some discontinuities have also yet to be fully explained. The 520 km discontinuity, for ex-

ample, which is probably caused by the transformation of wadsleyite to ringwoodite, seems not to be well resolved in all regions of the mantle, but has also been observed in some parts to be split into two separate discontinuities. As more and more detailed seismic observations such as these are reported, so the demand for equally detailed and accurate petrological models to explain these observations increases. ■

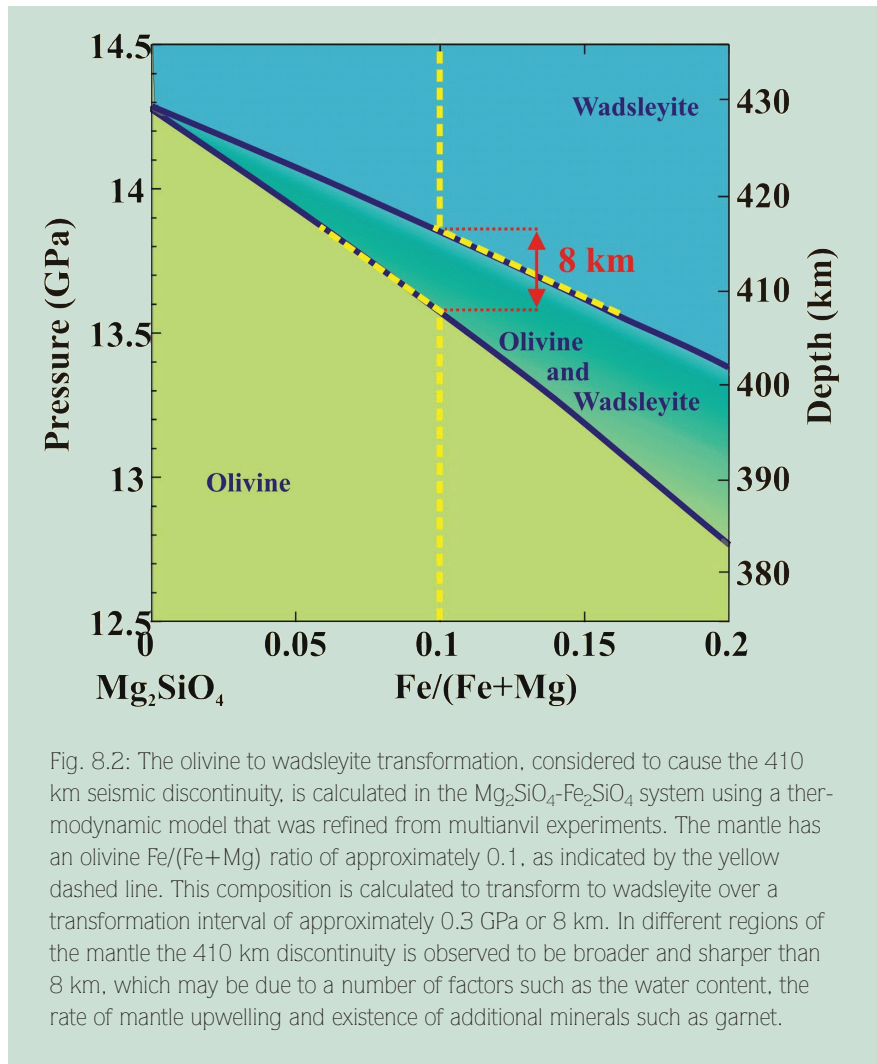
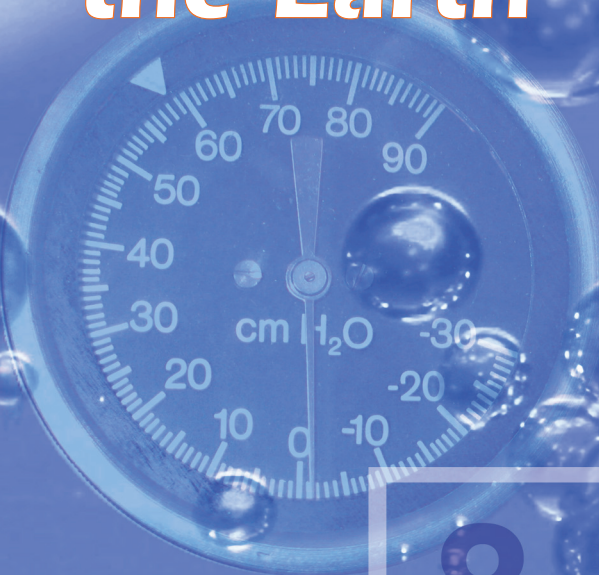


Fig. 8.2: The olivine to wadsleyite transformation, considered to cause the 410 km seismic discontinuity, is calculated in the Mg₂SiO₄-Fe₂SiO₄ system using a thermodynamic model that was refined from multianvil experiments. The mantle has an olivine Fe/(Fe+Mg) ratio of approximately 0.1, as indicated by the yellow dashed line. This composition is calculated to transform to wadsleyite over a transformation interval of approximately 0.3 GPa or 8 km. In different regions of the mantle the 410 km discontinuity is observed to be broader and sharper than 8 km, which may be due to a number of factors such as the water content, the rate of mantle upwelling and existence of additional minerals such as garnet.

9. The oxygen content of the Earth



8

15.9994

-2

90.18

50.35

1.429

$1s^2 2s^2 p^4$

Oxygen

Oxygen is the most abundant element in the Earth excluding its core, and one of the most important for us as living organisms. On its own, oxygen is a highly reactive gas, but readily combines with other elements to produce the oxides and silicates that make up the bulk of the Earth. Oxygen is not locked up permanently within crystal structures, however, and still maintains a degree of reactivity with its environment. A measure of this reactivity is oxygen fugacity, which can be described as the escaping tendency of oxygen from the phase assemblage. High oxygen fugacity implies oxidising conditions, while low oxygen fugacity implies reducing conditions. The depend-

ence of numerous mantle properties and processes on oxygen fugacity has shaped Earth development throughout its history. The evolution of the atmosphere, for example, may be linked to processes such as volcanism that connect the mantle with the outside (Fig. 9.1).

The measurement of oxygen fugacity is challenging compared to other intensive variables such as pressure or temperature. Most methods exploit the sensitivity of transition element valence, *e.g.* Fe^0 , Fe^{2+} or Fe^{3+} , to oxygen fugacity, highlighting the importance of methods that distinguish different valence states. Techniques such as Mössbauer spec-

Fig. 9.1: Volcanoes facilitate the exchange of water, carbon dioxide and other gases between the mantle and the atmosphere. Volcanic activity may have contributed to the evolution of oxygen in the Earth's atmosphere. The picture shows a night time eruption of the volcano Stromboli in Italy.



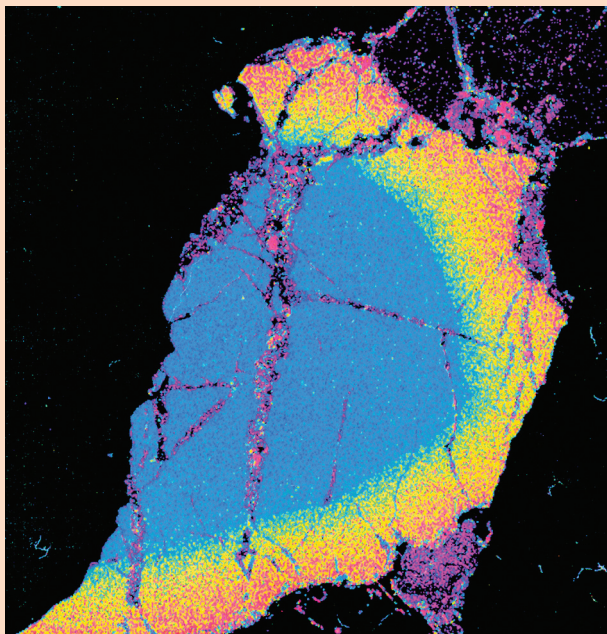


Fig. 9.2: An X-ray map shows the variation of Ca between high (blue) and low (red) concentrations in a xenolith garnet erupted in kimberlite. The zoned pattern results from fluid interaction over a period of more than 10,000 years, and studies of $\text{Fe}^{2+}/\text{Fe}^{3+}$ variation within the different zoned regions provides a measure of the redox history. The field of view is 0.7 mm across.

troscopy and Electron Energy Loss Spectroscopy (EELS) have been used extensively at Bayerisches Geoinstitut for the investigation of oxidation states at different length scales, and have contributed to the slowly emerging picture of mantle oxygen fugacity that has been constructed over the past decade. The small number of studies is likely to expand in coming years with the continued development of techniques such as X-ray absorption spectroscopy and electron-stimulated X-ray emission spectroscopy to quantitatively measure transition metal valence state distribution.

Direct measurements provide the most reliable estimates of oxygen fugacity; hence our knowledge is best in the upper part of the Earth from where most samples originate. The general picture shows a relatively oxidised upper mantle, equivalent to conditions where quartz (SiO_2), fayalite ($\text{Fe}^{2+}\text{SiO}_4$) and magnetite ($\text{Fe}^{2+}\text{Fe}^{3+}_2\text{O}_4$) are in equilibrium. The oxidising conditions arise from the peculiar aversion of olivine, the dominant mineral phase in the upper mantle, to incorporate Fe^{3+} in the crystal structure, which concentrates Fe^{3+} in minor phases such as spinel which effectively control oxygen fugacity. At greater depths where olivine transforms to wadsleyite and ringwoodite, the ability of these high-pres-

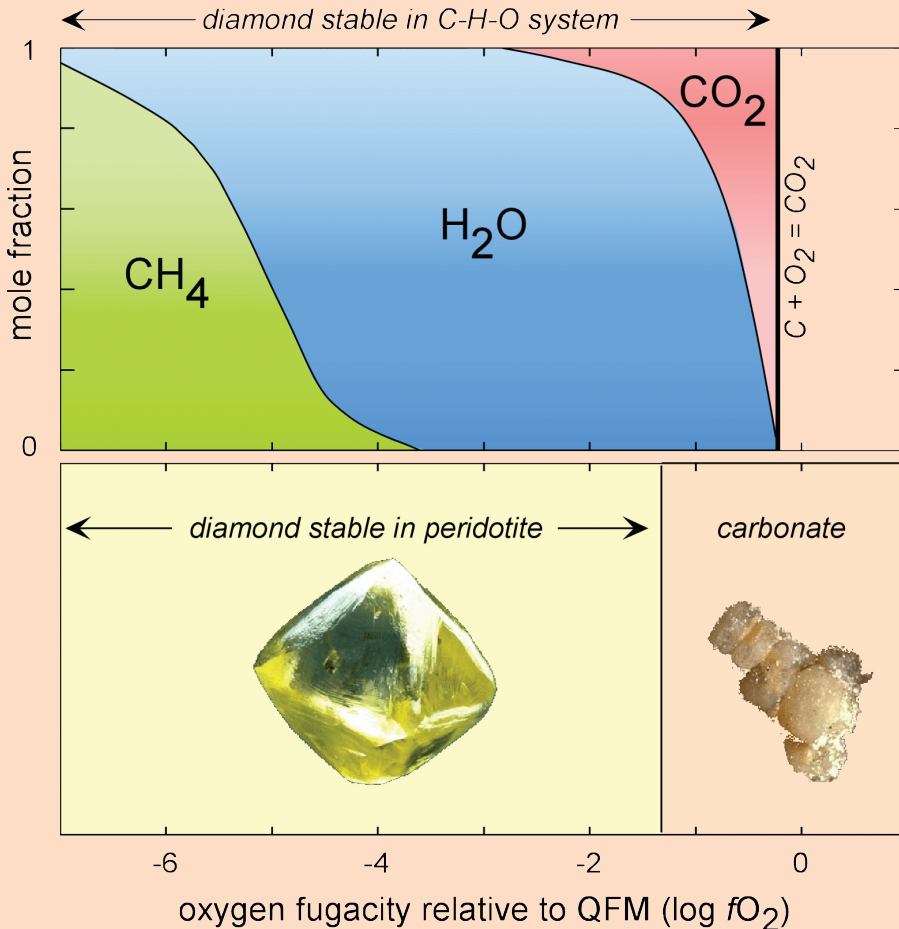
sure phases to incorporate Fe^{3+} probably lowers oxygen fugacity by several orders of magnitude. Superimposed on this homogeneous picture of oxygen fugacity, however, is the observation of significant heterogeneities in the upper mantle. For example rocks produced near mid-oceanic ridges are relatively reduced compared to rocks near subduction zones that show more oxidising conditions, while similar contrasts have been reported between modern rocks and more ancient ones. Although much work needs to be done, such results have already formed the basis of mod-

els for oxygen fugacity variation throughout the globe and over geologic time.

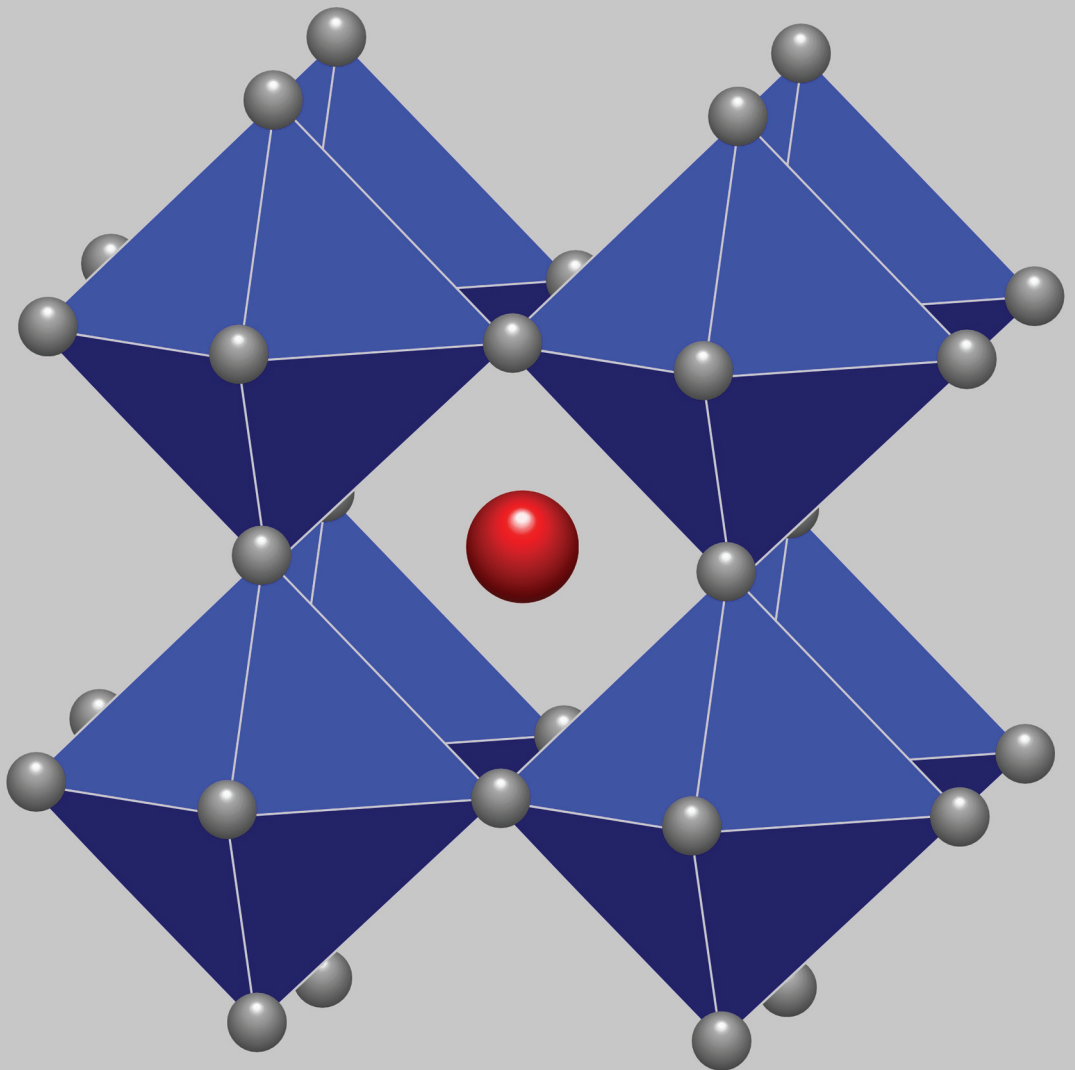
Studies of oxygen fugacity provide not only a snapshot of conditions at a given place or time, but also insight into dynamic processes within our planet. The action of fluids, for example, can effect dramatic changes in min-

eral chemistry. Sometimes a trace is left behind in the form of chemical zonation, and methods such as the Mössbauer milliprobe can be used to unravel the redox history (Fig. 9.2). Such results have important implications for diamond formation, which is often at the mercy of prevailing redox conditions (Fig. 9.3).

Fig. 9.3: The composition of C-H-O fluid in equilibrium with diamond at 5 GPa and 1100°C varies dramatically with oxygen fugacity (top graph). In the C-H-O system diamond is stable until it reacts with oxygen to form CO₂, but in a peridotite assemblage it is only stable until it reacts with olivine to form carbonate (bottom graph).



**10. The most common
but unseen
terrestrial mineral**



It is probably the most abundant mineral in the Earth, yet we cannot hold natural samples of it in our hands. High-pressure experiments over the past three decades have shown incontrovertible evidence that the perovskite structure dominates (to some 60 to 80%) a lower mantle assemblage with chondritic chemical composition. Since the Earth's lower mantle constitutes some 55% (by volume) of the Earth, high-pressure perovskite minerals are hence the most abundant mineral species in the Earth, but they have never been observed in terrestrial rocks due to their instability at low pressures.

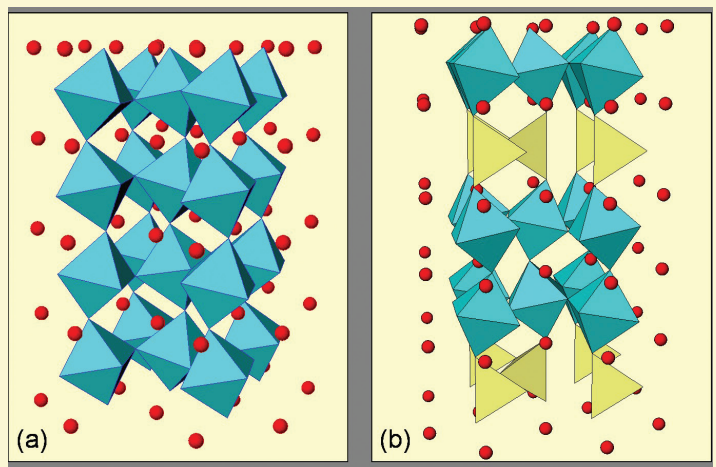
The mineral perovskite is ideally CaTiO_3 , a minor accessory mineral found only in limited quantities mainly within the Earth's crust. But it has given its name to all materials with similar structures, which can be described as a framework of corner-connected octahedra (e.g. TiO_6), with the large cation (e.g. Ca) occupying large interstices (Fig. 10.1a). The dominant perovskite-structured mineral in the lower mantle is a Mg-rich structure (ideally MgSiO_3), which coexists with a smaller amount of a Ca-rich silicate perovskite (ideally CaSiO_3). Both are stable only at high pressures and temperatures.

The perovskite structure is remarkably versatile, incorporating more than half of the stable elements in the periodic table. The wide range of chemical and

structural variations and well as possibilities for non-stoichiometry offer a wealth of interesting physical properties, including superconductivity, ferroelectricity, and ionic conductivity, to name but a few.

The chemistry of the Earth's mantle is complex; hence the lower mantle silicate perovskite minerals are almost certainly not the ideal end members MgSiO_3 and CaSiO_3 , but incorporate other elements as well. Of particular interest are trivalent cations, such as Al, Fe^{3+} , and Cr, since they can be incorporated in combination with oxygen vacancies. Such vacancies can significantly affect elastic properties, and in even small concentrations can produce high ionic conductivities. These ef-

Fig. 10.1: (a) The perovskite structure (ABO_3) consists of corner-shared BO_6 octahedra (blue) forming a framework around the large A cations (red). While the ideal structure is cubic, many structures have lower symmetry with octahedra tilted away from the vertical axis. (b) An oxygen-deficient perovskite-related structure shows the effect of oxygen atom removal where every third layer contains only sufficient oxygen atoms to form BO_4 tetrahedra (yellow). Oxygen vacancies are ordered into layers (not shown) that are perpendicular to the vertical axis.



fects depend on the nature of vacancy ordering, such as whether they are randomly distributed throughout the lattice or are ordered into individual layers (Fig. 10.1b). Other influences on physical properties include structural changes such as octahedral tilting in response to pressure, temperature and chemical composition. While little is currently known about the specific structures and properties of silicate perovskites in the lower mantle, it does appear likely (although it is not yet proven) that Mg-rich perovskite contains disordered oxygen vacancies only, while Ca-rich perovskites may show ordered arrangements in special mantle compositions (Fig. 10.2).

Investigation of lower mantle perovskite minerals is hampered by their metastability or even instability at atmospheric pressure. MgSiO₃-rich perovskites can be synthesised in the laboratory and examined optically (Fig.

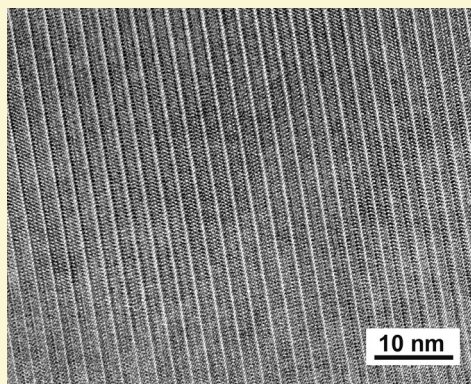
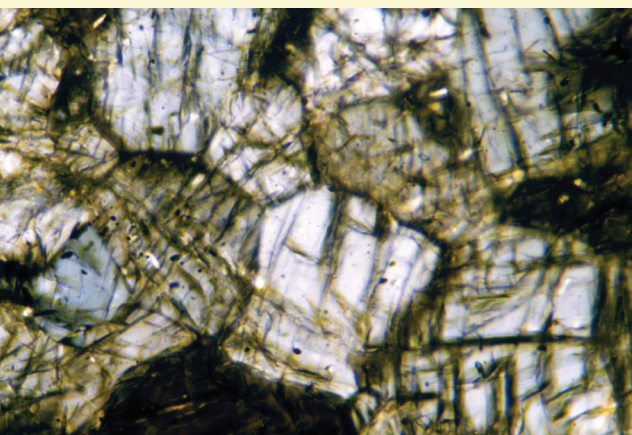


Fig. 10.2: High-resolution electron micrograph of CaFe_{0.4}Si_{0.6}O_{2.8} with a perovskite-related structure. The stripes correspond to layers with oxygen vacancies which are oriented in the [111] direction, referred to the cubic perovskite structure.

Fig. 10.3: The Earth's most abundant mineral, MgSiO₃-rich perovskite (shown here in thin section), can be synthesised at high pressure and temperature in the laboratory. The dark lines are cracks that formed in the crystals during decompression. The field of view is approximately 0.2 mm across.



10.3), but tend to decompose when crushed or probed with radiation such as electrons or intense X-rays. CaSiO₃-rich perovskites do not even survive decompression, as they transform rapidly to an amorphous (glassy) state upon pressure release. This accounts for the absence of silicate perovskites in terrestrial rocks, although some possibilities exist that they might eventually acquire an official mineral name. Mg-rich silicate perovskite was identified using electron diffraction several years ago in the Tenham meteorite, but unfortunately the sub-micron grains were too small for an X-ray structure determination, required for an approved mineral name. Perhaps better possibilities exist in the few minerals included in diamonds believed to come from the lower mantle (Fig. 10.4). MgSiO₃-rich inclusions have been identified based on their major and trace element chemistry to have crystallised as perovskite minerals in the lower mantle, but unfortunately were convert-

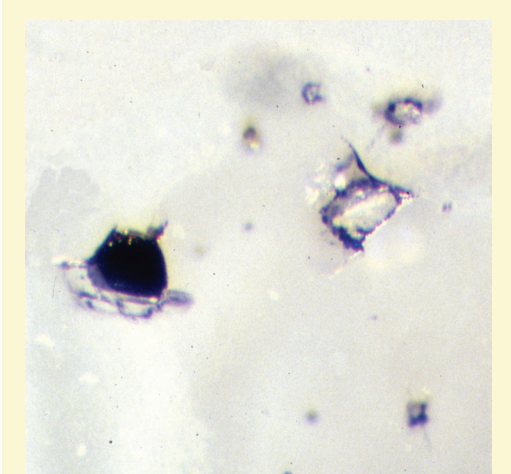


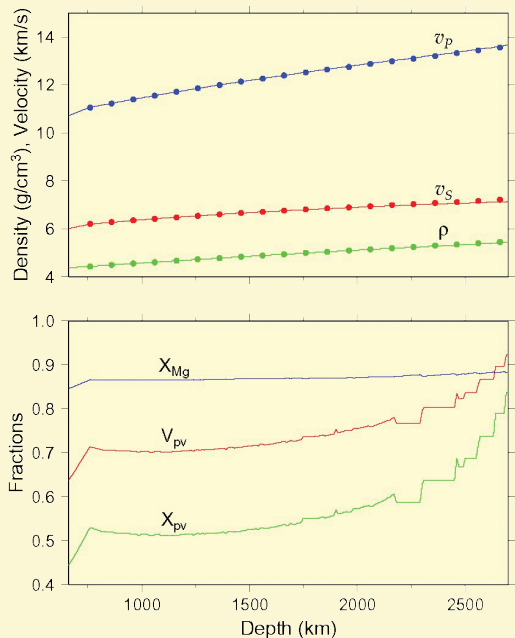
Fig. 10.4: Diamonds originating in the lower mantle have been sometimes found to contain inclusions of ferropericlase (black) and former MgSiO₃-rich perovskite (transparent). The latter phase was transformed upon exhumation to pyroxene, but the chemistry was preserved. The field of view is approximately 0.6 mm across.

ed to low-pressure structures upon exhumation. The ability of diamond to maintain high internal pressures and the advance of *in situ* techniques to examine such diamonds may provide the best possibility for successful recovery of the Earth's most abundant mineral.

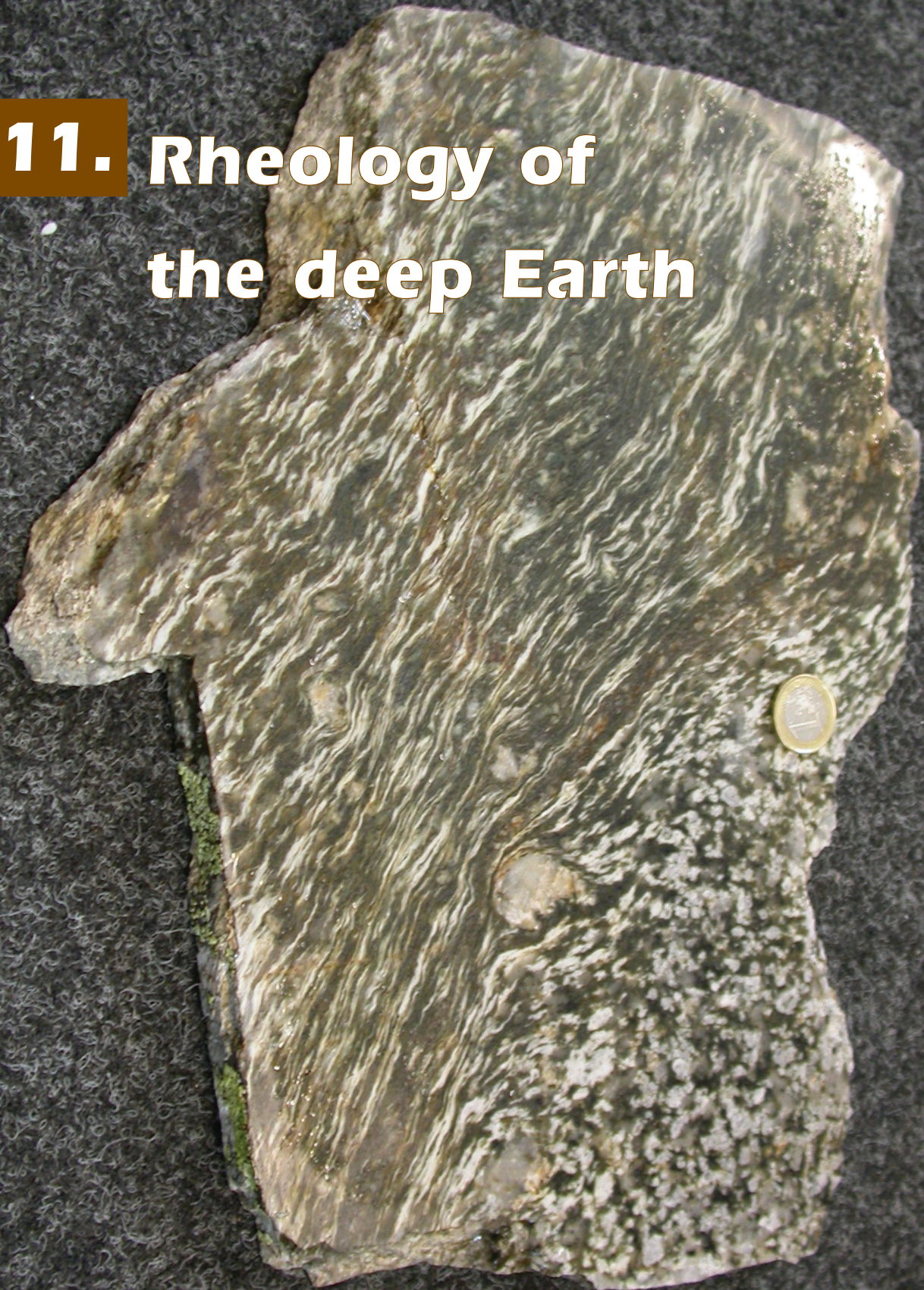
The metastability of perovskite minerals from the Earth's lower mantle can be readily overcome by quantum mechanical simulations, where the two end-member minerals can be studied over a wide compression range. Such studies are based on the self-consistent modelling of the electronic charge density of the crystal (see Fig. 2.6), from which the energetics and full thermodynamics of these phases can be computed. This ongoing effort has already yielded important information on the

physical properties of the Earth's deep interior. In particular, by combining results on the high temperature elasticity of (Mg,Fe)SiO₃ perovskite with those of other dominant mineral phase in the Earth's lower mantle, (Mg,Fe)O ferropericlase, one can obtain a depth dependent simplified compositional and mineralogical model of the lower mantle (Fig. 10.5). ■

Fig. 10.5: Best fitting compositional models of the lower mantle as a function of depth. The model is based on a simplified pyrolytic composition, and on results of the thermoelasticity of (Mg,Fe)SiO₃ perovskite and (Mg,Fe)O ferropericlase along a lower mantle adiabat (assuming a partition coefficient of $K=0.10$ for Fe-Mg between perovskite and ferropericlase). The magnesium content (fraction X_{Mg}) increases slightly from the top to the bottom of the lower mantle. V_{Pv} = volume fraction and X_{Pv} = mole fraction of perovskite. The upper panel compares the resulting fit in compressional v_p and shear wave v_s velocity as well as density ρ (lines) with seismic models of the lower mantle (dots). Modified from Phys. Earth Planet. Int. 134, F.C.Marton and R.E. Cohen, p. 239-252, 2002.



11. Rheology of the deep Earth

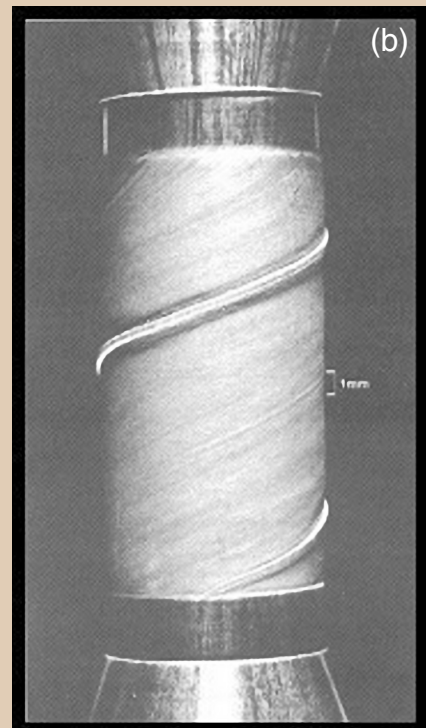


Dynamic processes within the Earth such as mantle convection cause deformation of minerals and rocks at length scales from sub-microns to hundreds of kilometres. The determination of the rheology of Earth materials (*i.e.* their mechanical response to applied stresses and strains) is therefore crucial to understanding the Earth's interior. Due to the high temperatures and pressures as well as the slow deformation rates, rocks in the deep Earth generally behave plastically (Fig. 11.1a). The rheology of minerals or rocks is described by flow laws which relate the applied stresses to the deformation rates. Many additional factors such as temperature, pressure, grain size, oxygen fugacity as well as other physical and chemical parameters may affect the flow stress of a material. At Bayerisches Geoinstitut we attempt to determine the flow laws of the most common phases of the Earth's interior by recording their mechanical response to applied stresses under controlled experimental conditions.

Ferropericlase (Mg,FeO) is believed to be the second most abundant mineral in the lower mantle, and is most likely much weaker than the predominant silicate perovskite phase. Ferropericlase may therefore determine the rheological behaviour in this part of the Earth. In deformation experiments its mechanical behaviour was tested in torsion (Fig. 11.1b), and showed little weakening after the initial yield and the development of a steady state microstructure and crystallographic preferred orientation (Fig. 11.2). The preferred alignment of crystals causes a significant anisotropy of physical properties in the resulting material, which may serve



Fig. 11.1: (a) High-pressure shear zones can be observed in natural rocks such as in this meta-quartzdiorite. (b) Shear strains can also be generated in the laboratory, shown by this experimental sample deformed in torsion geometry; the cylinder was twisted twice around its vertical axis



as a possible explanation for the observed seismic wave anisotropy in different parts of the lower mantle.

Seismic anisotropy developed during deformation will depend on the direction in which glide within the crystal occurs, the so-called slip system. Deformation experiments of olivine in the multi-anvil press (Fig. 11.3a) indicate that the slip system in this mineral may change with increasing pressure. Microstructures and textures in these samples show that slip in the [001] direction is preferred over slip in the [100] direction, which is dominant at low pressures. Macroscopically, this leads to an alignment of the [001] direction in the shear direction instead of

[100]. The results may have direct implications for the interpretation of the shear-wave splitting observed for the Earth's upper mantle, since the oscillation direction of the fastest shear wave coincides with the [100] direction in olivine, and therefore that direction has been interpreted as the direction of shear (or transport) due to convective flow in the upper mantle. Since it is difficult to distinguish the influence of confining pressure and differential stresses in multi-anvil deformation experiments up to now, experiments with assemblies that allow for separate control of those two factors such as the D-DIA type press (Fig. 11.3b) are highly desirable. ■

Fig. 11.2: Shear stress-shear strain curve of a sample deformed to a shear strain (γ) of 16 at 1300K (solid line). The microstructure maps (lower row) and {111} pole figures (upper row) are (from left to right): the starting material, two samples deformed to a shear strain of 1.1 and 3.4, respectively, and the sample for which the stress-strain curve is shown. The sections are perpendicular to the horizontal shear plane and the shear sense is dextral.

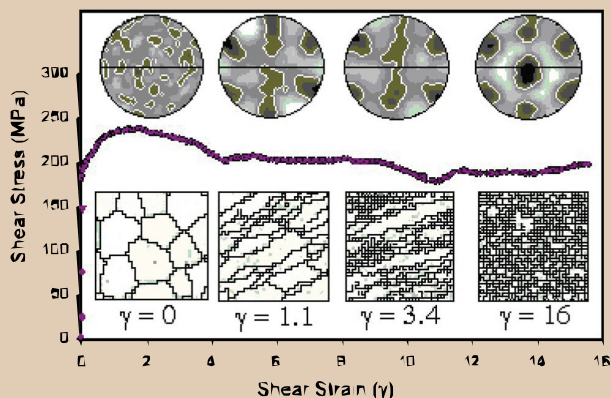
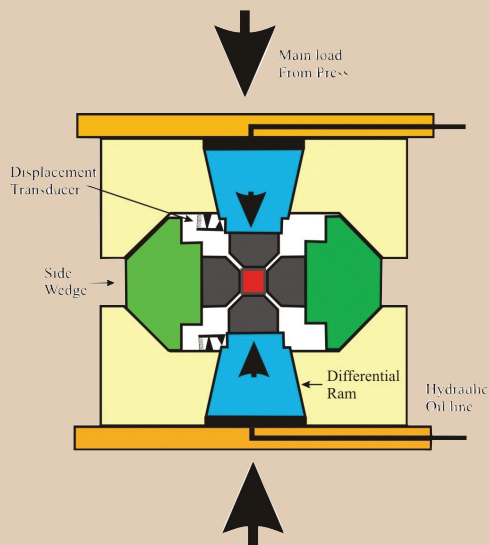


Fig. 11.3: Experimental rock deformation at mantle pressures. (b) Axial compression in the D-DIA type press. Note that in the latter case the differential stresses can be controlled independently from the confining pressure due to the separate movement of the anvils marked in blue.



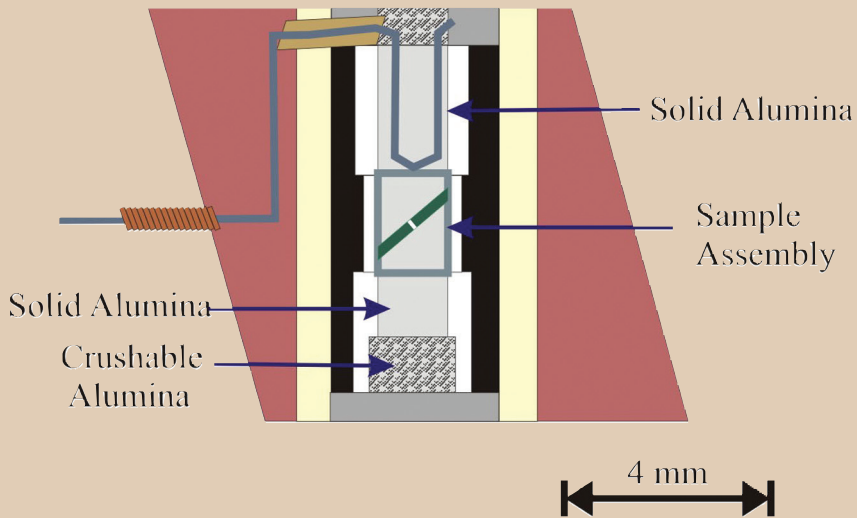
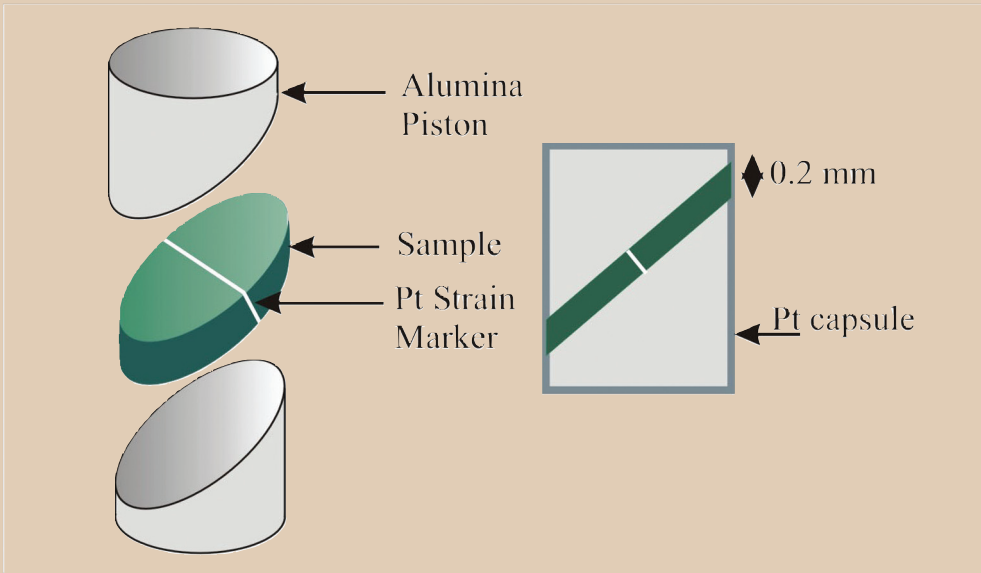
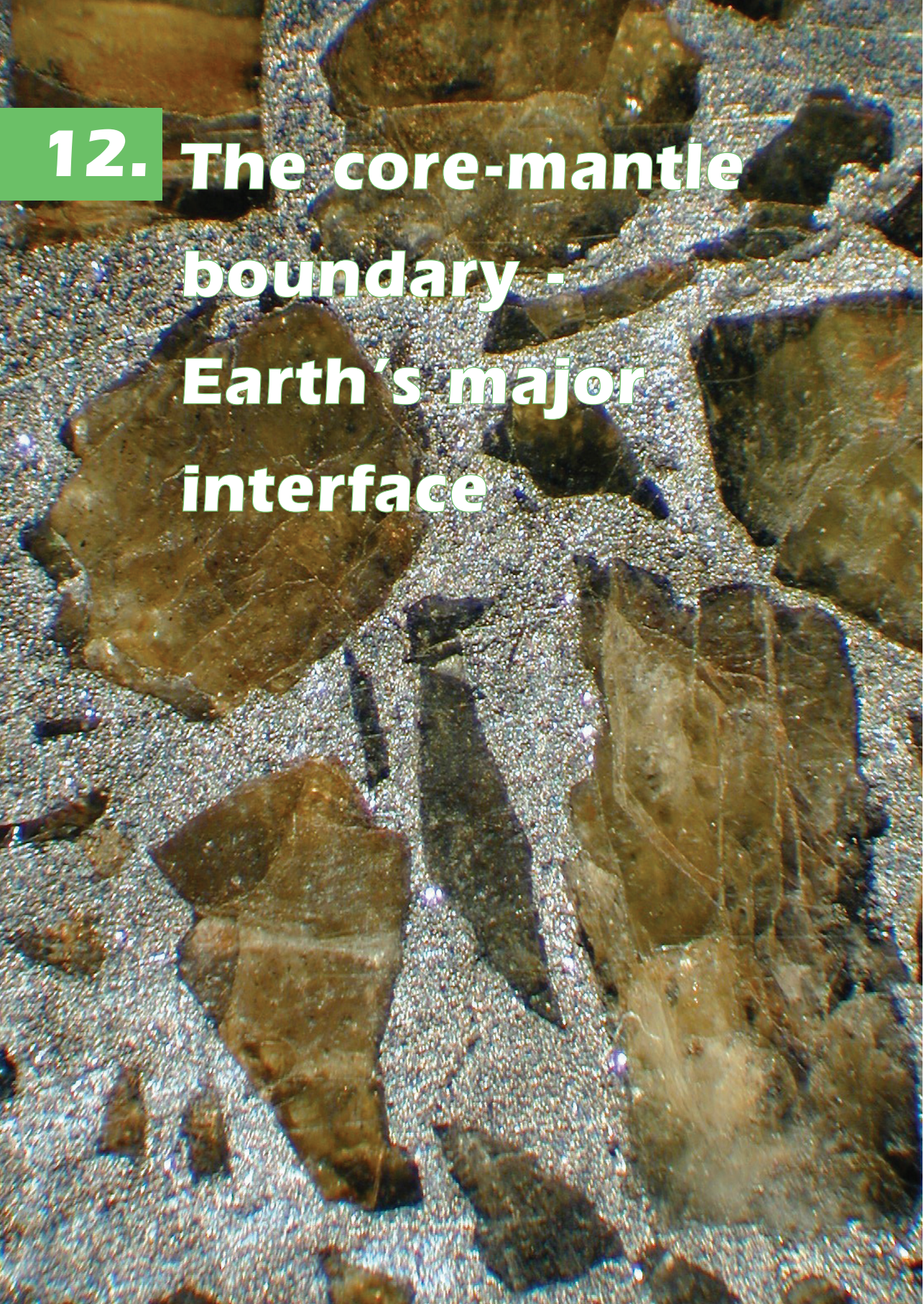


Fig. 11.3: Experimental rock deformation at mantle pressures.

(a) Direct shear in the multi-anvil press;



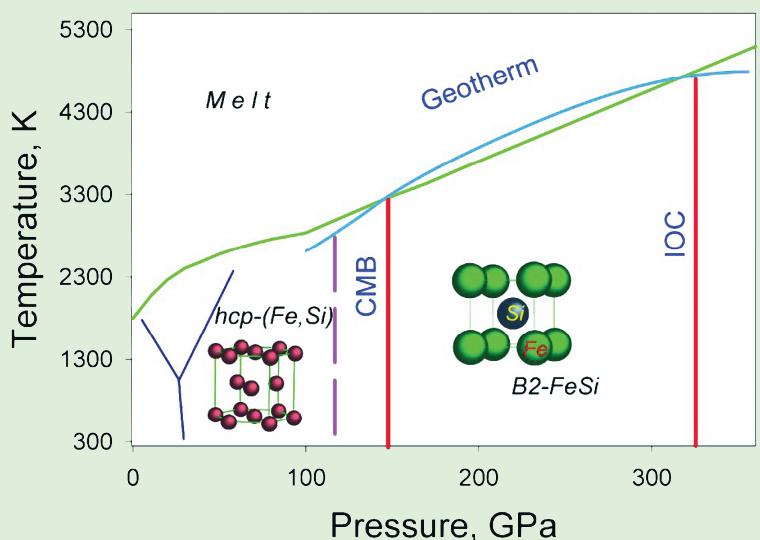
**12. The core-mantle
boundary -
Earth's major
interface**

The boundary between the Earth's mantle and the core is actually a narrow zone (ca. 100 km in thickness), the so-called D'' layer. It is characterised by steep gradients in temperature and marked changes in properties with depth. The seismologically observed changes in density and sound wave velocities, for example, are 2-3 times greater than across the air-rock (or air-seawater) interface at the Earth's surface. Moreover, the difference in materials across the boundary, with predominantly crystalline rock above and liquid iron alloy below, is among the most profound in the Earth. In this sense, the core-mantle boundary (CMB) can be considered the primary "surface" of the planet, and it is simply because of its remoteness that it has attracted less study than the top of the Earth's crust. On the other hand, processes at the CMB directly or indirectly affect us. There are a number of geophysical, geochemical and seismological arguments which link processes at the D'' layer with those at the surface of the Earth. For example, super plumes originating at the core-mantle boundary are thought to manifest themselves as hot-spot volcanoes on Hawaii.

Experimental studies of processes at the CMB are challenging due to the ex-

tremely high pressures and temperatures required (at least 140 GPa and ca. 2600°C, see Fig. 1.7), and only laser heating in diamond anvil cells can generate the appropriate conditions (Fig. 12.1). However the samples are exceptionally small (typically 35-50 μm in diameter, less than 10 μm in thickness, with masses about 10⁻⁷ g) and only combinations of the most powerful techniques (e.g. synchrotron X-ray diffraction, luminescence and absorption methods, analytical transmission electron microscopy, Mössbauer milliprobe spectroscopy) can shed light on the processes occurring at the CMB.

Fig. 12.2: Schematic phase diagram of iron and iron-silicon alloys. Phase relations between α (bcc), γ (fcc), and ε (hcp) pure iron phases are shown by dark blue lines, the tentative melting curve of iron is green, and the boundary separating hcp-(Fe,Si) alloy from coexisting iron-rich alloy and B2-structured FeSi is indicated by the dashed magenta line. The geotherm is light blue, while the core-mantle boundary (CMB) and the inner-outer core boundary (IOC) are both shown as red lines.



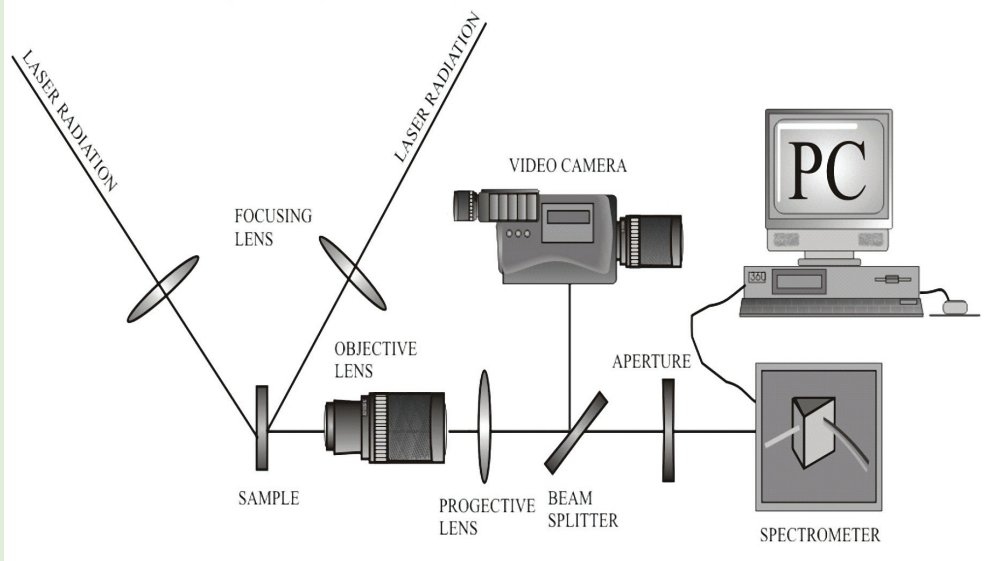
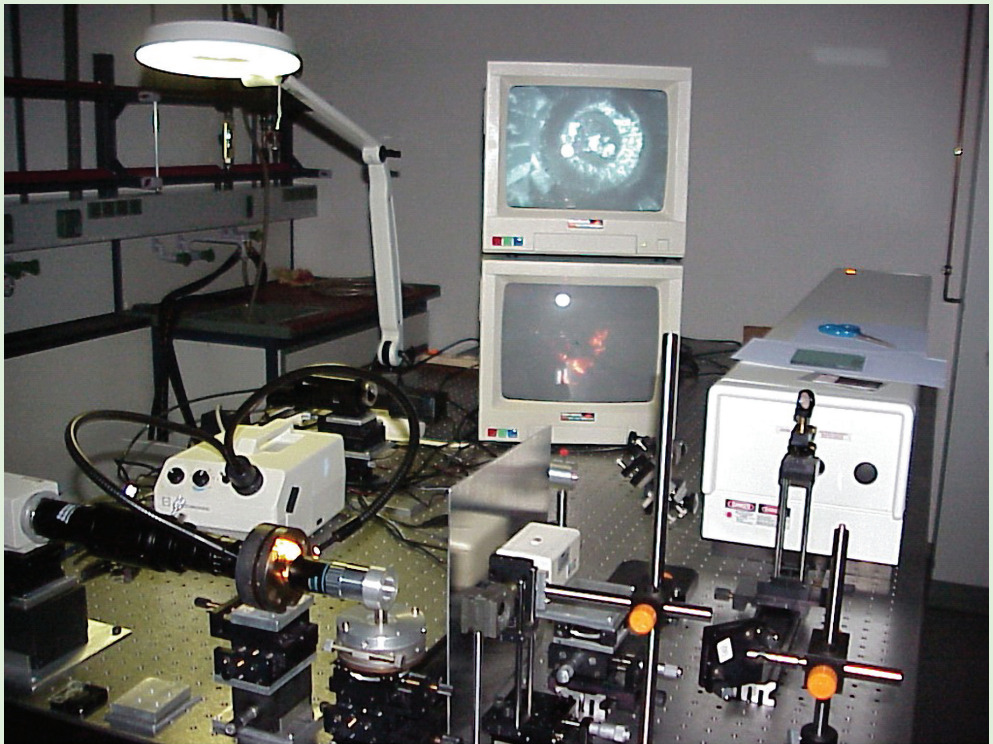


Fig. 12.1: General view (top) and schematic diagram (bottom) of the double-sided Yttrium Lithium Fluoride (YLF) laser-heating set up for experiments involving diamond anvil cells at Bayerisches Geoinstitut.

Chemical properties and reactions can be quite unusual at such extreme pressures. For example, iron is more electronegative than aluminium at ambient conditions, but significantly changes its chemical nature at pressures above 60 GPa and temperatures above 2200 K. At these conditions it can reduce aluminium oxide to metallic aluminium, thus providing a possible source of aluminium for the Earth's core. Similarly, iron and silicon react easily at high temperatures and low pressures, but not at high temperatures and high pressures where iron-silicon alloys dissociate into almost pure iron and the CsCl-structured (B2) FeSi compound (Fig. 12.2). Experimental observations suggest that during formation and differentiation of the proto-Earth, iron alloy segregating in a deep magma ocean (thus containing several wt% Si) would subsequently decompose into a mixture of Si-poor iron phase and silicon-rich B2 phase in the core. The metallic silicon-rich B2 phase produced by this reaction (or produced at the CMB due to reaction between iron and silicate) is denser than lower mantle material and lighter than liquid iron in the Earth's outer core, and should hence accumulate at the CMB. The presence of B2 FeSi at the base of the Earth's lower mantle could explain the anomalously high electrical conductivity of this region (Figs. 12.2 and 12.3).

Further studies of possible chemical reactions between iron and its alloys (which represent the Earth's core) and complex Mg-Fe-Si-Al oxides (which model the composition of the Earth's lower mantle) will help to elucidate many of the enigmatic properties of this region and to answer many perplexing questions about this most drastic of Earth's interfaces. For example, what is the degree of chemical equilibrium between the core and lower mantle, given the hypothesis that the D'' layer is a temporary repository for subducted material that then rises again in the form of superplumes? What is the spin state of iron at these depths and how does it affect chemical equilibria and physical properties? Among all the questions about the D'' layer, however, one point appears to be undebated: This is where the action is. ■

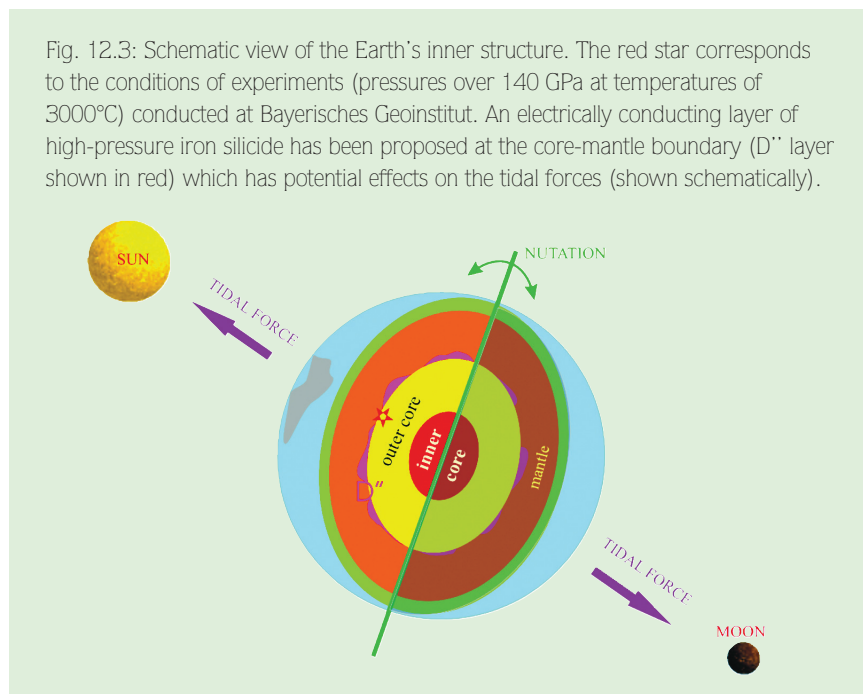
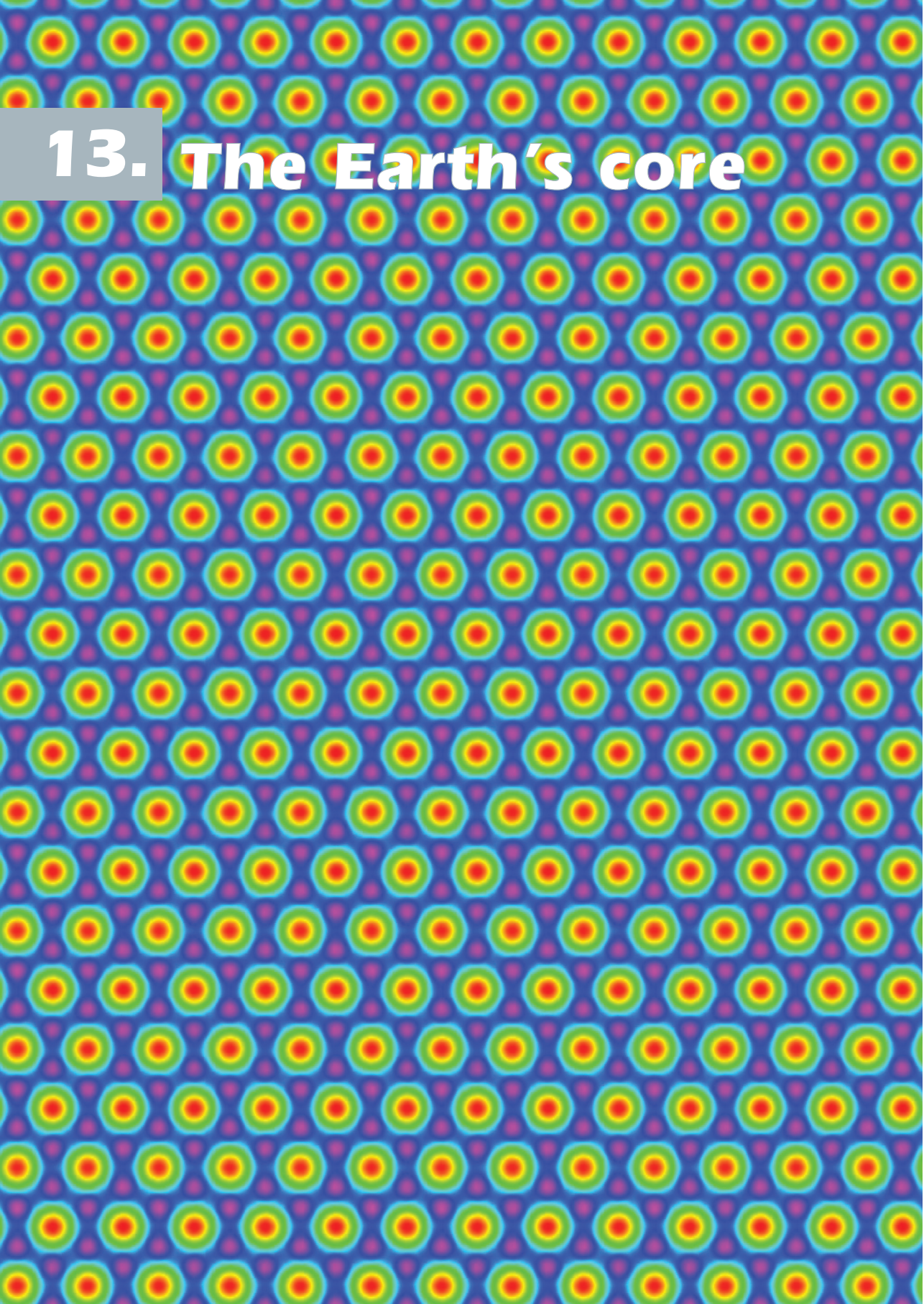


Fig. 12.3: Schematic view of the Earth's inner structure. The red star corresponds to the conditions of experiments (pressures over 140 GPa at temperatures of 3000°C) conducted at Bayerisches Geoinstitut. An electrically conducting layer of high-pressure iron silicide has been proposed at the core-mantle boundary (D'' layer shown in red) which has potential effects on the tidal forces (shown schematically).



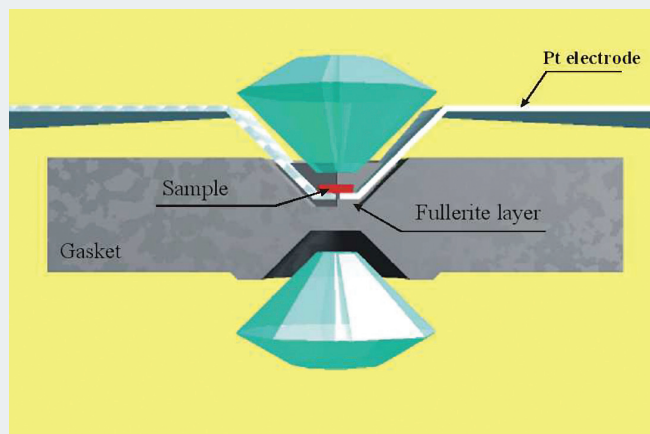
13. The Earth's core

The Earth's core is the most remote region of our planet as shown in Fig. 1.1. Not only do we have no samples from the core, but we really do not ever expect to get them. Our knowledge of the physical state and composition of the core comes from the interpretation of indirect observation through results of laboratory experiments or molecular modelling. Arguments from cosmochemistry and meteorites (high abundance of iron in the universe), seismology (density of the core compatible with density of iron at corresponding conditions), geochemistry (depletion of iron in Earth's crust and mantle), and geomagnetism and geodynamics (existence of long-lived dynamic magnetic field) suggest that the major component of the Earth's core is an iron-nickel alloy with 5 to 15% of nickel. However, pure iron-nickel alloy does not satisfy the seismological observations of the fluid outer core – it is too dense by approximately 10% to agree with both the observed density and bulk modulus along any plausible geotherm. The presence of one or more light elements has therefore been inferred, but their identity and concentrations are still uncertain. Based primarily on cosmochemical arguments, one third of the elements lighter than iron have been

proposed as candidates, including H, C, O, Mg, Si, and S. However the lack of information on the chemical behaviour, phase stability and physical properties of solutions between iron and such light elements at extreme pressures and temperatures means that any modelling of outer core compositions is very difficult. On the other hand, in the inner core the density-pressure relation and the equation of state of iron at high temperatures are in good agreement, hence the composition of the inner core is assumed to be close to pure iron or iron-nickel alloy.

A fundamental problem that is closely linked to studies of the Earth's core and melting curves of alloys between iron, nickel, and possible light elements is the determination

Fig. 13.1: (a) Schematic diagram of the electrical wire-heating assemblage in a diamond anvil cell, where a rhenium gasket of $250\ \mu\text{m}$ thickness is indented to about $30\ \mu\text{m}$ between diamonds with $300\ \mu\text{m}$ culets. The gasket is covered by an electrically isolating fullerite layer, and a platinum wire of $0.2\ \text{mm}$ diameter flattened to a thickness less than $10\ \mu\text{m}$ serves as electrical leads.



of the temperature profile within the Earth. There are no direct methods for temperature measurement of the Earth's lower mantle and core. However, seismological data provide evidence that the Earth's outer core is liquid. If one could measure melting temperatures of iron-nickel-light element(s) alloys at *ca.* 140 GPa (core-mantle boundary) and *ca.* 330 GPa (inner-outer core boundary), this would constrain the minimum temperature at the CMB and fix the temperature at the inner-outer core boundary, paving the way to derive a temperature profile of the entire Earth. So far dynamic studies (shock wave), static experiments (laser heating in diamond anvil cells) and theoretical calculations have not given consistent results,

partly due to technical difficulties; hence development of a new wire-heating method for diamond anvil cells at Bayerisches Geoinstitut provides a new perspective for resolving the problem (Fig. 13.1).

The physical properties of pure iron govern the behaviour of the inner core to the extent that the inner core is composed of pure iron. In particular, if the aggregate elastic properties of iron and the inner core are in agreement at a particular temperature, we can use this temperature to constrain the thermal state of the Earth's deepest interior. Such results now provide an independent estimate of the temperature within the core (Fig. 13.2).

Fig. 13.1: (b) Photograph of a Fe-10%Ni alloy wire in the sample chamber of the diamond anvil cell heated at 107 GPa to 2850 K by a DC current.

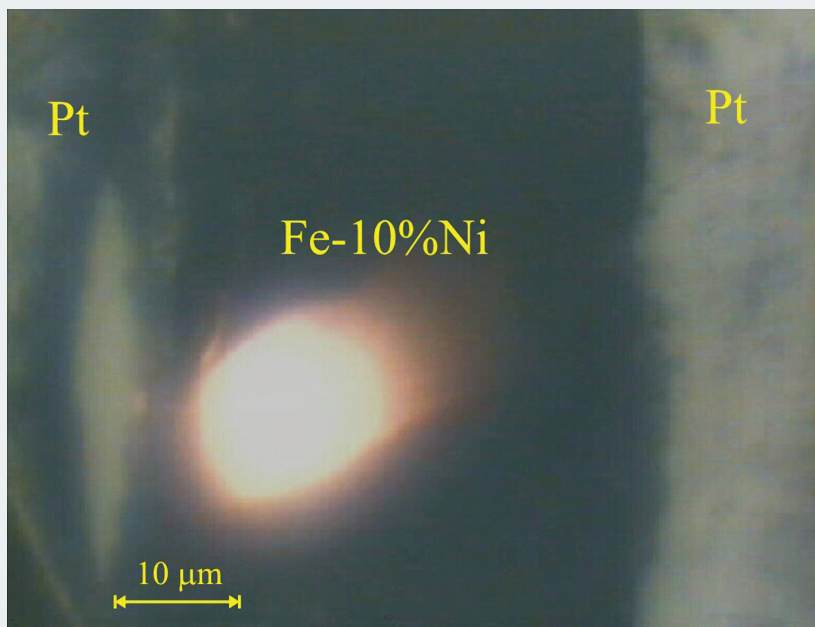
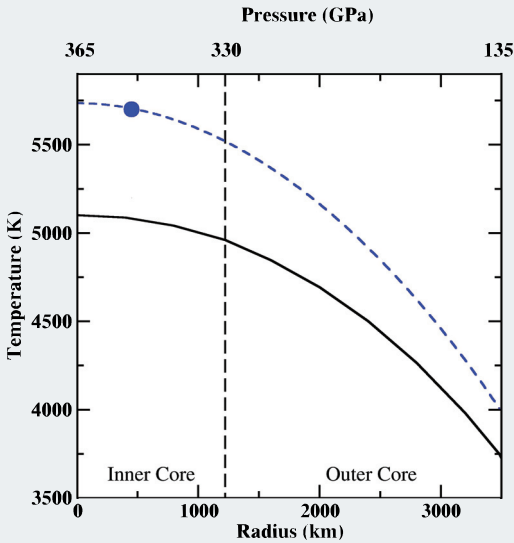


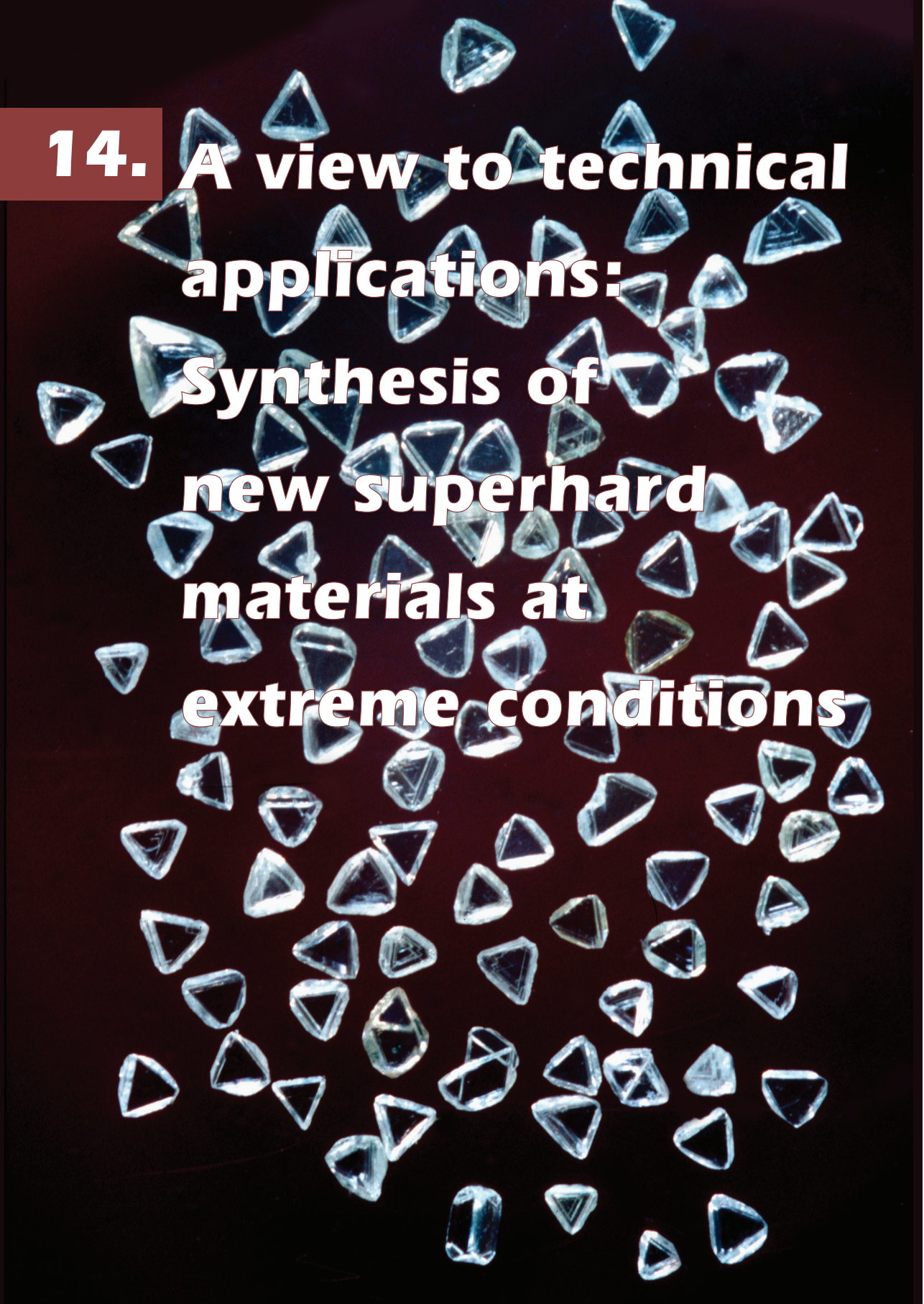
Fig. 13.2: Temperature in the Earth's core. A temperature point in the inner core (solid blue circle) was calculated based on a comparison of inner core aggregate elasticity with that of pure iron at high temperature. The dashed blue line represents an adiabat through the inner and outer core, while the black line indicates a conventional geotherm.



command considerable attention and are still hotly debated, while knowledge of the behaviour and properties of Fe-Ni alloys in the multi-megabar pressure range and at high temperatures is very limited. Even relatively small amounts of additional components can significantly affect the structure (face-centered cubic “fcc” versus hexagonal close-packed “hcp”), phase relations and thermophysical properties of iron alloys. For example, extrapolation of data collected for Fe-10%Ni to outer core conditions suggests that the Earth's inner core could contain coexisting fcc- and hcp-structured iron-nickel alloys. Also, at 330 GPa the molar volume of fcc-Fe-10%Ni alloy is expected to be *ca.* 0.5% higher than the molar volume of the hcp phase. Such differences could be

The past decade has brought many fascinating discoveries related to the properties and dynamics of the Earth's solid inner core. This region, approximately 2400 km in diameter and comparable in mass to our moon, was long considered to be essentially inert and featureless. The discovery of anisotropy, super-rotation (where the inner core rotates faster than the rest of the Earth), and fine-scale heterogeneity of the Earth's inner core revolutionised the field and brought questions to the foreground about the chemical and mineralogical composition, as well as elastic and rheological properties of core-forming alloys. Currently studies of pure iron at extreme conditions

important for the dynamics of the Earth's core and could contribute to its fine- or large-scale heterogeneity. Moreover, the thermoelastic properties of cubic fcc and hexagonal hcp phases are expected to be rather different; hence the microtextures and mechanical properties of two-phase (fcc and hcp) mixtures could be quite different from the properties of the pure hcp-phase. Similarly, the incorporation of other elements into iron can affect the crystal structure of the alloy considerably. Investigation of the aggregate and anisotropic elastic properties of the Earth's inner core will require explicit consideration of the phase heterogeneity of the constituent material. ■



**14. A view to technical applications:
Synthesis of new superhard materials at extreme conditions**

The study of Earth materials teaches us that crystal structures and properties change with pressure and temperature (Fig. 14.1), and that these parameters are therefore useful tools for the synthesis of novel materials in general. Basically, pressure allows the precise tuning of a single fundamental parameter, interatomic distance, which in turn controls the electronic structure and virtually all of the interatomic interactions that determine material properties.

The hardness of materials is unquestionably one of the properties most suited for a detailed intercomparison and semi-quantitative evaluation. Although hardness is a macroscopic phenomenon, the crystal structure, which describes bonds lengths, bond angles and their variations as well as coordination numbers and so on, is the decisive factor for the strength of any material. The classical example is diamond *versus* graphite, where the industrial production of diamond by high-pressure synthesis recently celebrated its 50th anniversary. Diamonds are generally considered to be the hardest known material due to the directed covalent sp^3 bonds between carbon atoms that gives rise to a very rigid, hard structure. In contrast, graphite contains three strong short bonds within the sheets and a very long bond between sheets. The easy shear between graphite sheets makes it an ideal material for old-fashioned pencils and high-tech lubricants; whereas the hardness of diamond makes it an exceptional abrasive for many applications. Unfortunately diamonds cannot be used to machine ferrous metals, presu-

ably because a metal carbide is formed under the high-temperature conditions encountered during the machining process, or because iron catalyses the transformation of diamond back to graphite. Hence there is a great need for thermally stable materials with hardness approaching (or even greater than) that of diamond for use in the machining of ferrous metals.

So far it has been hard to imagine that the outstanding properties of diamond could be significantly improved. However studies of nanomaterials have shown that their properties (*e.g.* hardness and thermal stability) may exceed those of bulk materials. In particular, it was suggested that carbon

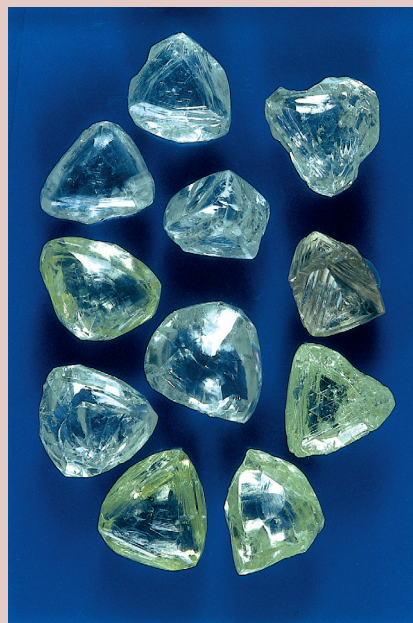


Fig. 14.1: Nearly perfect but too valuable for industrial use: natural diamonds.

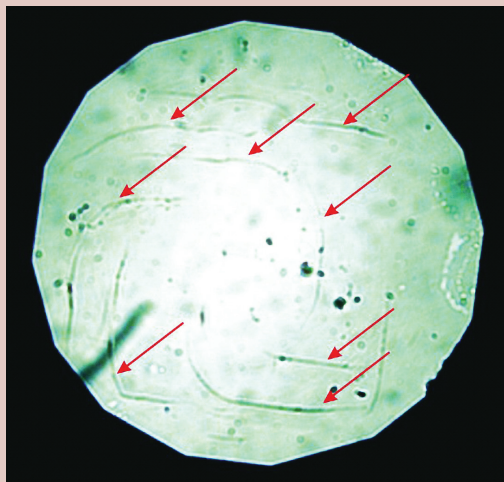


Fig. 14.2: Photograph of the “hardest” (111) face of natural diamond scratched by synthetic nanodiamond (arrows). The edge of the picture is 350 μm across.

clusters with a diamond-like structure (“nanodiamond”) with diameters less than about 5 nm (1 nm = 1 billionth of a metre) may actually be more stable than graphite-like clusters of the same size. Recently we synthesised a sample of nanocrystalline cubic diamond with crystallite sizes of 5–12 nm. We found that the hardness of the new material exceeded that of single crystal diamond. As shown in Fig. 14.2, these materials scratch the hardest face of diamond and are therefore harder – a revival of the Mohs scale of hardness test. This nanocrystalline diamond is even thermally and kinetically more stable than conventional diamonds – its oxidation in air or

transformation to graphite are slower at high temperature than for coarse-grained diamond.

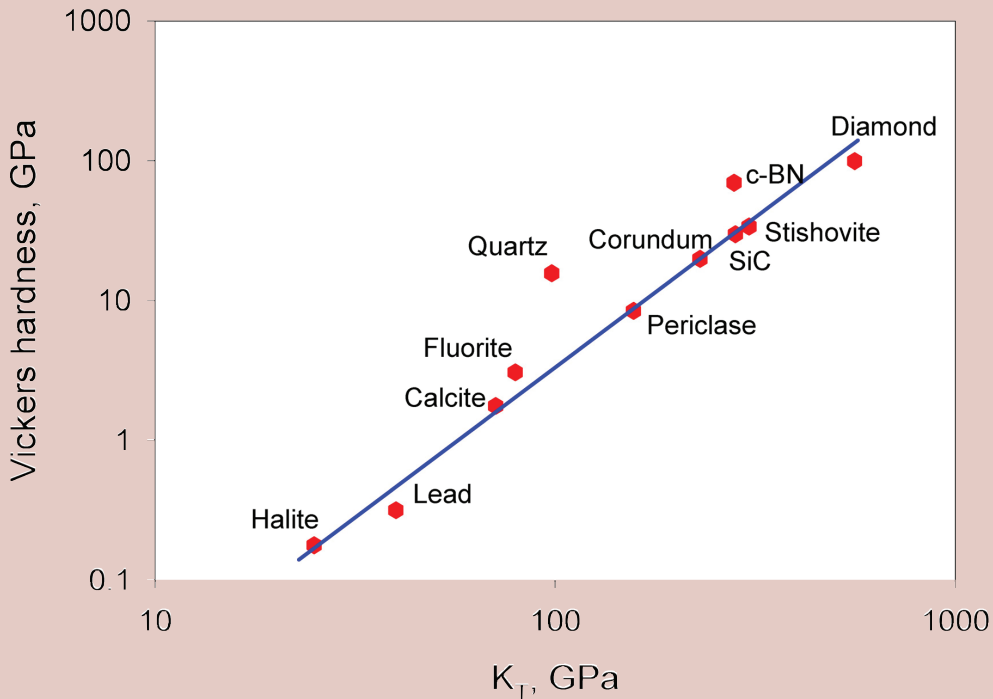
In searching for new superhard materials the main direction has been to look for materials that contain small, strongly bonded atoms and are isoelectronic with diamond. For example, boron nitride (BN) fulfils these criteria and forms a diamond-like structure (*c*-BN) at high pressure with hardness similar to diamond; it is stable against oxidation and can be used as an abrasive for ferrous metals. Solid solutions between diamond and boron nitride have been proposed as superhard materials and significant progress in this direction was recently achieved when cubic BC_2N (harder than *c*-BN) was synthesised at Bayerisches Geoinstitut.

Research on superhard materials is not exclusively confined to diamond-like structures, however. Hard and superhard materials are also encountered among oxides, nitrides and carbides, and some of these are important from both a geophysical and a technological perspective. The results of studies of high *P-T* polymorphs of silica, titania, and silicon nitride have shown that stishovite (rutile-type SiO_2), α - PbO_2 -like silica, cotunnite-type TiO_2 , and cubic Si_3N_4 are all harder than Al_2O_3 (recall that corundum has a hardness of 9 on the Mohs scale), which make them among the hardest

known polycrystalline materials. Methodologically, hardness is a difficult parameter to assess in newly synthesised hard materials since sufficiently large quantities of material are needed, and hardness (generally measured as Vickers hardness using a diamond indenter) is not defined when the hardness of a material exceeds that of diamond. On the other hand, the isothermal bulk modulus K_T of a material (see section 7) can be easily measured with high

precision, and is closely related to hardness as illustrated in Fig. 14.3. Through the combination of various synthesis methods (electrically heated diamond cell for extreme pressures, multianvil presses for larger volumes) with advanced methods of *in situ* or *ex situ* characterisation (for example using X-rays, vibrational or Mössbauer spectroscopy), we have the potential to discover new materials that have innovative technical applications. ■

Fig. 14.3: Diagram showing the relationship between Vickers hardness H and the isothermal bulk modulus K_T for a number of materials. Note the logarithmic scales.



An aerial photograph of a large, modern university building complex. The main building is a large, multi-story structure with a white facade and a dark blue roof. It features a central courtyard with a paved area and several trees. The building is surrounded by green lawns and winding paths. In the foreground, there is a parking lot with several cars parked. The text "About Geoinstitut" is overlaid on the top left of the image in a white, bold font, with a red rectangular background behind the word "About".

About Geoinstitut

Mission: Bayerisches Geoinstitut is a central research facility of the University of Bayreuth. The institute was founded in 1986 with the goal to investigate processes in the Earth's interior through experimental studies using a multidisciplinary approach.

Staffing and structure: The institute currently has three professorships, one junior professorship, five tenured and three untenured scientific staff positions, a technical and administrative staff of 14, a visiting scientists' programme (see below), Ph.D. students and a variable, but generally high number of both short-term and long-term visitors. The professors are also *ad personam* members of the Faculty for Biology, Chemistry and Geosciences. The institute is headed by an acting director. The absence of a formal group structure and an "open lab door" philosophy helps to overcome barriers between disciplines. The "Kommission für Geowissenschaftliche Hochdruckforschung" of the "Bayerische Akademie der Wissenschaften" in Munich acts as an advisory body.

National and international collaboration: Through the institute's visiting scientists' programme, EU-funded exchange programmes for junior and senior scientists, fellowship and award programmes of the Alexander-von-Humboldt Foundation, *etc.*, the institute offers a truly international and



challenging atmosphere. This spirit, combined with the expertise of the staff, the state-of-the art equipment in a wide range of experimental methods and the excellent technical support staff, makes the institute attractive for Ph.D. students, postdoctoral fellows and senior scientists, *e.g.* those on sabbatical leave. Further international and national contacts are established through participation in priority programmes of the German Science Foundation (DFG), network programmes of the European Union and joint projects with other universities, and also by conferences arranged in Bayreuth or abroad, and participation in experiments at large-scale facilities such as synchrotrons.

Teaching: The staff of the institute teaches basic geology and mineralogy to students in geocology in the Faculty for Biology, Chemistry and Geosciences, and advanced courses in geophysics to physics students. Once a year, a laboratory course on "High pressure experimental techniques and applications to the Earth's interior" is held by members of the institute, with a strong international participation from graduate and postgraduate students. Ph.D. students at

View of the Bayerisches Geoinstitut building on the campus of the University of Bayreuth

Equipment: Major equipment includes

I. High-pressure apparatus

- 5000, 1200, and 1000 tonne multianvil presses (25 GPa, 3000 K)
- 500 tonne multianvil press (20 GPa, 3000 K)
- 3 piston-cylinder presses (0.5" and 0.75"; 4 GPa, 2100 K)
- Cold-seal hydrothermal vessels (700 MPa, 1000 K, H₂O), TZM vessels (300 MPa, 1400 K, gas) rapid-quench hydrothermal vessels
- Internally-heated autoclave (1 GPa, 1600 K)

II. Structural and chemical analysis

- 3 X-ray powder diffractometers, one with furnace and cryostat
- X-ray powder microdiffractometer
- Single-crystal X-ray cameras
- 2 automated single-crystal X-ray diffractometers
- 2 Mössbauer spectrometers (1.5 - 1300 K)
- Mössbauer millispectrometer
- FTIR spectrometer with IR microscope
- FEG transmission electron microscope, 200 kV analytical, with EDS and PEELS
- FEG scanning electron microscope with BSE detector, EDS, EBSD and CL
- High-resolution solid-state NMR spectrometers (100, 200, 300 MHz)
- 2 Micro-Raman spectrometers
- JEOL JXA-8200 electron microprobe; fully-automated with 14 crystals, 5 spectrometer configuration, EDX, capability for light elements
- Cameca SX-50 electron microprobe
- ICP-AES sequential spectrometer

III. In situ determination of properties

- 1 calorimeter (77 - 1000 K) scanning
- 1 dilatometer (to 1800 K)
- Diamond anvil cells for powder and single crystal X-ray diffraction, Mössbauer, IR, Raman, optical spectroscopy and electrical resistivity measurements in the megabar pressure range
- Facility for in situ hydrothermal studies in DAC
- Externally electrically heated DACs for in situ studies at pressures to 100 GPa and 1200 K
- 1-atm furnaces (to 1873 K, gas mixing) equipped with zirconia fO₂ probes
- Paterson HP/HT deformation apparatus
- 1-atm high-temperature creep apparatus
- 2 high frequency ultrasonic interferometers (crystalline and molten materials)
- Gigahertz ultrasonic interferometer with interface to resistance-heated diamond-anvil cells
- Heating stage for fluid inclusion studies
- Impedance/gain-phase analyser for electrical conductivity studies
- Apparatus for in situ measurements of thermal diffusivity at high P and T

the institute are fully integrated into the research and receive an in-depth supervision by multiple members of the staff.

Funding: Bayerisches Geoinstitut is supported by the Free State of Bavaria through the Science Ministry and the University of Bayreuth. Important complementary funds come from the European Union through various programmes, the German Science Foundation (DFG), the Fonds der Chemischen Industrie, *etc.* and by high-level awards to staff members, *e.g.* the Kovalevskaja programme of the Alexander-von-Humboldt Foundation. Many visitors bring their own funds in the form of stipends or awards from the Alexander-von-Humboldt Foundation, DAAD, EU, and national agencies abroad.

Annual Report: The institute issues a comprehensive Annual Report on its scientific activities once a year, giving summaries of recent projects, a list of publications by staff members, lectures held, conferences organised, visitors hosted, *etc.* These Annual Reports can also be viewed on the institute's web page (www.bgi.uni-bayreuth.de).

The Building: Bayerisches Geoinstitut is based on the campus of the University of Bayreuth and occupies the major fraction of the "BGI" building, with four large laboratories (400 m², multianvil, deformation, piston-cylinder, internally heated autoclaves), some 760 m² of additional lab space, 450 m² of office space, 280 m² of machine shops and 70 m² of infrastructure space (including seminar room, institute library, *etc.*), and it also has access to the central machine

shops, central library, computer centre, *etc.* of the University of Bayreuth.

The Geoinstitut is provided with well equipped machine shops, electronic workshop and sample preparation laboratories. It operates a 19 node HPTC linux cluster, and has also access to the university computer centre. 



Four Humboldt awardees meet at Bayerisches Geoinstitut. From left: Bill Durham/Livermore, USA; Jean-Paul Poirier/Paris, France; Joe Smyth/Boulder, USA; Hartmut Spetzler/Boulder, USA.

Source of Figures, copyright information

We are grateful to the following copyright holders for permission to reproduce the figures in this brochure.

Fig. 1.1	© GEO 4/94, modified
Fig.1.2	© Dapeng Zhao, Uhima University, Japan
Figs. 1.3, 3.1, 3.2, 3.3, 3.4, 3.5, 3.6	© F. Langenhorst, Bayreuth
Fig.1.4	© R. Hollerbach, Köln
Fig.1.5	© J.J.Gurney, Cape Town
Fig. 1.6	© F. Marton, Bayreuth
Fig.1.7	© F. Seifert, Bayreuth
Figs. 2.1, and page 71	© Bayerisches Geoinstitut, Bayreuth
Figs. 2.2, 2.3	© Bayerisches Geoinstitut, Bayreuth, S. Weber
Figs. 2.4, 12.1, 12.2, 12.3, 13.1	© L. Dubrovinsky, Bayreuth
Fig. 2.5	© Min. Soc. Great Britain, see also www.minersoc.org , and courtesy T.Arlt, Marly, Switzerland
Figs. 2.6, 7.6, 13.2	© G. Steinle-Neumann, Bayreuth
Figs. 4.1, 4.3	© H. Terasaki, Bayreuth
Fig. 4.2	© W. K. Hartmann, Tucson (www.psi.edu/hartmann/index.html)
Figs. 5.1, 5.2	© H. Terasaki, C. Liebske, Bayreuth
Figs. 6.1, 6.5	© G. Bromiley, Bayreuth
Fig.6.2	Courtesy of NOAA Central Library, USA (www.photolib.noaa.gov)
Fig. 6.3	© a,b Mineralogical Society of America, c. M. Terry, Bayreuth
Fig. 6.4	© S. Demouchy, Bayreuth
Figs. 7.1, 7.2, 7.4, 7.5	© S. Jacobsen, Bayreuth
Fig. 7.3	© S. Jacobsen, T. Boffa Ballaran, Bayreuth
Figs.8.1, 8.2, 11.3	© D. Frost, Bayreuth
Fig. 9.1	© F. Becker, U. Küppers, Univ. München
Figs. 9.2, 9.3, 10.4	© C. McCammon, Bayreuth
Fig. 10.1	© A.I. Becerro, Sevilla, Spain
Fig. 10.2	© F. Langenhorst, U. Bläß, Bayreuth
Fig. 10.3	© S. Lauterbach, Darmstadt
Fig. 10.5	© Elsevier and F. Marton, Bayreuth
Fig. 11.1a, 11.2	© F. Heidelbach, Bayreuth
Fig.11.1b	© I. Stretton, Bayreuth
Fig.14.1	© Dr Heinz Malzahn, Berlin, www.rohdiamant.de
Figs. 14.2, 14.3	© N. Dubrovinskaia, Bayreuth

Frontispieces:

Page 6	© F. Langenhorst, Bayreuth
Page 12	© A. Gaube, Bayreuth
Page 16	© A. Bischoff, F. Bartschat, Univ. Münster
Page 20	© W.K. Hartmann, Tucson
Page 24	© A. Gaube, Bayreuth
Page 28	© H. Hürter, Westerstede
Page 34	© GeoZentrum KTB, Windischeschenbach
Page 40	© N. Bolfan Casanova, CNRS, Clermont-Ferrand
Page 44	© www.istockphoto.com , modified and composed by A. Gaube
Page 48	© C. McCammon, Bayreuth
Page 52	© F. Heidelbach, Bayreuth
Page 56	© Dan Frost, Bayreuth
Page 60	© G. Steinle-Neumann, Bayreuth
Page 64	© Dr Heinz Malzahn, Berlin, www.rohdiamant.de
Page 68	© A. Türk, Bayreuth

The publications cited in the following give suggested further reading material for individual sections of the brochure. For most of these papers staff members of Bayerisches Geoinstitut have been authors or coauthors

Section 3

Langenhorst F, Shavranovsky GI, Masaitis VL, Koivisto M (1999): Discovery of impact diamonds in a fennoscandian crater and evidence for their genesis by solid-state transformation. *Geology* 27, 747-750

Langenhorst F, Poirier J-P (2000) Anatomy of black veins in Zagami: Clues to the formation of high-pressure phases. *Earth Planet Science Letters* 184:37-55

Langenhorst F, Poirier J-P, Deutsch A, Hornemann U (2002a) Experimental approach to generate shock veins in single-crystal olivine by shear melting. *Meteoritics Planet Sci* 37:1541-1553

Langenhorst F, Boustie M, Deutsch A, Hornemann U, Matignon CH, Migault A, Romain JP (2002b): Experimental techniques for the simulation of shock metamorphism: A case study on calcite. In *High-Pressure Shock Compression of Solids V – Shock Chemistry with Applications to Meteorite Impacts* (eds. L. Davison, Y. Horie, T. Sekine), Springer, 1-2

Langenhorst F (2002) Einschlagskrater auf der Erde – Zeugen kosmischer Katastrophen. *Sterne und Weltraum* 6:34-44

Section 4

Holzheid A, Sylvester P, O'Neill HSC, Rubie DC, Palme H (2000) Evidence for a late chondritic veneer in the Earth's mantle from high-pressure partitioning of palladium and platinum. *Nature* 406: 396-399

Gessmann CK, Rubie DC (2000) The origin of the depletions of V, Cr, and Mn in the mantles of the Earth and Moon. *Earth Planet Science Letters* 184:95-107

Gessmann CK, Wood BJ, Rubie DC, Kilburn MR (2001) Solubility of silicon in liquid metal at high pressure: Implications for the composition of the Earth's core. *Earth Planet Science Letters* 184:367-376

Fortenfant, SS, Günther D, Dingwell DB, Rubie, DC (2003) Temperature dependence of Pt and Rh solubilities in a haplobasaltic melt. *Geochim Cosmochim Acta* 67:123 - 131

Rubie DC, Melosh HJ, Reid JE, Liebske C, Righter K (2003) Mechanisms of metal-silicate equilibration in the terrestrial magma ocean. *Earth Planet Science Letters* 205: 239-255

Section 5

Liebske C, Behrens H, Holtz F, Lange RA (2003) The influence of pressure and composition on the viscosity of andesitic melts. *Geochim Cosmochim Acta* 67: 473-485

Suzuki A, Ohtani E, Funakoshi K, Terasaki H, Kubo T (2002) Viscosity of albite melt at high pressure and high temperature. *Phys Chem Minerals* 29:159-165

Terasaki H, Kato T, Urakawa S, Funakoshi K, Suzuki A, Okada T, Maeda M, Sato J, Kubo T, Kasai S (2001) The effect of temperature, pressure, and sulfur content on viscosity of the Fe-FeS melt. *Earth Planet Science Letters* 190:91-102

Reid JE, Suzuki A, Funakoshi K-I, Terasaki H, Poe BT, Rubie DC, Ohtani E (2003) The viscosity of CaMgSi₂O₆ liquid at pressures up to 13 GPa. *Physics of the Earth and Planetary Interiors* 139:45-54

Section 6

Demouchy S, Gaillard F, Stern CR, Mackwell S (2003) Water diffusion as a natural process in olivine crystal from garnet-peridotite xenoliths in basalts. *Geophys Res Abs*, 5:03216

Bromiley GD, Pawley AR (2002) The high-pressure stability of Mg-sursassite in a model hydrous peridotite: a possible mechanism for the deep subduction of significant volumes of H₂O. *Contr Mineral Petrol* 142:714-723

Terry MP, Robinson P, Ravna RJK (2000) Kyanite eclogite thermobarometry and evidence for thrusting of UHP over HP metamorphic rocks, Nordoyane, Western Gneiss Region, Norway. *Am Mineral* 85: 1637-1650

Section 7

High-Temperature and High-Pressure Crystal Chemistry. RM Hazen and RT Downs, Eds. *Reviews in Mineralogy and Geochemistry* Vol 41, Mineralogical Society of America, pp 596, Washington D.C. (2001)

Boffa-Ballaran T, Angel RJ, Carpenter MA (2000) High pressure transformation behaviour of the cummingtonite-grunerite solid solution. *Eur J Mineral* 12:1195-1213

Jacobsen SD, Reichmann HJ, Spetzler HA, Mackwell SJ, Smyth JR, Angel RA, McCammon CA (2002) Structure and elasticity of single-crystal (Mg,Fe)O and a new method of generating shear waves for gigahertz ultrasonic interferometry. *J Geophys Res* 107(B2), 2037, doi: 10.1029/2001JB000490.

Spetzler H, Shen A, Chen G, Herrmannsdoerfer G, Schulze H, Weigel R (1996) Ultrasonic measurements in a diamond anvil cell. *Phys Earth Planetary Int* 98: 93-99

Steinle-Neumann G, Stixrude L, Cohen RE (1999) First-principles elastic constants for the hcp transition metals Fe, Co, and Re at high pressure. *Phys Rev B* 60:791-799

Section 8

Frost DJ (2003) The structure and sharpness of $(\text{Mg,Fe})_2\text{SiO}_4$ phase transformations in the transition zone. *Earth Planet Science Letters* 216(3):313-318

Frost DJ (2003) Fe^{2+} -Mg partitioning between garnet, magnesiowüstite and $(\text{Mg,Fe})_2\text{SiO}_4$ phases of the transition zone. *Am Mineral* 88:387-397

Smyth JR, Frost DJ, (2002) The effect of water on the 410-km discontinuity: An experimental study. *Geophys Res Letters* 29:10.1029/2001GL014418.

Frost DJ, Langenhorst F (2002) The effect of Al_2O_3 on Fe-Mg partitioning between magnesiowüstite and magnesium silicate perovskite. *Earth Planet Science Letters* 199:227-241

Frost DJ, Langenhorst F, van Aken PA (2001) Fe-Mg partitioning between ringwoodite and magnesiowüstite and the effect of pressure, temperature and oxygen fugacity. *Phys Chem Minerals* 28:455-470

Section 9

McCammon CA, Griffin WL, Shee SH, O'Neill HSC (2001) Oxidation during metasomatism in ultramafic xenoliths from the Wesselton kimberlite, South Africa: Implications for the survival of diamond. *Contrib Mineral Petrol* 141: 287-296

McCammon CA (2002) From diamonds to defects: New ideas about the Earth's interior. *Hyper Inter* 141/142:73-81

McCammon CA, Ross NL (2003) Crystal chemistry of ferrous iron in $(\text{Mg,Fe})(\text{Si,Al})\text{O}_3$ majorite with implications for the transition zone. *Phys Chem Minerals* 30:206-216

Section 10

McCammon CA (2001) Deep diamond mysteries. *Science* 293:813-814

Xu Y, McCammon CA (2002) Evidence for ionic conductivity in lower mantle $(\text{Mg,Fe})(\text{Si,Al})\text{O}_3$ perovskite. *J Geophys Res* 107: 10.1029/2001JB000677

McCammon CA, Becerro AI, Lauterbach S, Bläß U, Marion S, Langenhorst F, Angel RJ, van Aken P, Seifert F (2002) Oxygen vacancies in perovskite and related structures: Implications for the lower mantle. *Mat Res Soc Symp Proc* 718:109-114

Tomioka N, Fujino K (1997) Natural $(\text{Mg,Fe})\text{SiO}_3$ -ilmenite and -perovskite in the Tenham meteorite. *Science* 277:084-1086

Marton FC, Cohen RE (2002) Constraints on lower mantle composition from molecular dynamics simulations of MgSiO_3 perovskite. *Phys Earth Planet Int* 134:239-252

Section 11

Heidelbach F, Stretton I, Langenhorst F, Mackwell S (2003) Fabric evolution during high shear-strain deformation of magnesiowüstite $(\text{Mg}_{0.8}\text{Fe}_{0.2}\text{O})$ *J Geophys Res* 108(B3): 10.1029/2001/JB001632

Holtzman BK, Kohlstedt DL, Zimmerman ME, Heidelbach F, Hiraga T, Hustoft J (2003) Melt segregation and strain partitioning: Implications for seismic anisotropy and mantle flow. *Science* 301: 1227-1230

Section 12

Dubrovinsky L, Annersten H, Dubrovinskaia N, Westman F, Harryson, Fabrichnaya O, Carlson S, (2001) Chemical interaction of iron and corundum as a source of heterogeneity at the core-mantle boundary. *Nature* 412:527-529

Dubrovinsky L, Dubrovinskaia N, Langenhorst F, Dobson D, Rubie D, Geßmann C, Abrikosov I, Johansson B (2003) Iron-silica interaction at extreme conditions and the nature of the electrically conducting layer at the base of Earth's mantle. *Nature* 422:58-61

Section 13

Dubrovinsky L, Dubrovinskaia NA (2003) High-pressure crystallography at elevated temperatures: experimental approach. NATO Meeting/NATO ASI Series, NATO Publishing Unit, Vol. High-pressure crystallography, 2003

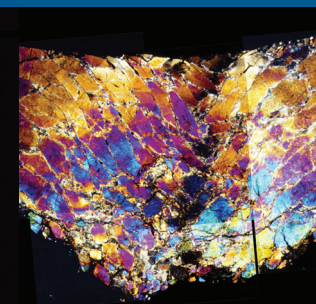
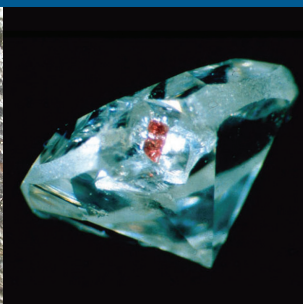
Steinle-Neumann G, Stixrude L, Cohen RE, Gülsersen O (2001) Elasticity of iron at the temperature of the Earth's inner core. *Nature* 413:57-60

Steinle-Neumann G, Stixrude L, Cohen RE (2003) Physical Properties of Iron in the Inner Core, in Core dynamics, structure, and rotation, Geodynamics Series, vol. 31, ed. Dehant V et al., pp. 137-162, Am Geophys Union, Washington, DC USA

Section 14

Dubrovinskaia NA, Dubrovinsky LS, Ahuja R, Prokopenko VB, Dmitriev D, Osorio-Guillen JM, Johansson B (2001) Experimental and theoretical identification of new high-pressure TiO_2 polymorph. *Phys Rev Letters*. 87: 27, 275501-4

Dubrovinskaia N, Dubrovinsky L (2003) Whole-cell heater for the diamond anvil cell, *Rev Sci. Instr* 74: 3433-3477



Bayerisches Geoinstitut
Universität Bayreuth
D-95440 Bayreuth
Germany

Tel. +49 (0) 9 21 - 55 37 00
Fax +49 (0) 9 21 - 55 37 69

e-mail bayerisches.geoinstitut@uni-bayreuth.de
Homepage: <http://www.bgi.uni-bayreuth.de>